SKI Report 2004:17

Research

Vault-Scale Modelling of pH Buffering Capacity in Crushed Granite Backfills

Steven Benbow
Sarah Watson
David Savage
Peter Robinson

April 2004

ISSN 1104–1374
ISRN SKI-R-04/17-SE

SKI

SKI perspective

Background

Concrete and cement are used in constructions as well as in conditioning of waste in repositories for radioactive waste. If it can not be excluded that groundwater in the backfill and bedrock adjacent to the backfill becomes highly alkaline, all potential consequences (influence on the bedrock and the EBS components, influence on sorption and radionuclide solubility etc.) must be evaluated in the performance assessment context. In the SKI review of SKB's preliminary safety assessment of the repository for long-lived low- and intermediate-level waste (SFL 3-5), SKI questioned the SKB results regarding neutralisation of high pH in a backfill.

In an earlier SKI study scoping calculations were carried out on a particle scale to investigate uncertainties encountered by different dissolution models, mineral compositions and diffusional transport (SKI Report 02:39). The results of the study indicate that the accessibility of buffering is limited, and that the SKB claim that cementitious pore water leached from the concrete would be neutralised in the backfill is questionable.

Purpose of the project

The purpose of this project was to develop a repository (vault) scale model, to investigate if and under what circumstances high pH water could leave the vault. This included a range of flow scenarios and modelling of the pH development within the vault for these scenarios.

Results

The results of the modelling show that a gravel backfill (in this case represented by quartz) is in general capable of retarding the migration of high pH pore fluids generated by concrete leaching. However, in some of the investigated flow scenarios the pH at the backfill/host rock boundary increases to about 11, especially beneath the waste packages (where the backfill layer is thin) or at outflow regions. It should be noted that the accessibility of pH-buffering of the backfill though may have been overestimated due to model simplifications.

Effects on SKI work

The modelling shows that it is not sufficient to use simple scoping calculations for estimating pH-buffering capacities of backfills. The effects of high pH water reaching the rock could be studied in further detail, by e.g. developing the representation of chemical kinetics or by including the chemical reactions of the surrounding bedrock more explicitly.

A general conclusion is that the effects of high pH must be analysed in performance assessments of cementitious repositories, and the project results will be used as one

basis in coming SKI reviews of SKB's safety assessments of repositories for spent fuel (SFL 2) and low-and intermediate level waste (SFR, SFL 3-5).

Project information

Responsible for the project at SKI has been Christina Lilja.
SKI reference: 14.9-020951/02231

The report is also available as an electronic version (e.g. at the SKI web site www.ski.se, in which some of the black and white figures presented in the paper report are shown in colour.

SKI Report 2004:17

Research

Vault-Scale Modelling of pH Buffering Capacity in Crushed Granite Backfills

Steven Benbow[1]
Sarah Watson[2]
David Savage[1]
Peter Robinson[1]

[1]Quintessa Limited
Dalton House
Newton Road
Henley-on-Thames
Oxfordshire, RG9 1HG
UK

[2]Geo-Analysis
23 Tuckers Road
Faringdon
Oxfordshire, SN7 7YQ
UK

April 2004

Contents

Summary

Some engineered barrier designs for geological repositories for radioactive wastes rely upon the use of cement as chemical conditioning agents for the wastes. Although the hyperalkaline pore fluids characteristic of cements may have a positive effect upon near-field performance, their migration into the geosphere poses problems regarding potentially deleterious interactions along groundwater flow paths, e.g. change of sorption or matrix diffusion properties of the host rock. To counteract these potential effects, SKB has developed the concept of a gravel backfill for its SFL 3-5 repository, where it is anticipated that the gravel would act as a 'sacrificial' reactive barrier between cement conditioned wastes and the geosphere. This role is dependent upon the reaction of silicate and aluminosilicate minerals in the gravel through hydroxyl ion-catalysed mineral dissolution reactions and the associated precipitation of hydroxyl ion bearing solids, such as calcium silicate hydrates. This barrier concept has been evaluated by the simulation of groundwater flow and chemical reaction of cement pore fluid through a realistic backfill geometry and various potential groundwater flow scenarios.

Potential groundwater flow conditions through gravel backfill for the SFL 3-5 repository concept were modelled in 3D using MODFLOW. The regional groundwater flow field was assumed to be horizontal and its interaction with a homogeneous backfill of dimensions in accordance with published designs for the SKB SFL 3-5 repository, with uniform physical and hydraulic properties was investigated. The host rock also had uniform properties, except where simulations explicitly represented transmissive features.

Calculations of cement pore fluid migration and reaction with backfill were carried out using *Raiden2*, a fully-coupled reaction-transport simulator. Flow fields generated in 3D with MODFLOW were converted to 2D 'slices' for reaction-transport calculations. The backfill was assumed to consist of grains of quartz of uniform size of either 4 or 32 mm diameter. The cement pore fluid diffusing from the waste package was assumed to be pure water saturated with portlandite [$Ca(OH)_2$] at 25 °C. The pore fluid saturating the backfill was assumed to be pure water equilibrated with quartz at 25 °C. A number of different simulations were carried out for both 4 and 32 mm diameter gravel backfill grains:

1. A 2D horizontal slice through the vault length with a transmissive feature in the host rock parallel to the vault length, but positioned roughly two vault widths from the vault.
2. As (1) above, but considering a 2D *vertical* slice through the vault.

3. A 2D horizontal slice through the vault *width* with a transmissive feature in the host rock normal to the vault length.
4. A 2D horizontal slice through the vault length with a transmissive feature in the host rock intersecting the vault at 45 ° to the vault.

An additional simulation was also carried out for the geometry considered in model variant (4) above where reaction of quartz was excluded so that only the reaction of $Ca(OH)_2$-saturated fluid with ambient groundwater was simulated.

The results of the model variants incorporating reaction of quartz were broadly similar, with few differences apparent for the different orientations of the transmissive feature in the host rock. Most simulations showed that the gravel backfill was capable of maintaining pH < 11 in the backfill adjacent to the waste package and pH < 9.5 adjacent to the host rock, at timescales up to 10 000 years. However, some model variants showed pH ~11 in the backfill adjacent to the host rock at certain locations (beneath the waste package in some simulations, or at outflow regions in others). In all simulations, gradients of pH across the backfill were marked. Appreciable amounts of quartz (in the order of 10^4 moles after 10 000 years in a representative 1 m thick slice through the backfill) were dissolved in the gravel adjacent to the waste package to achieve pH buffering. All of the dissolved quartz was converted to CSH solids (tobermorite and gyrolite). Reactions in simulations with the 4 mm diameter backfill grains were slightly faster, but the results were otherwise identical to those for the 32 mm diameter grains.

The model variant with no chemical reaction of the backfill particles was considerably different from the other simulations with pH > 11 throughout the backfill volume after 3000 years of simulated time. Only trace amounts of a CSH solid (tobermorite) precipitated in this simulation, reflecting the minor amount of silica in the backfill pore fluid. This simulation highlighted the role of quartz/granite reactivity in retarding the migration of the hyperalkaline pore fluid.

The results of the modelling reported here broadly show that a gravel backfill (here represented by quartz) is capable of retarding the migration of high pH pore fluids derived from hydrolysis of a cement/concrete waste package. However, some model variants investigated here suggest that pore fluid pH at the backfill-host rock boundary may increase to pH ~11, particularly beneath waste packages or at outflow regions of the EBS. These pore fluids have a pH considerably above that expected for groundwaters in Swedish granites and may thus be reactive with respect to minerals lining groundwater pathways. Dissolution of fracture-lining silicates and carbonates may be expected, with concomitant precipitation of solids such as zeolites. These reactions may serve to increase radionuclide retardation, but may need to be considered explicitly in safety assessment.

Moreover, there are a couple of non-conservative assumptions in the modelling conducted here which create further uncertainty in the ability of a gravel backfill to buffer pH:

- The granite backfill is not wholly composed of quartz, so that the amount of silica available for reaction with cement pore fluids is less than that modelled, probably by 30-40 %.
- The reactive surface area of granite gravel grains will decrease with time due to 'armouring' by reaction products. This will result in decreased reactivity (less buffering capacity) with time.

The effects of these assumptions could be investigated in further studies of this type.

1 Introduction

Some engineered barrier designs for geological repositories for radioactive wastes rely upon the use of cement as a chemical conditioning agent for the wastes. Concrete may also be used as a structural engineering material, such as hydraulic plugs for vaults. Pore fluids in cements and concretes are hyperalkaline (pH > 12.5) due to the hydrolysis of constituent solids such as portlandite [$Ca(OH)_2$] and calcium silicate hydrate gel, e.g. see Börjesson, 1997. Although hyperalkaline pore fluids may have a positive effect upon near-field performance through minimisation of radioelement solubility and maximisation of sorption, their migration into the geosphere poses problems regarding potentially deleterious interactions along groundwater flow paths, e.g. change of sorption or matrix diffusion properties of the host rock.

To counteract these potential effects, SKB has developed the concept of a gravel backfill for its SFL 3-5 repository. In this design, it is anticipated that the gravel would act as a 'sacrificial' reactive barrier between cement conditioned wastes and the geosphere. This role is dependent upon the reaction of silicate and aluminosilicate minerals in the gravel through hydroxyl ion-catalysed mineral dissolution reactions and the associated precipitation of hydroxyl ion bearing solids, such as calcium silicate hydrates (Karlsson et al., 1999). Karlsson et al. (1999) have suggested that OH^- ions in the migrating cement pore fluids may be wholly consumed by dissolution of quartz in gravel backfills of broad 'granitic' composition and subsequent precipitation of calcium silicate hydrate (CSH) solids.

The validity of this approach was questioned by a review and particle-scale modelling work carried out by SKI (Benbow et al., 2002). Benbow et al. (2002) provided evidence that suggested SKB had used non-conservative assumptions concerning the amount and available surface area of quartz required to achieve retardation of OH^- in the backfill and that hyperalkaline fluids may not be fully retarded by reaction within the gravel backfill.

The aim of the work presented here is to further investigate the issues raised by Benbow et al. (2002) by carrying out reactive transport modelling of the potential pH buffering process in the gravel backfill envisaged by SKB for the SFL 3-5 repository. These model calculations have employed realistic engineered barrier geometries, published laboratory data concerning mineral reaction kinetics, and a number of plausible groundwater flow scenarios to test the validity of SKB's claims for the performance of this proposed engineered barrier design for SFL 3-5.

Groundwater flow calculations for the repository site domain are presented in Section 2. The calculations were performed using the MODFLOW code (McDonald and

Harbaugh, 1988). Results for two and three-dimensional calculations are presented for various fracture geometries in the host rock neighbouring the vault.

In Section 3, vault-scale geochemical modelling calculations are presented. The calculations were performed using the Raiden2 geochemical modelling tool. The geochemical calculations are based on two-dimensional slices through the vault region, with the applied flow fields taken from the three-dimensional modelling results of Section 2. The geochemical modelling uses the same level of discretisation as was used in the flow modelling calculations. Calculations were performed for various backfill particle sizes over a range of two-dimensional slices through the modelling scenarios considered in the flow modelling.

A summary of the geochemical modelling results and conclusions are presented in Section 4. Comparisons with the conclusions drawn by Karlsson et al. (1999) are given and some suggestions for enhancements to the geochemical are made.

Due to the difficulties encountered when attempting to present graphs of two-dimensional geochemical modelling results in a concise format, also a CD has been produced with colour images and movies from the geochemical simulations that may help to describe better the results. An electronic copy of this report is available (e.g.at the SKI web site www.ski.se) in which some of the black and white figures presented in the paper report are shown in colour.

2 Flow modelling

2.1 Introduction and scope

The current project addresses the question of whether a granite backfill is sufficient to buffer a high pH plume emanating from a cementitious (SFL 3-5) repository. It involves the development of a vault-scale geochemical model to investigate whether or not the gravel backfill currently proposed by SKB would limit the migration of high pH porefluids. The work includes the assessment of a range of potential flow scenarios and models the pH development within the vault for each of these. To generate realistic flow scenarios for the geochemical model on the vault scale, repository site domain scale flow models have been considered so that the impact of the repository on the regional flow fields can be represented.

Although it is possible to use various analytical approaches to estimate the groundwater flow field within the disposal vault for various idealised geometries, it is appropriate to model groundwater flow in the SFL 3-5 system using a (simple) three-dimensional model. It is not possible to represent the three-dimensional geometry of the encapsulated waste, surrounding backfill and any transmissive features that might intersect the vault in an appropriate way using an analytical model. This geometry is key to determining the distribution of flow through the gravel backfill and encapsulated waste.

The following section describes the groundwater flow calculations that were carried out to produce flow fields for use in the *Raiden2* geochemical model. Results of the groundwater flow calculations are presented in 2.3.

2.2 Specification

2.2.1 Background

A sealed waste repository will have a permeability that is different from that of the surrounding rock. The groundwater flow field in the immediate vicinity of the repository will be modified by the presence of the repository. At the simplest level, this modification to the flow can be calculated analytically using the equations more usually applied to electrostatics to obtain a 'flow enhancement' factor. If the inclusion has a higher permeability than the host rock, flow is focussed through the inclusion and if it is less permeable the opposite occurs. The degree of flow enhancement depends on both the dimensions of the inclusion (aspect ratio etc) and on the orientation of the inclusion relative to the regional groundwater flow field. This approach has been used to estimate

groundwater flow through the repository in a number of radioactive waste programmes worldwide.

The approach can be extended to cope with the slightly more complex geometry of vaults such as the SFL 3-5 system in which the encapsulated waste (which has a relatively low permeability) is completely surrounded by backfill which has a significantly higher permeability than either the encapsulated waste or the host rock. In this case it is expected that flow will be mostly through the high permeability backfill such that a 'hydraulic cage' is established around the encapsulated waste. The backfill is termed a positive flow barrier by some workers.

Probably the most complete and accessible analytical treatment of the effect of an inclusion with different permeability to the host rock on the local groundwater flow field is that of Holmén in SKB Report TR-97-10 (1997). This report was reviewed as part of the current study and provides the justification for model parameters such as the overall size of the modelled domain. SKB Report R-99-13 (Skagius et al., 1999) contains a useful compilation of physical parameters appropriate to the types of site being considered by SKB for SFL 3-5. Other relevant reports from the SKB programme were also consulted.

2.2.2 Model geometry

A relatively simple groundwater flow model, which nevertheless captures the key features of the system, is required. Some key features of the model are listed below:

- Simplified representation of generic SFL3 or 5 vault with geometry based on R-99-13;
- No interactions with neighbouring SFL3 (or 5) vault or with the network of SFL4 tunnels;
- Concrete holding encapsulated waste treated as homogeneous – internal structure not represented;
- Transmissive feature extending over the full height of the domain which may intersect the vault, otherwise uniform host rock properties;
- Gravel backfill has uniform properties;
- Regional groundwater flow field is horizontal.

The geometry is based on the design given in SKB R-99-13. However, the concrete building holding the encapsulated waste is placed in the centre of the vault rather than allowing a large loading area at one end. The encapsulated waste package is founded on a 0.5 m thick layer of gravel and surrounded by gravel backfill that entirely fills the remaining vault space. It is assumed that the construction is such that the layer of

gravel forming the building foundation is in hydraulic contact with the gravel backfill so that they function as a single hydrogeological unit.

The key vault dimensions are shown in the following table.

Parameter	**Value**
Vault length	133 m
Vault width	14 m
Vault height	19 m (Curved top starts at 16.8 m)
Encapsulated waste length	114.6 m
Encapsulated waste width	10.8 m
Encapsulated waste height	10.7 m
Thickness of gravel beneath waste	0.5 m
Thickness of backfill either side of waste	1.6 m
Thickness of gravel above waste	7.8 m

Table 2.1: Vault dimensions used in the flow modelling

As noted above, the presence of the vault affects the groundwater flow field in the region immediately surrounding the vault. The model domain must be sufficiently large that boundary effects resulting from the necessarily finite size of the model domain are acceptably small. The data in Holmén (1997) can be used to estimate the size of model domain required. From the analyses presented in that report it appears that an appropriate rule of thumb to ensure that boundary effects are negligible (less than order 1%) is that the boundary should be located at least the tunnel length away from the tunnel. For the current model, this implies that the boundaries should be at least 130 m away from the tunnel.

2.2.3 Groundwater flow parameters

The hydrogeological parameters were chosen to be representative of those that might reasonably be expected to prevail at the SFL site. Report SKB R-99-13 contains a summary of the hydrogeological conditions at Aberg, Beberg and Ceberg, the three hypothetical sites studied by SKB during their 1997 assessment. The parameters used were based on those given for the Beberg site. However, the results given in TR-97-10 indicate that the permeability contrasts in the system are such that the overall distribution of flow (in relative terms) does not change greatly if the regional

groundwater flow rate changes so the results should scale to larger (Aberg) or smaller (Ceberg) overall groundwater flows.

Groundwater flow at Beberg is predicted to be sub-horizontal (downwards flow at 6º relative to horizontal). For simplicity, it has been assumed in the current study that groundwater flow is horizontal. The orientation of the vault relative to the direction of regional groundwater flow is not known. Therefore three different flow directions will be considered : regional flow along the long axis of the vault; regional flow at 45º to the long axis of the vault; and regional flow at right angles to the vault.

SKB Report R-99-13 also gives values for the expected hydrogeological parameters for the other components of the system. The hydraulic conductivity of intact structural concrete is very low (order 10^{-11} to 10^{-12} m/s) but it is expected that there will be some cracking of the concrete. Therefore hydraulic conductivity of concrete that contains some penetrating cracks was used for the encapsulation structure (concrete plus waste). A value of 10^{-8} m/s is suggested as an appropriate effective hydraulic conductivity for partially cracked concrete.

Groundwater flow at the potential SFL 3-5 sites is largely through a network of fracture zones and there is expected to be relatively little flow through the 'intact' rock. The fracture zones at the various sites have been mapped and in some cases their hydrogeological properties have been determined. The spacing of the fracture zones appears to be of the order of 100 m so it is likely that the SFL 3-5 vault will be intersected by one or more such features which are likely to have a significant influence on the groundwater flow through the vault. A simple representation of the intersection of one of these features with the vault is therefore included in the model.

There does not appear to be a readily available summary of the form given in R-99-13 (Skagius et al., 1999) for parameters such as fracture zone widths and transmissivities. However, SKB Report R-01-49 (Marsic et al., 2001) tabulates the widths and hydraulic conductivities of the fracture zones used in the recent modelling of Beberg. From this report it appears that the fracture zones of interest in the current modelling are often subvertical, are of order 35 m in width and have an average transmissivity of order 10^{-3} to 10^{-4} m^2/s. In practice, once the effective hydraulic conductivity of the fracture zone is more than an order of magnitude greater than that of the background rock it will dominate the flow.

The groundwater flow parameters used in the models are summarised in the following table.

Parameter	Value
Specific Flow (Darcy Velocity)	3 l/m^2/year (9.5 10^{-11} m/s)
Hydraulic conductivity of host rock (effective)	10^{-8} m/s
Hydraulic conductivity of transmissive features	10^{-6} m/s
Width of transmissive features	order 35 m
Hydraulic conductivity of encapsulation structure	10^{-8} m/s
Hydraulic conductivity of gravel backfill	10^{-4} m/s

Table 2.2: Groundwater flow parameters

The analyses presented in Holmén (1997) demonstrate that there is a 'threshold' value of the ratio of the permeability of the tunnel to that of the host rock above which the flow enhancement factor is effectively constant. For the tunnel geometry considered in the current study the threshold value is about 1000; hence the choice of 10^{-4} m/s for the hydraulic conductivity of the backfill should be sufficiently large to give the maximum possible flow rates through the backfill.

2.2.4 Numerical model

The groundwater flow calculations were carried out using MODFLOW (McDonald and Harbaugh, 1988). The MODFLOW SURFACT PCG4 solver was used for many of the models. The model was constructed and the results were analysed using the Groundwater Vistas graphical interface. MODFLOW is a finite difference code which imposes certain constraints on the construction of the model owing to the regular Cartesian grid used by the code. Key features of the numerical implementation are as follows.

- The vault is aligned along rows/columns of a finite difference grid. In the 45º case flow in the host rock will be at 45º to the rows/columns.
- All features are at least two cells thick to maintain the continuity of the feature when it is not aligned with the rows/columns.
- Refinement is concentrated in the central part of the grid.
- The ratio of adjacent cell sizes is always between 0.75 and 1.3.
- The model measures 527 x 500 x 302 m. For the 45º case, the model is approximately square in plan view with a side length of approximately 355 m.
- The grid contains 284142 cells (69 x 71 x 58 cells). For the 45º case, 229854 cells are active.

The boundary conditions applied are as follows.

- Specified head on the upstream boundary such that the total flow is equal to 3 $l/m^2/yr$ averaged over the whole boundary. For cases that included transmissive features, the overall head drop across the model was reduced to achieve the desired overall flow.
- Specified head on the downstream boundary.
- No flow on all other lateral boundaries.

The head drops across each model are given in the Table 2.3.

Model	Description	Head drop
1	Flow along vault, no transmissive feature	5 m
2	Flow across vault, no transmissive feature	5 m
3	Flow at 45º to vault, no transmissive feature	3.5 m
4	Flow along vault, vertical section	5 m
5	Flow along vault, transmissive feature	1.5 m
6	Flow across vault, transmissive feature	1.5 m
7	Flow at 45º to vault, transmissive feature	1.0 m

Table 2.3: Head drops across each model

The procedure used to set up the model was as follows.

1. Set up the desired geometry with the vault hydrogeological properties set equal to the host rock (plus transmissive features) properties.
2. Run the model to produce the background regional flow field. Adjust the boundary conditions and properties of the transmissive features so that the desired undisturbed uniform flow field is obtained.
3. Set the hydrogeological properties of the vault to the desired values and carry out the flow calculation using the regional flow field as the initial guess.

The large contrast in permeability between the backfill and the host rock / waste plus encapsulation makes the models relatively difficult to solve because of the large off diagonal entries in the matrices. In particular, it was necessary to specify a very strict

convergence criterion of 10^{-7} m (the convergence criterion for the MODFLOW solvers is head change) in order to ensure that the solution was fully converged. For less strict criteria, the solution appeared to be plausible but detailed inspection of the flow vectors and pathlines showed that it was not in fact fully converged.

2.3 Results

Calculations were carried out in both 2D and 3D for cases with and without a transmissive feature. The 2D models represent a plane through the centre of the waste stack (horizontal and vertical). The results are summarised in the following subsections.

2.3.1 Two dimensional models

2D Model 1: Flow along vault; no transmissive feature

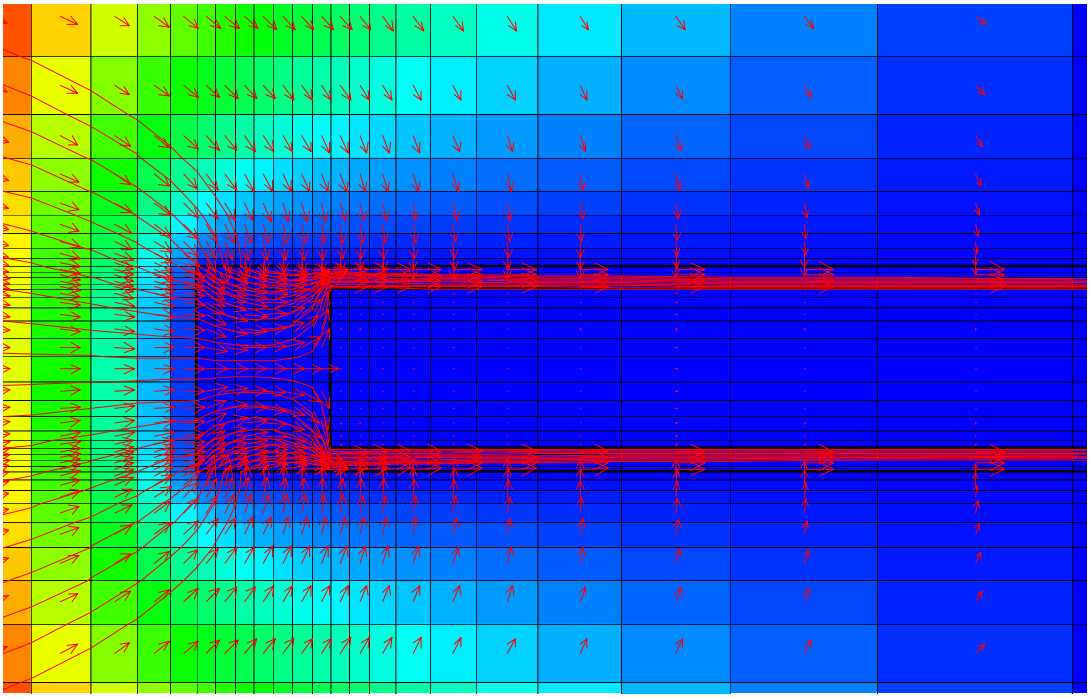

Figure 2.1: 2D Model 1 flow field. The figure is shaded according to head and shows velocity vectors (length proportional to log of magnitude) and particle tracks.

Representative Darcy velocities in the model are:

Location	**Darcy velocity (m/s)**
Undisturbed background flow	1×10^{-10}
Backfill upstream/downstream of waste	4×10^{-10}
Backfill either side of waste	4×10^{-9}
Encapsulated waste	4×10^{-13}

2D Model 2: Flow across vault; no transmissive feature

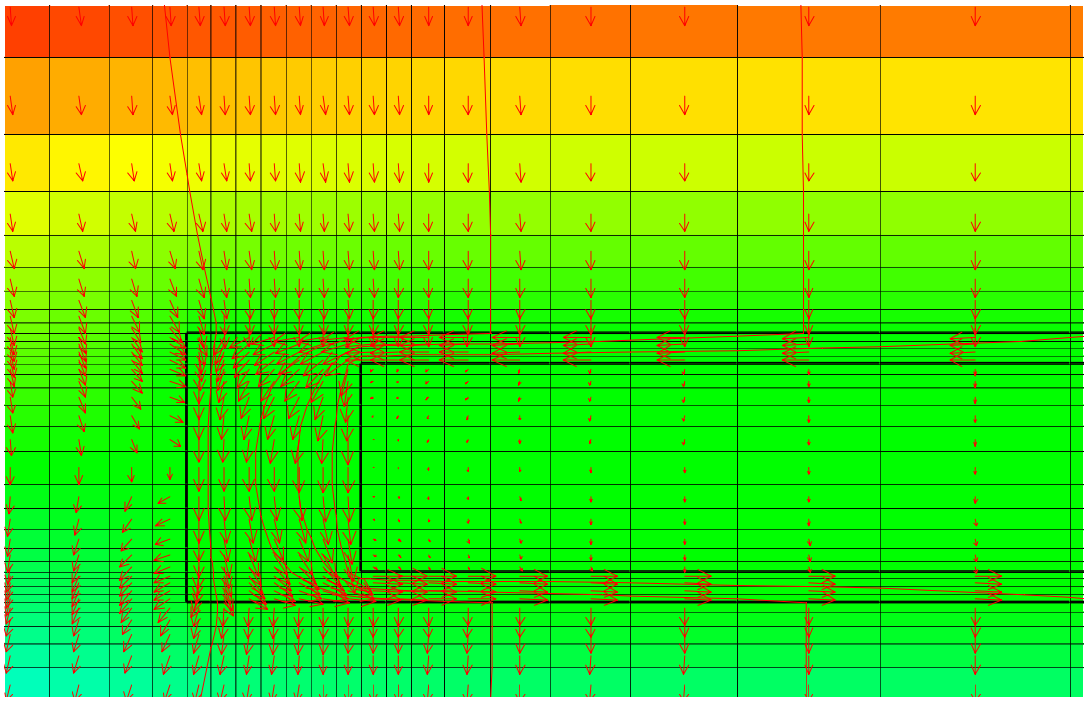

Figure 2.2: 2D Model 2 flow field. The figure is shaded according to head and shows velocity vectors (length proportional to log of magnitude) and particle tracks.

Representative Darcy velocities in the model are:

Location	**Darcy velocity (m/s)**
Undisturbed background flow	1×10^{-10}
Backfill upstream/downstream of waste	1×10^{-9}
Backfill either side of waste	2×10^{-9}
Encapsulated waste	2×10^{-12}

2D Model 3: Flow at 45° to vault; no transmissive feature

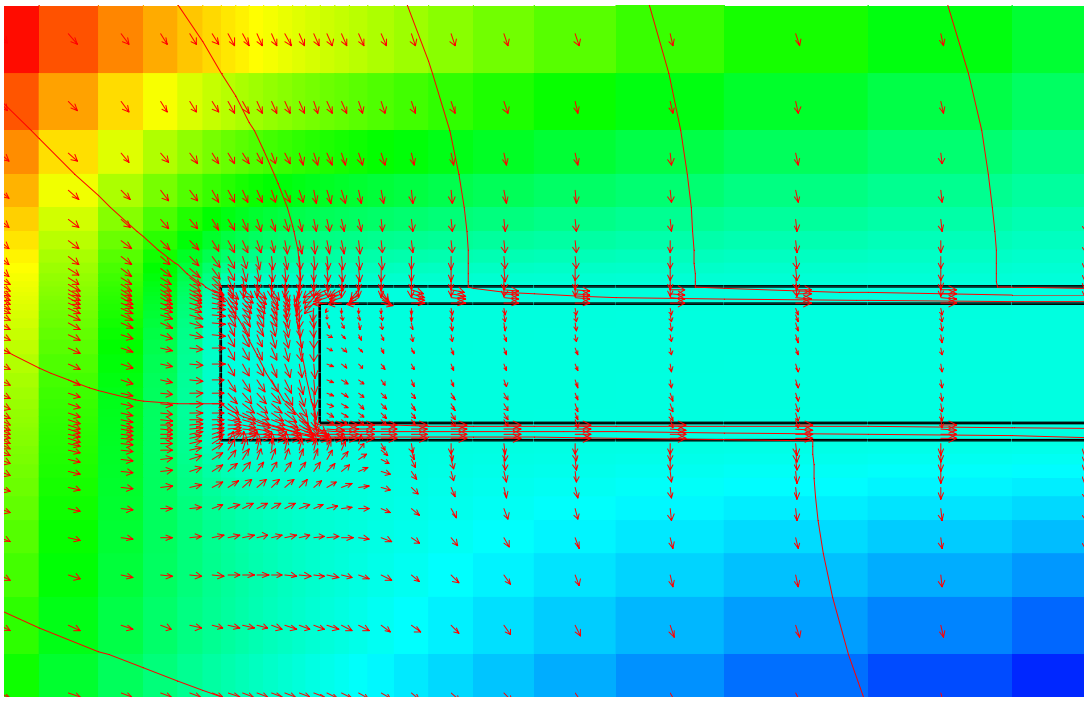

Figure 2.3: 2D Model 3 flow field. The figure is shaded according to head and shows velocity vectors (length proportional to log of magnitude) and particle tracks.

Representative Darcy velocities in the model are:

Location	**Darcy velocity (m/s)**
Undisturbed background flow	1×10^{-10}
Backfill upstream/downstream of waste	7×10^{-10}
Backfill either side of waste	3×10^{-9}
Encapsulated waste	1.5×10^{-12}

2D Model 4: Vertical section along vault; no transmissive feature

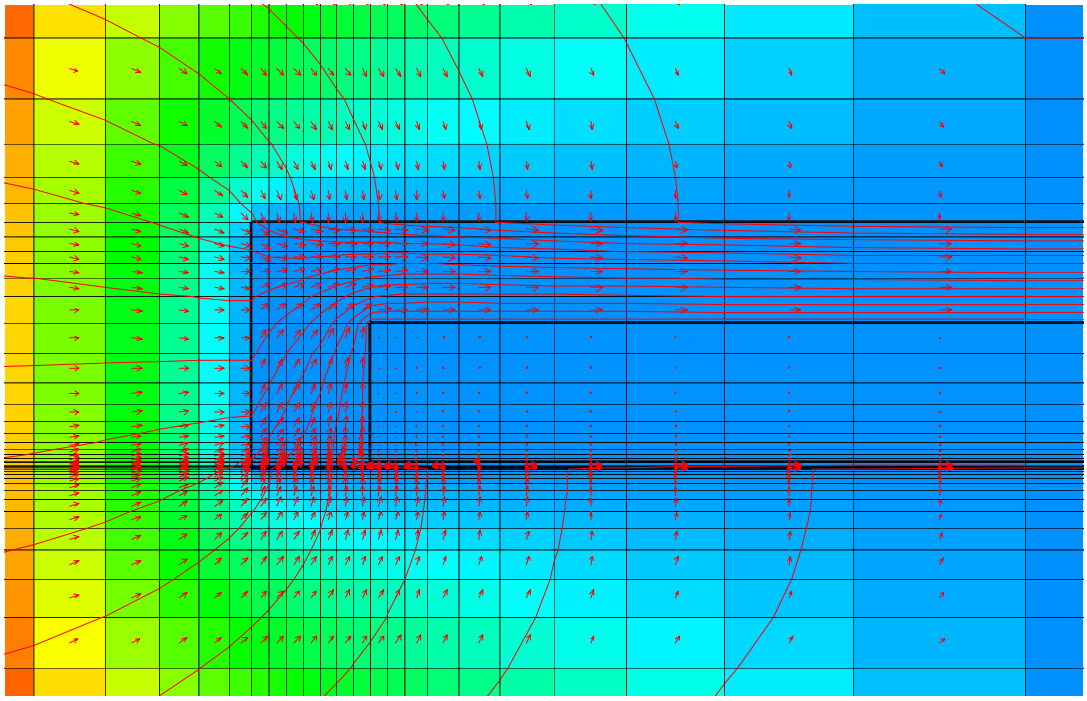

Figure 2.4: 2D Model 4 flow field. The figure is shaded according to head and shows velocity vectors (length proportional to log of magnitude) and particle tracks.

Representative Darcy velocities in the model are:

Location	**Darcy velocity (m/s)**
Undisturbed background flow	1×10^{-10}
Backfill upstream/downstream of waste	6×10^{-10}
Backfill above waste	2×10^{-9}
Backfill below waste	3×10^{-9}
Encapsulated waste	4×10^{-13}

The 'backflow' in the backfill at below the waste near the upstream end of the waste block is noted. In 3D this backflow is not expected to occur, as the water is able to flow through the backfill either side of the waste.

If the backfill under the waste is removed, the flow through the waste increases to about 10^{-11} m/s.

2D Model 5: Flow along vault; transmissive feature

In this case, a transmissive feature was introduced into the model parallel to the vault and at a distance of approximately 2 vault widths from the vault.

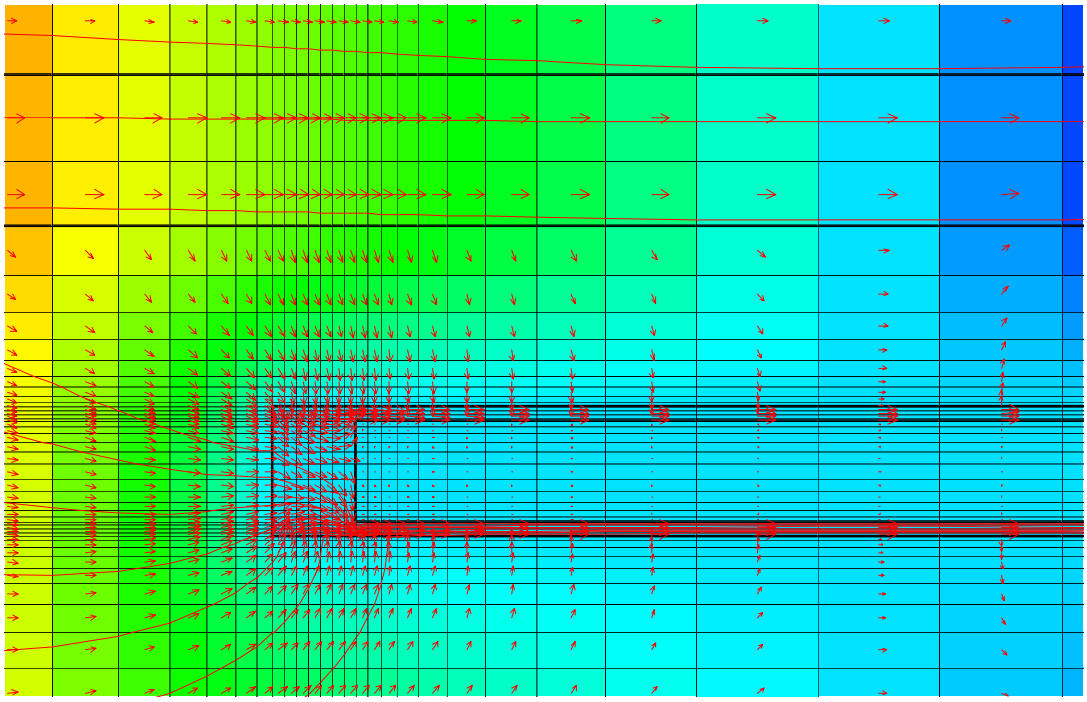

Figure 2.5: 2D Model 5 flow field. The figure is shaded according to head and shows velocity vectors (length proportional to log of magnitude) and particle tracks.

The presence of the transmissive feature has subtly modified the flow through the vault by introducing an asymmetry into the flow. Representative Darcy velocities in the model are:

Location	**Darcy velocity (m/s)**
Undisturbed background flow	3×10^{-11}
Undisturbed flow in transmissive feature	3×10^{-9}
Flow upstream / downstream of waste	1.75×10^{-10}
Flow either side of waste	2×10^{-9}
Encapsulated waste	2×10^{-13}

2D Model 6: Flow across vault; transmissive feature

In this case, a transmissive feature intersecting the vault about a third of the way along was introduced into the model.

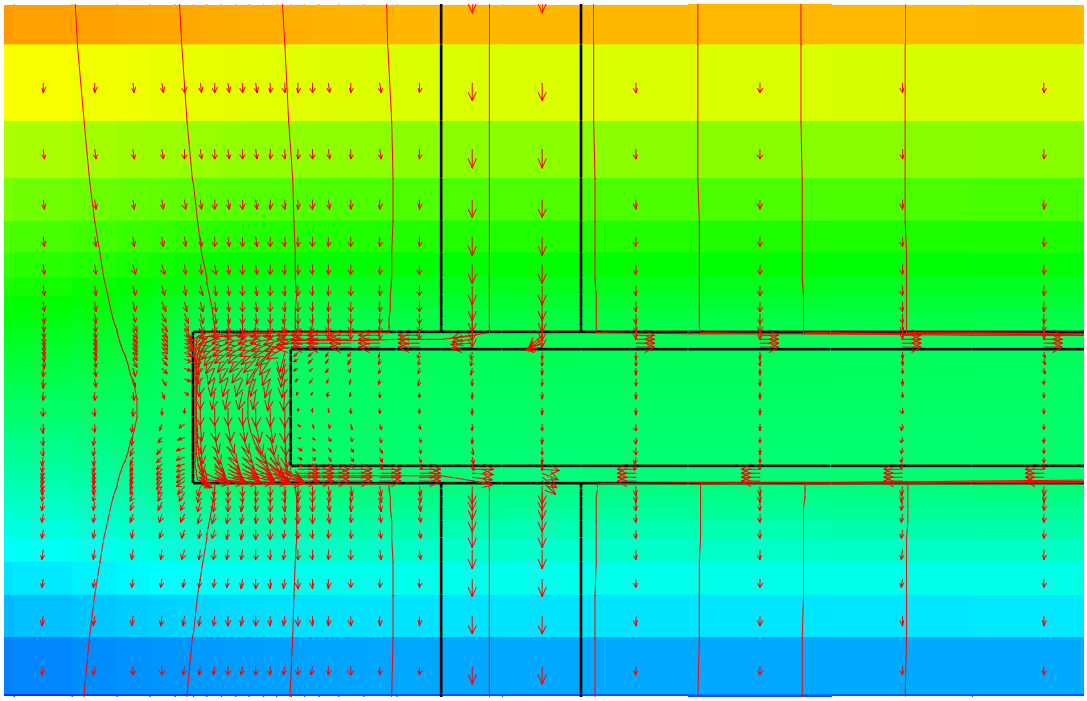

Figure 2.6: 2D Model 6 flow field. The figure is shaded according to head and shows velocity vectors (length proportional to log of magnitude) and particle tracks.

The presence of the transmissive feature has a significant effect on the flow through the vault. The 'flow divide' is now located at the edge of the transmissive feature that is closer to the vault centreline. All of the flow from the transmissive feature flow around one end of the waste stack. Representative Darcy velocities in the model are:

Location	**Darcy velocity (m/s)**
Undisturbed background flow	3×10^{-11}
Undisturbed flow in transmissive feature	3×10^{-9}
Backfill at ends of waste	4×10^{-9} / 1×10^{-9}
Backfill either side of waste	2×10^{-8} / 5×10^{-9}
Encapsulated waste	$4\text{-}8\times10^{-12}$

2D Model 7: Flow at 45° to vault; transmissive feature

In this case, a transmissive feature intersecting the vault about a third of the way along was introduced into the model.

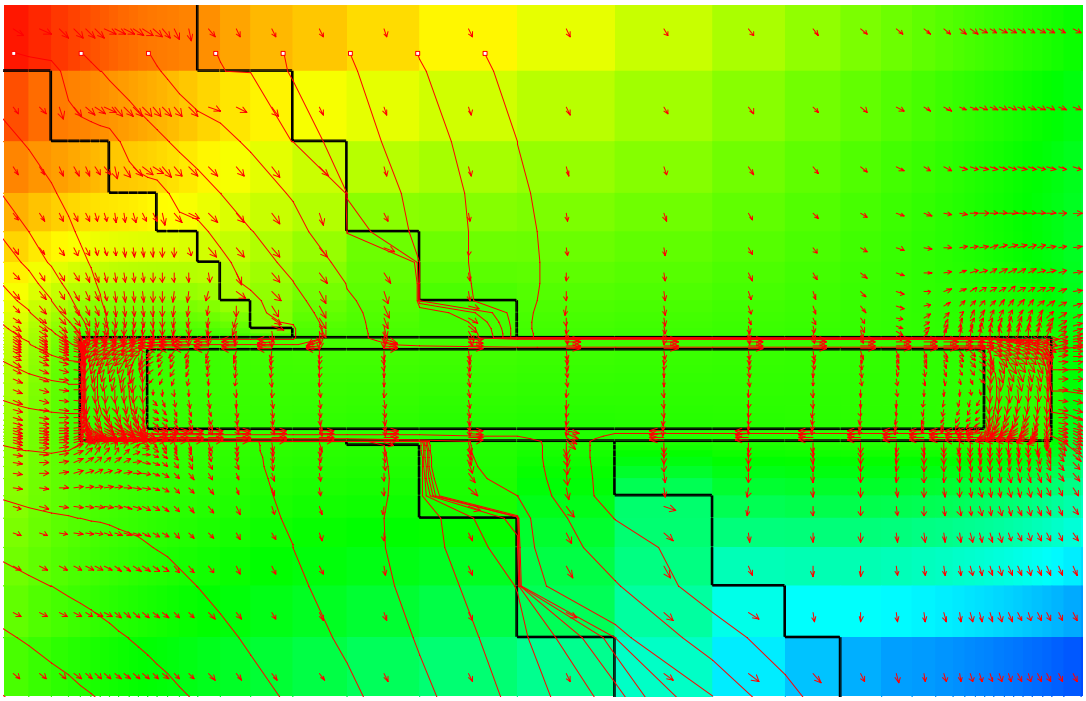

Figure 2.7: 2D Model 7 flow field. The figure is shaded according to head and shows velocity vectors (length proportional to log of magnitude) and particle tracks.

The transmissive feature modifies the flow field such that the flow divide round the waste is located at the intersection with the transmissive feature. Flow rates through the waste in the vicinity of the transmissive feature are significantly increased compared with the case when it is not present. Representative Darcy velocities in the model are:

Location	**Darcy velocity (m/s)**
Undisturbed background flow	3×10^{-11}
Undisturbed flow in transmissive feature	3×10^{-9}
Backfill at ends of waste	3×10^{-9}
Backfill either side of waste	$1\text{-}2\times10^{-8}$
Encapsulated waste	2×10^{-12} - 1×10^{-11}

2.3.2 Three dimensional models

3D Model 1: Flow along vault; no transmissive feature

(In the electronic document, downwards flows are in blue and upwards flows are in red.)

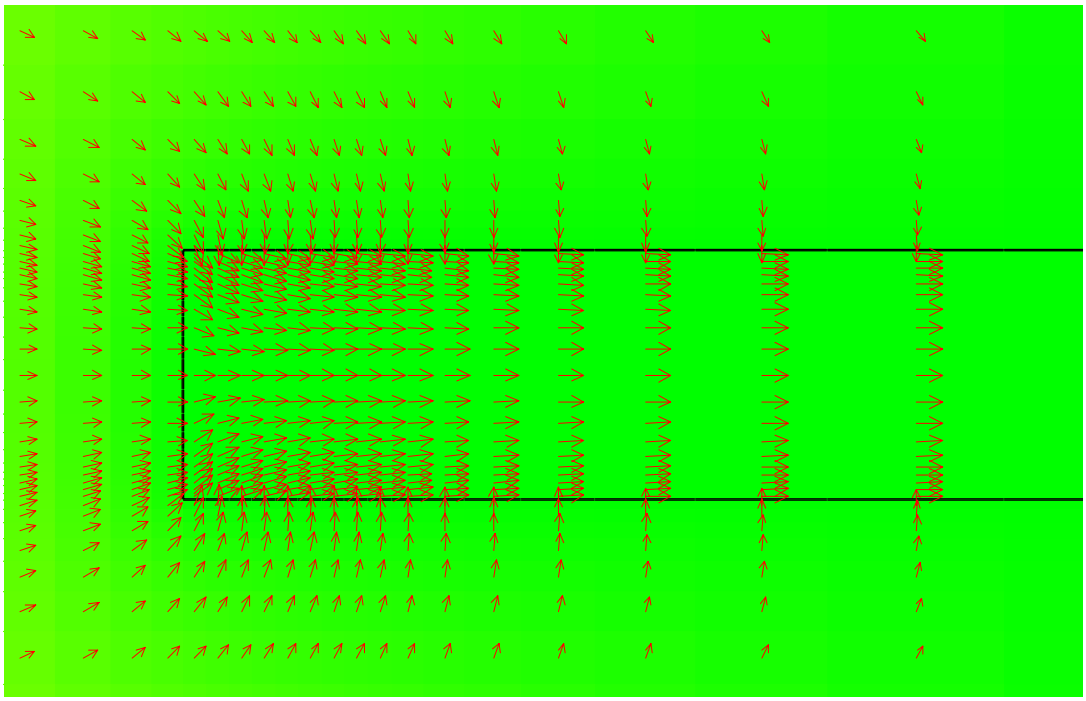

Figure 2.8: Velocity field close to the top of the backfill

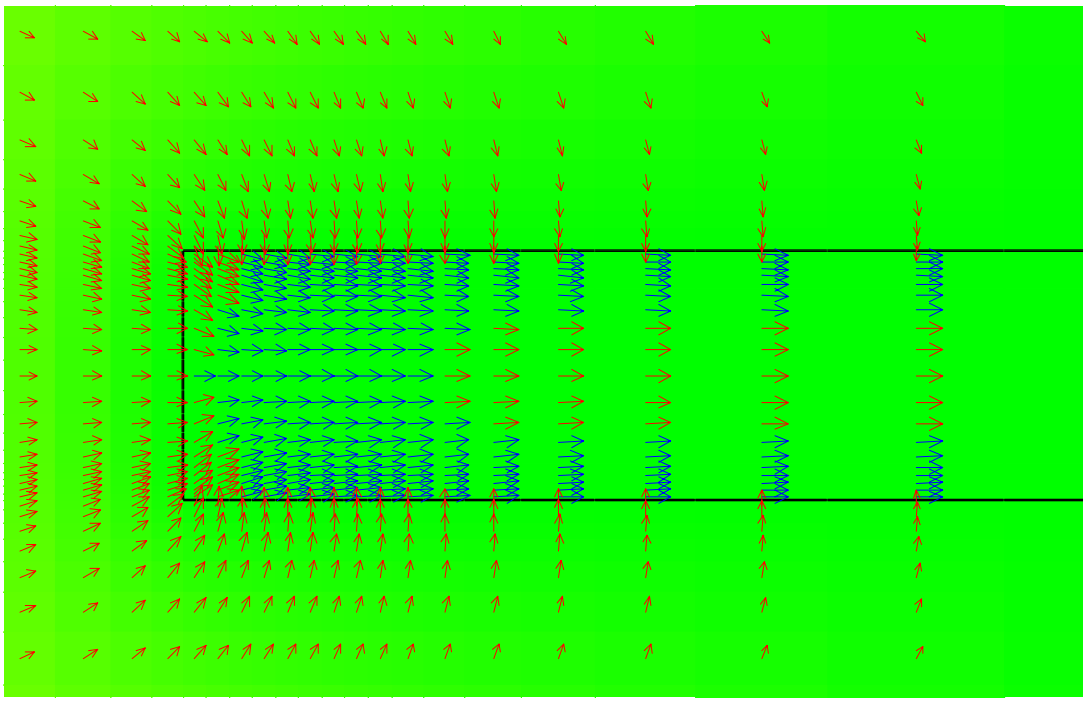

Figure 2.9: Velocity field about a third of the way up the backfill

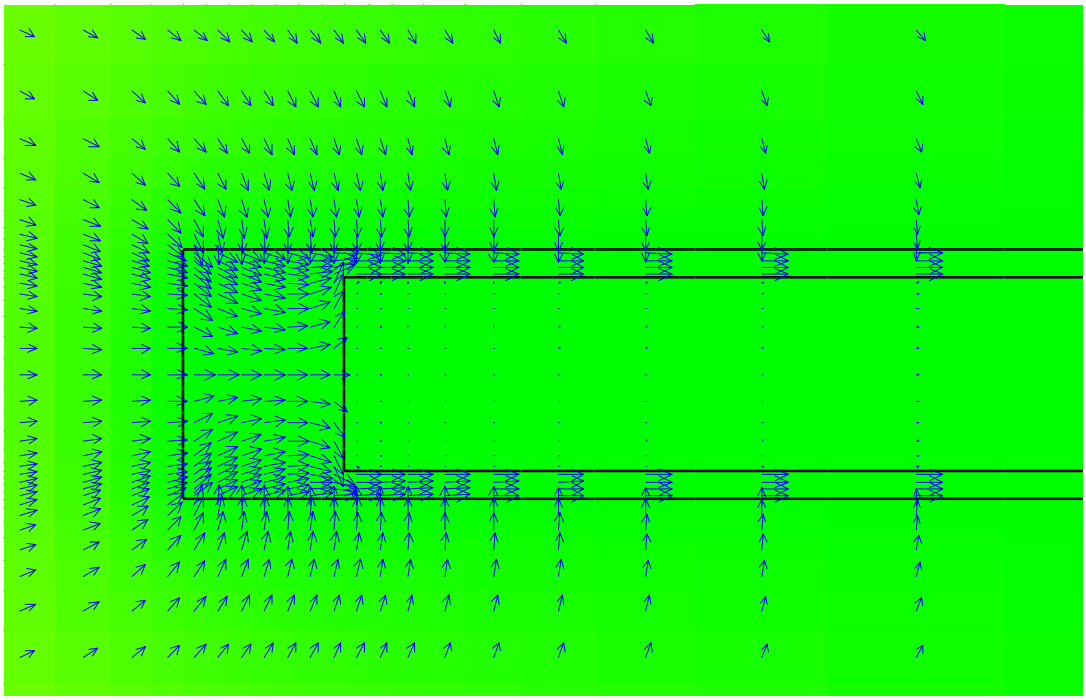

Figure 2.10: Velocity field about half way up the waste

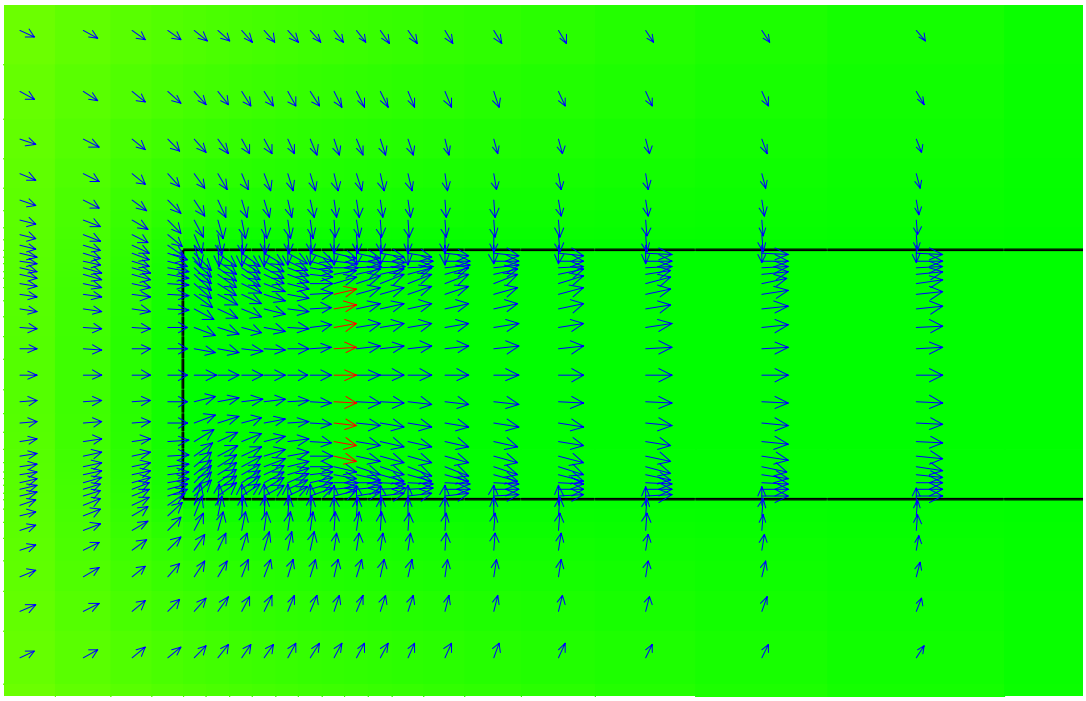

Figure 2.11: Velocity field in the backfill below the waste

The figures show the velocity field on horizontal slices through the model. Flow is focussed into the region of backfill immediately upstream of the waste and then flows up and over the waste. Typical Darcy velocities in the model are summarised in the following table.

Location	**Darcy velocity (m/s)**
Undisturbed background flow	1×10^{-10}
Backfill upstream/downstream of waste	1×10^{-9}
Backfill above waste	6×10^{-9}
Backfill either side of waste	6×10^{-9}
Backfill below waste	7×10^{-9}
Encapsulated waste	7×10^{-13}

3D Model 2: Flow across vault; no transmissive feature

(In the electronic document, downwards flows are in blue and upwards flows are in red.)

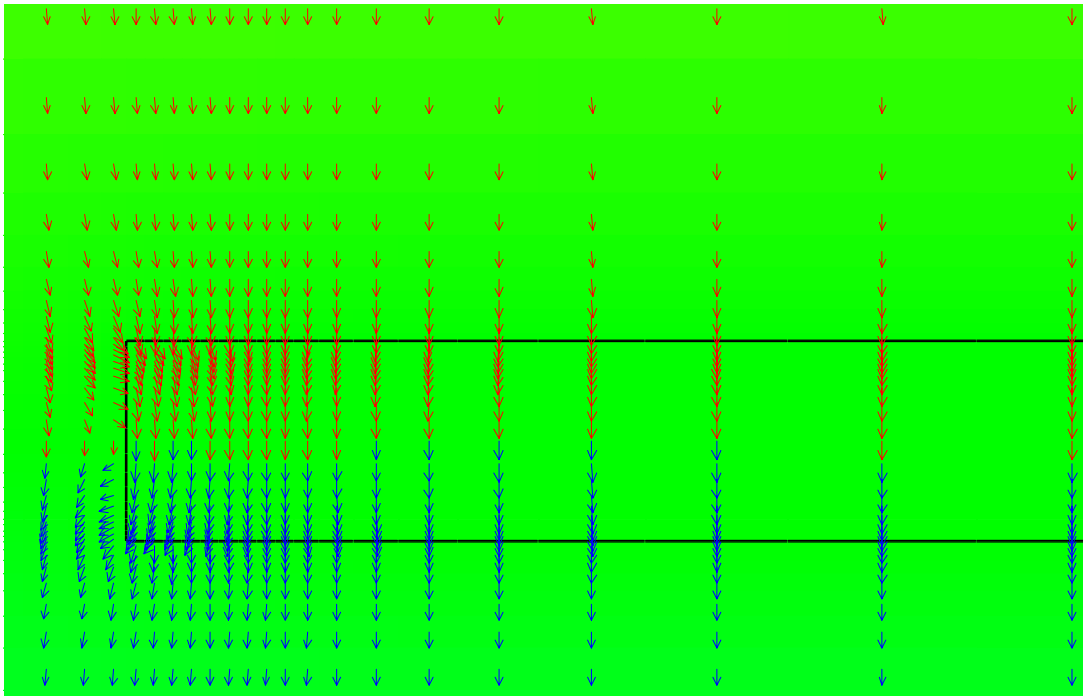

Figure 2.12: Velocity field close to the top of the backfill

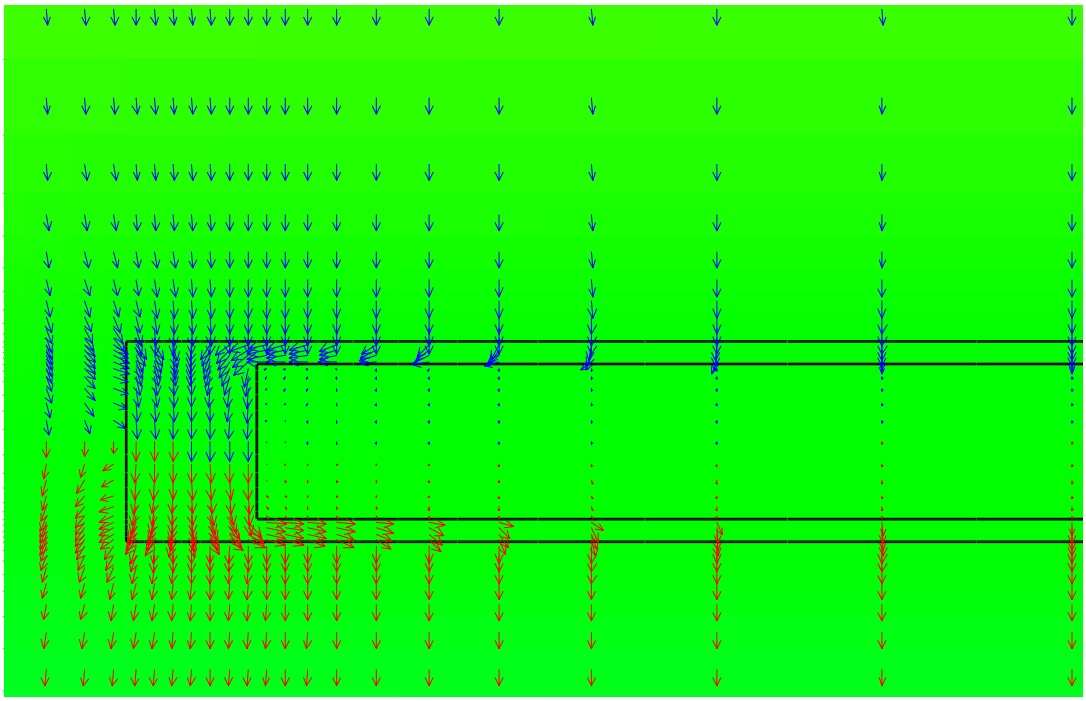

Figure 2.13: Velocity field about half way up the waste

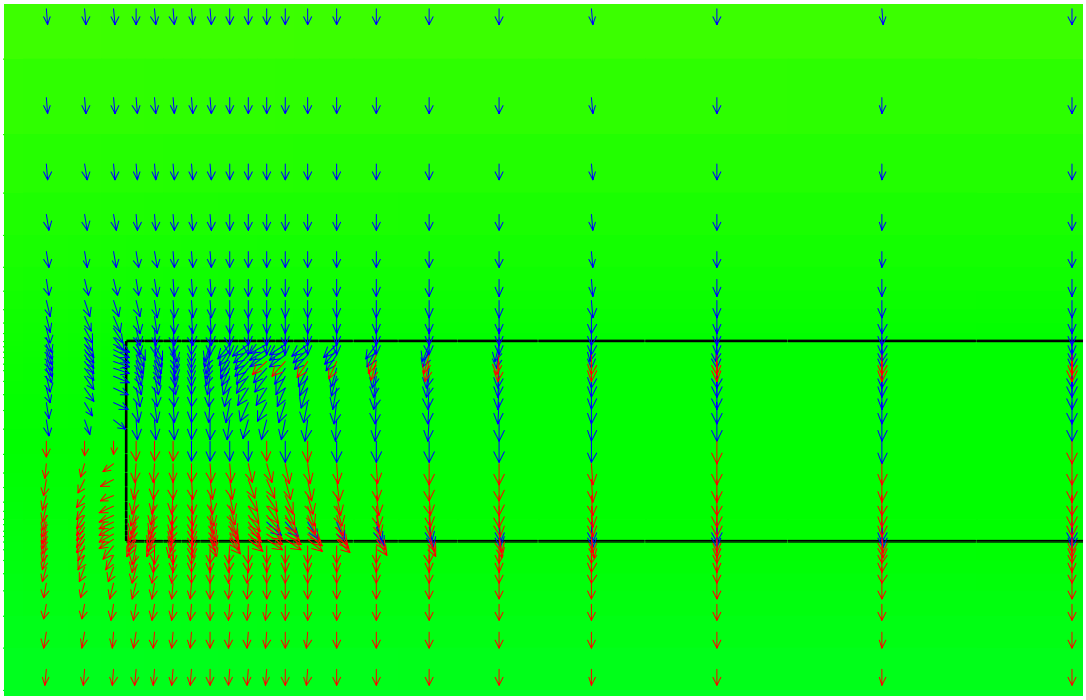

Figure 2.14: Velocity field in the backfill below the waste

The figures show the velocity field on horizontal slices through the model. Flow is concentrated through the backfill at either end of and above the waste. Typical Darcy velocities in the model are summarised in the following table.

Location	**Darcy velocity (m/s)**
Undisturbed background flow	1×10^{-10}
Backfill upstream/downstream of waste	4×10^{-10}
Backfill above waste	4×10^{-10}
Backfill either side of waste	2×10^{-10}
Backfill below waste	1.5×10^{-9}
Encapsulated waste	1.5×10^{-13}

3D Model 3: Flow at 45° to vault; no transmissive feature

(In the electronic document, downwards flows are in blue and upwards flows are in red.)

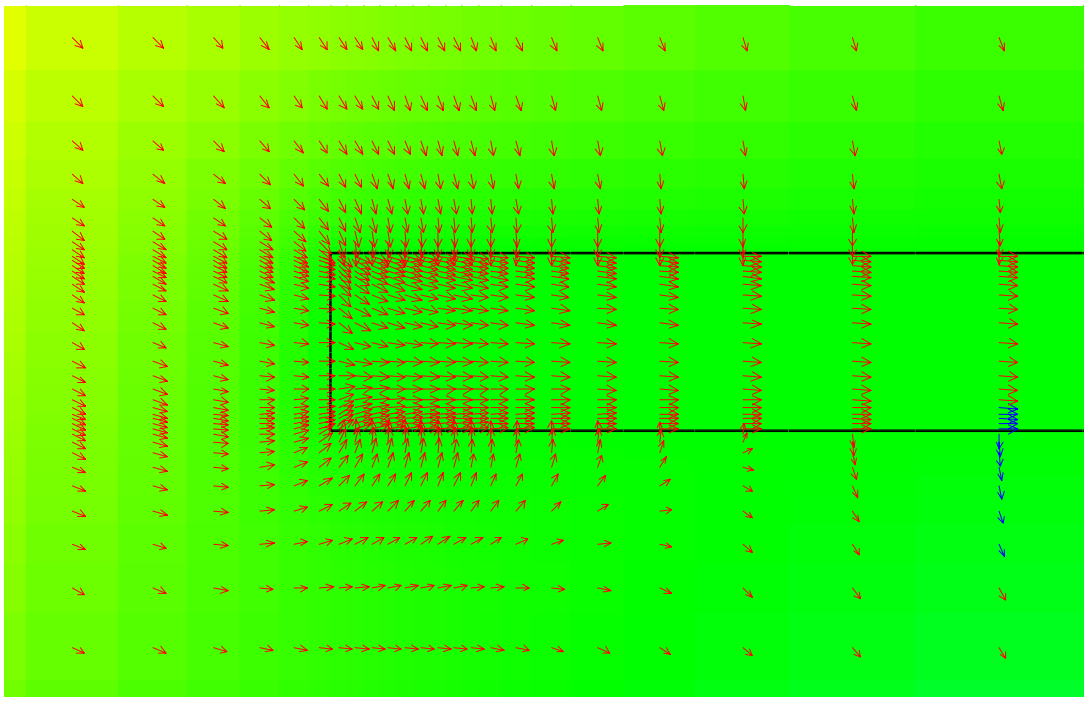

Figure 2.15: Velocity field close to the top of the backfill

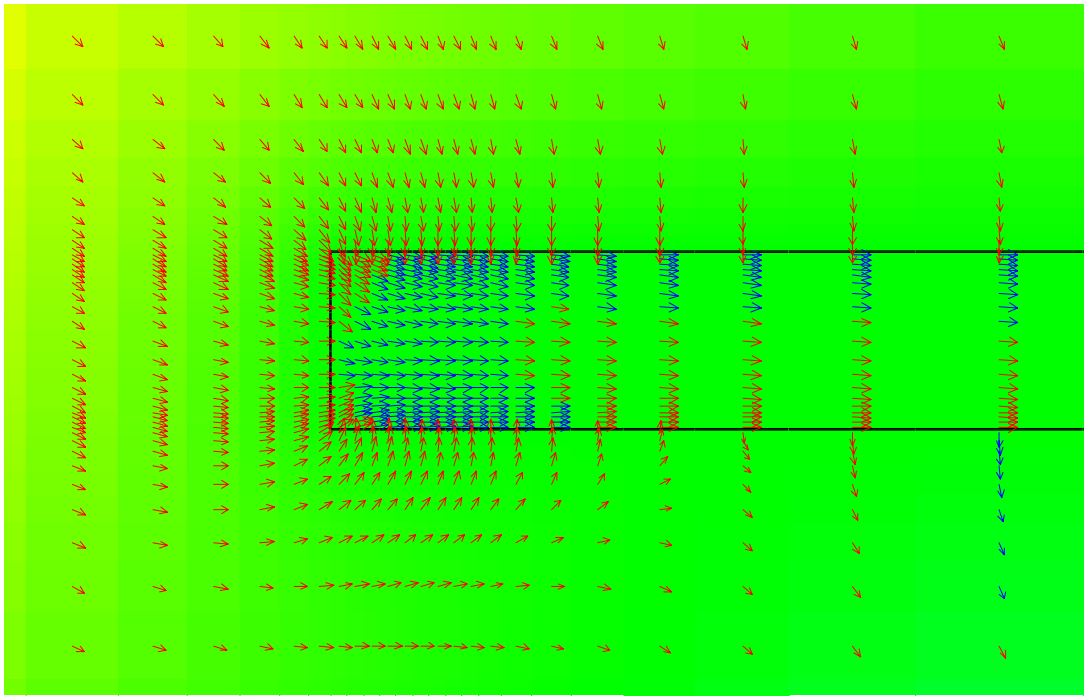

Figure 2.16: Velocity field about a third of the way up the backfill

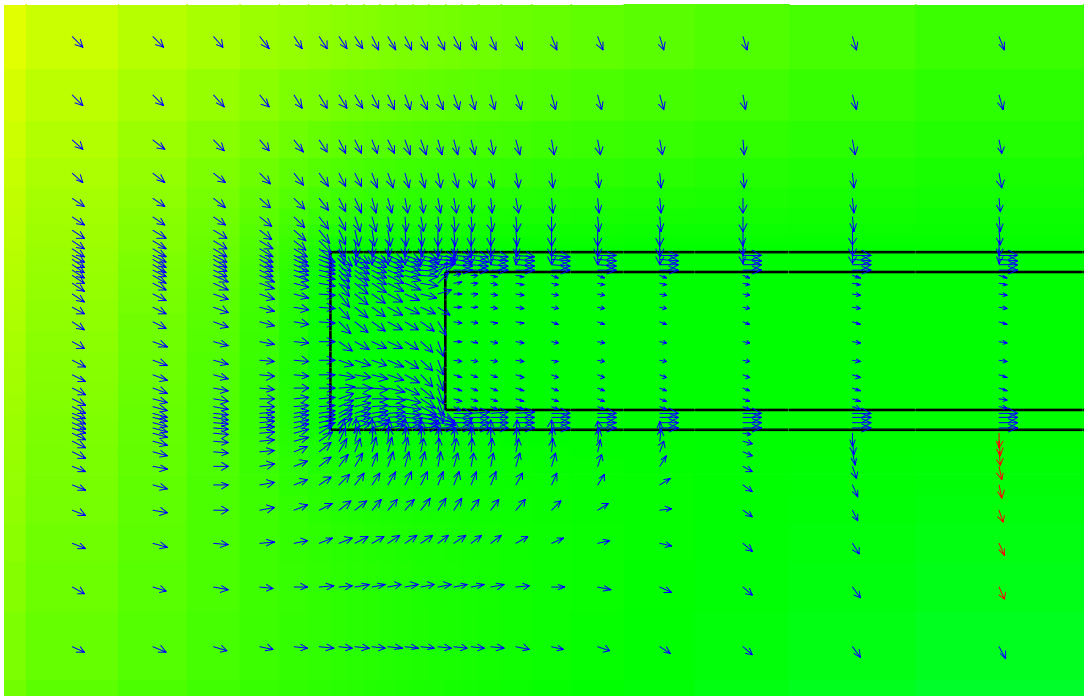

Figure 2.17: Velocity field about half way up the waste

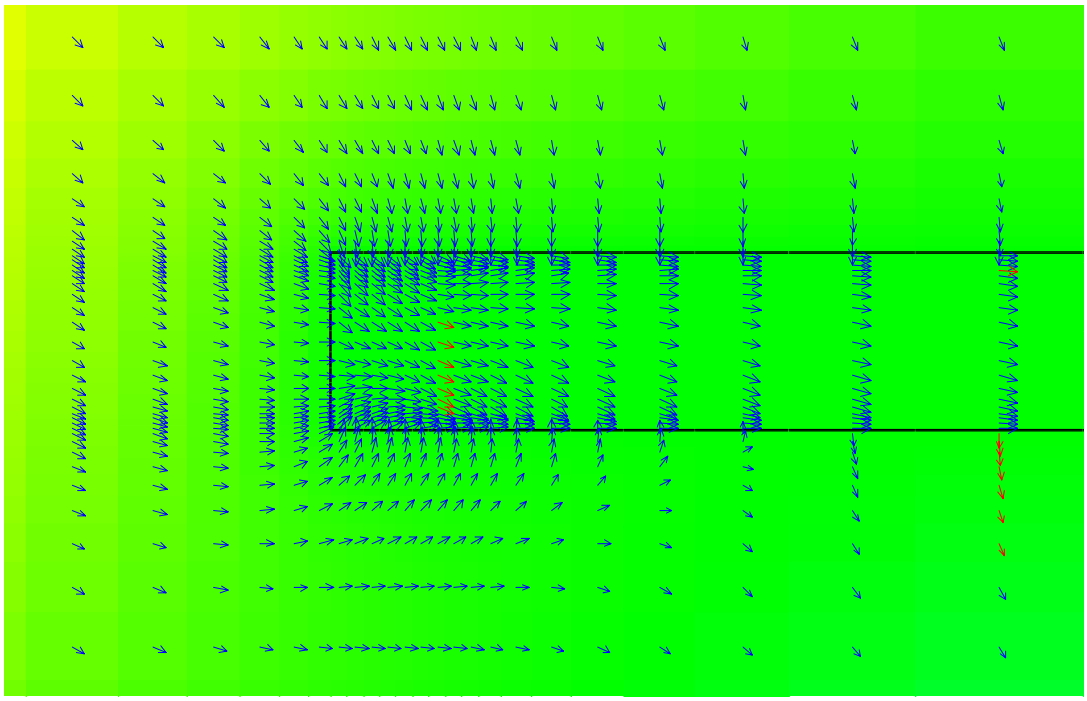

Figure 2.18: Velocity field in the backfill below the waste

The figures show the velocity field on horizontal slices through the model. Flow is focussed into the region of backfill immediately upstream of the waste and then flows up and over the waste. Typical Darcy velocities in the model are summarised in the following table.

Location	**Darcy velocity (m/s)**
Undisturbed background flow	1×10^{-10}
Backfill upstream/downstream of waste	1×10^{-9}
Backfill above waste	5×10^{-9}
Backfill either side of waste	5×10^{-9}
Backfill below waste	5×10^{-9}
Encapsulated waste	5×10^{-13}

3D Model 5: Flow along vault; transmissive feature

(In the electronic document, downwards flows are in blue and upwards flows are in red.)

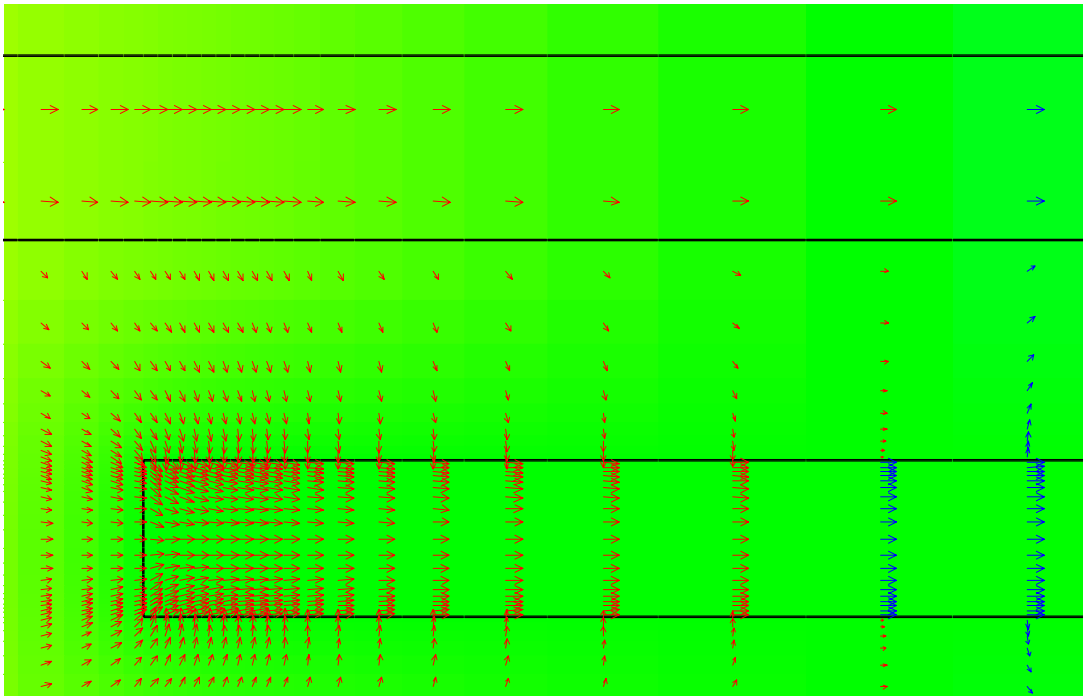

Figure 2.19: Velocity field close to the top of the backfill

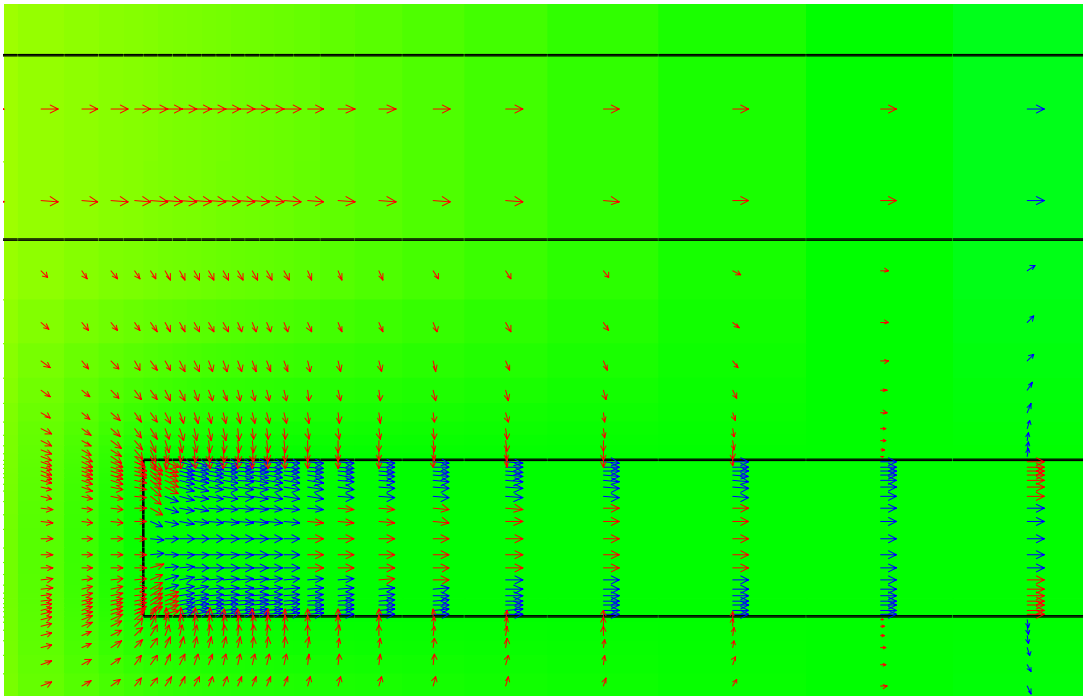

Figure 2.20: Velocity field about a third of the way up the backfill

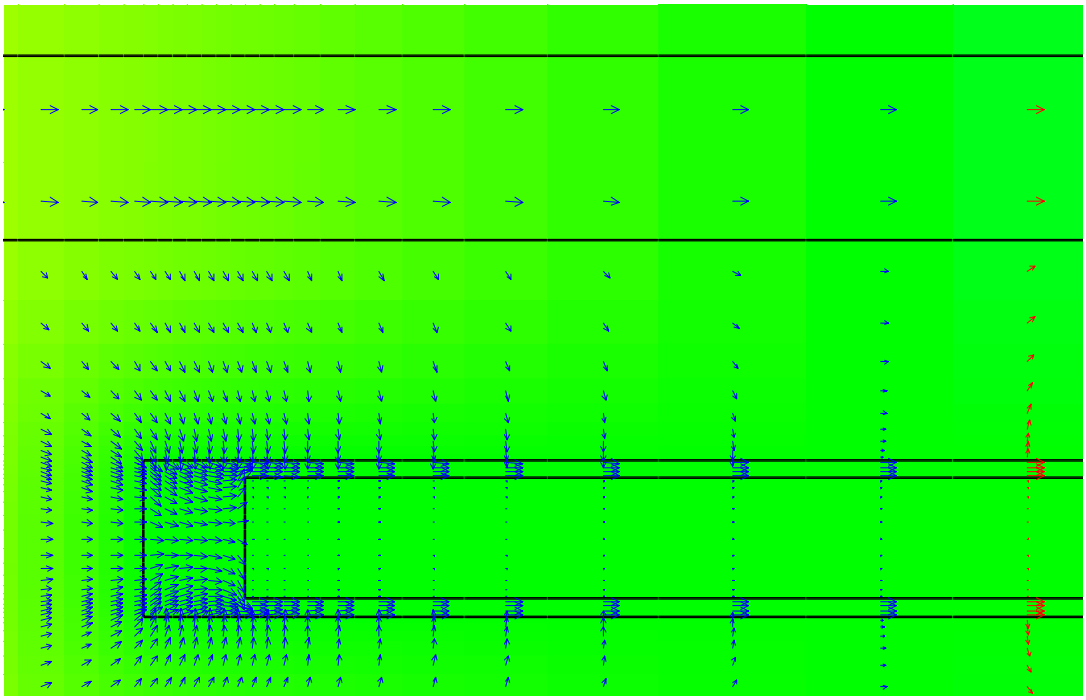

Figure 2.21: Velocity field about half way up the waste

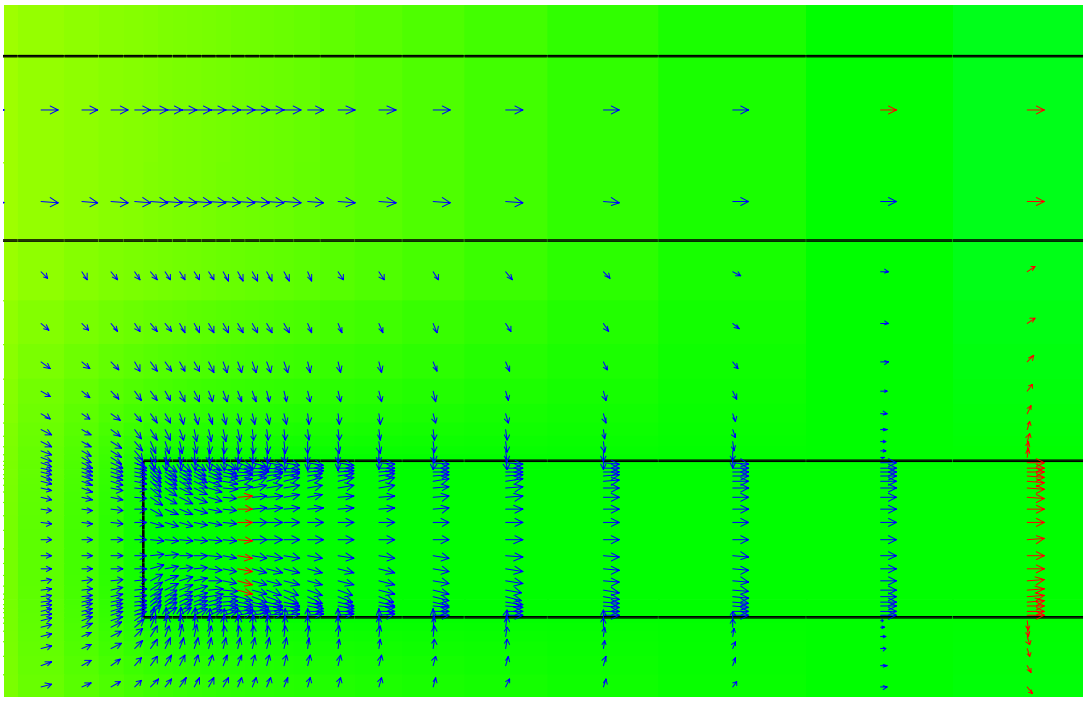

Figure 2.22: Velocity field in the backfill below the waste

The figures show the velocity field on horizontal slices through the model. Flow is focussed into the region of backfill immediately upstream of the waste and then flows up and over the waste. Comparison with the case in which no transmissive feature present shows that the presence of the transmissive feature has only a very small influence on the pattern of flow within the backfill and waste. The influence of the

transmissive feature is smaller than in the two-dimensional version of this case. Typical Darcy velocities in the model are summarised in the following table.

Location	**Darcy velocity (m/s)**
Undisturbed background flow	3×10^{-11}
Flow in transmissive feature	3×10^{-9}
Backfill upstream/downstream of waste	4×10^{-10}
Backfill above waste	2.5×10^{-9}
Backfill either side of waste	2.5×10^{-9}
Backfill below waste	2.5×10^{-9}
Encapsulated waste	2.5×10^{-13}

3D Model 6: Flow across vault; transmissive feature

(In the electronic document, downwards flows are in blue and upwards flows are in red.)

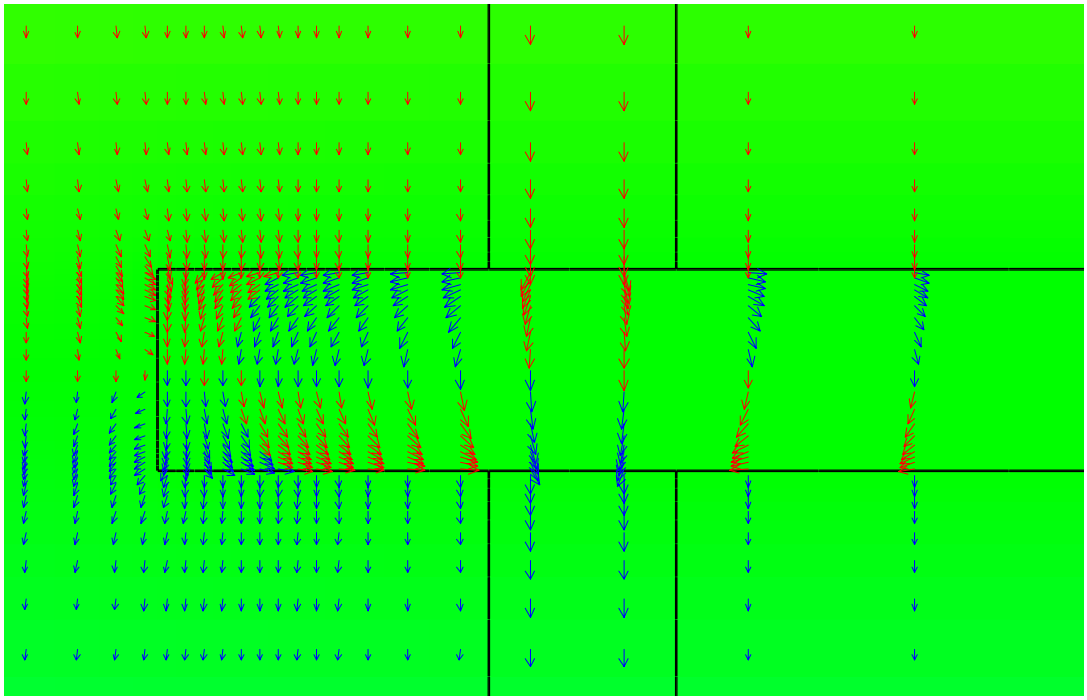

Figure 2.23: Velocity field close to the top of the backfill

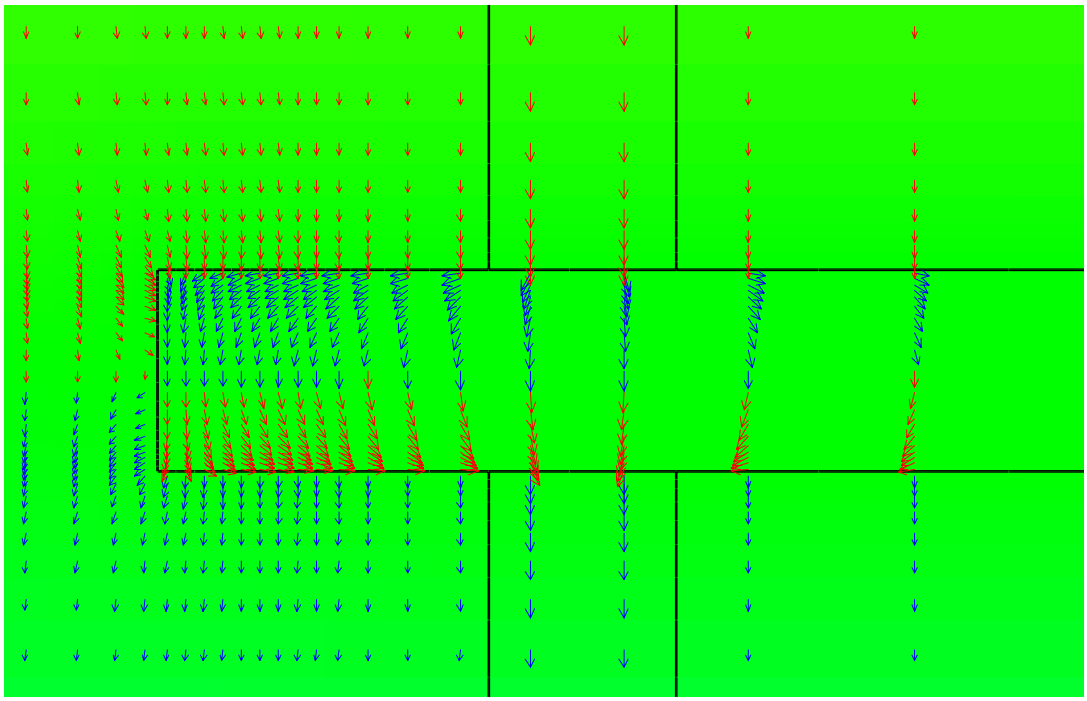

Figure 2.24: Velocity field about a third of the way up the backfill

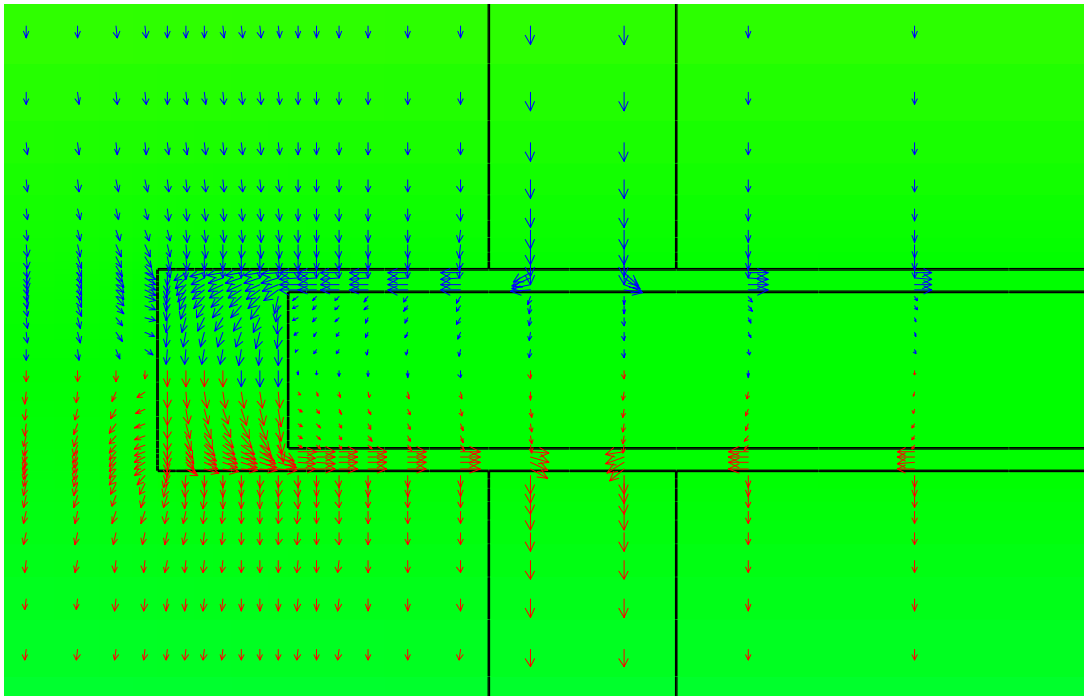

Figure 2.25: Velocity field about half way up the waste

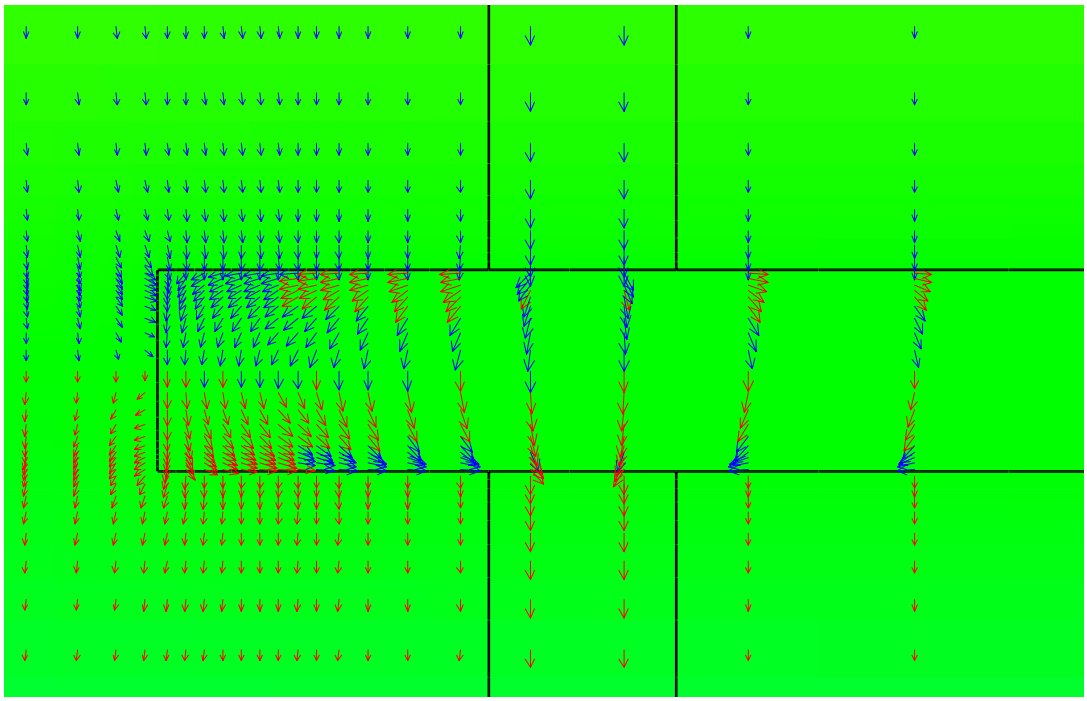

Figure 2.26: Velocity field in the backfill below the waste

The figures show the velocity field on horizontal slices through the model. The transmissive feature has a significant influence on the flow patterns within the backfill and on flow rates within the waste. Typical Darcy velocities in the model are summarised in the following table.

Location	**Darcy velocity (m/s)**
Undisturbed background flow	3×10^{-11}
Flow in transmissive feature	3×10^{-9}
Backfill upstream/downstream of waste	$1 - 5\times10^{-10}$
Backfill above waste	1×10^{-10} / 7×10^{-9}
Backfill either side of waste	4×10^{-9} / 3×10^{-10}
Backfill below waste	1.5×10^{-9} / 2×10^{-8}
Encapsulated waste	1×10^{-13} / 2×10^{-12}

3D Model 7: Flow at 45° to vault; transmissive feature

(In the electronic document, downwards flows are in blue and upwards flows are in red.)

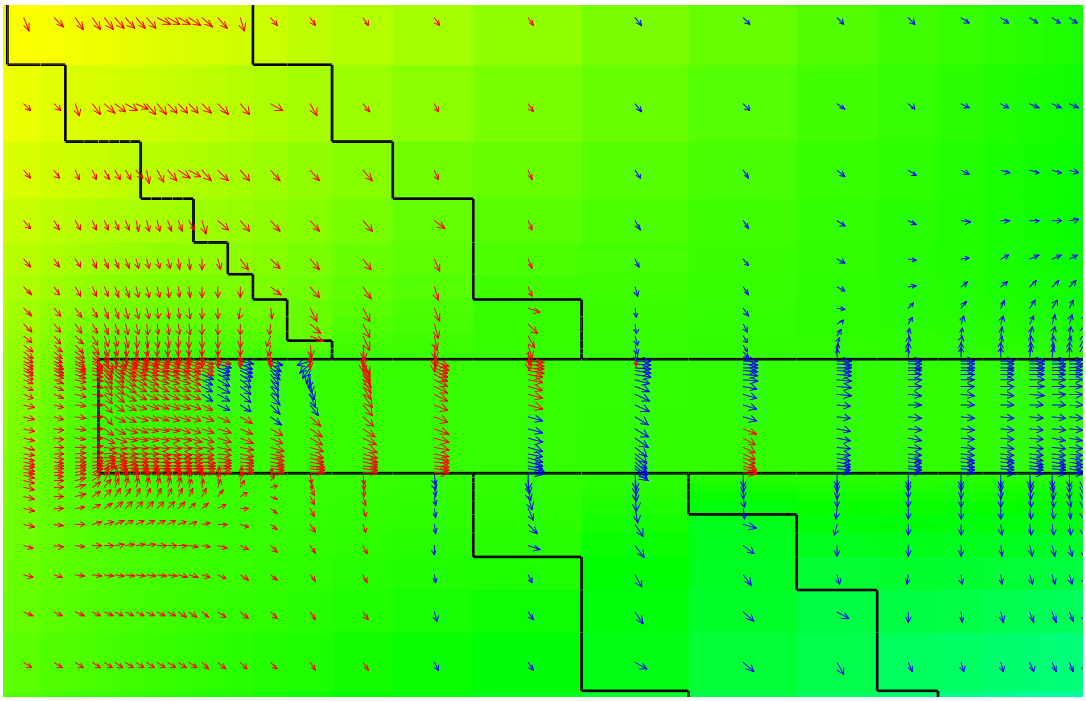

Figure 2.27: Velocity field close to the top of the backfill

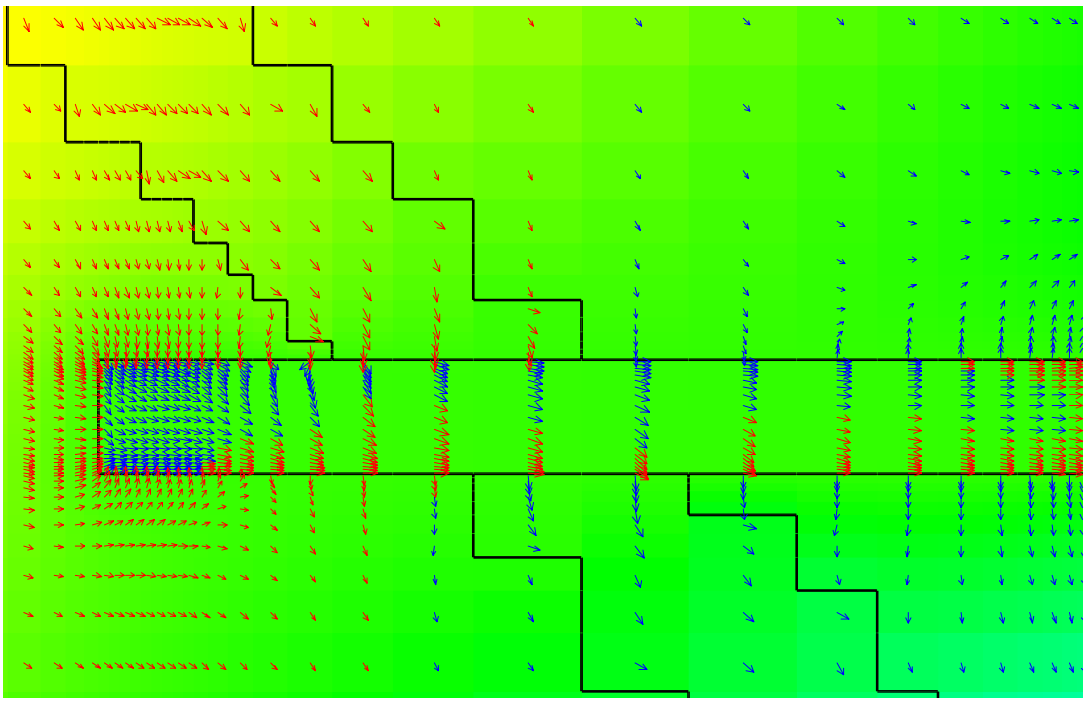

Figure 2.28: Velocity field about a third of the way up the backfill

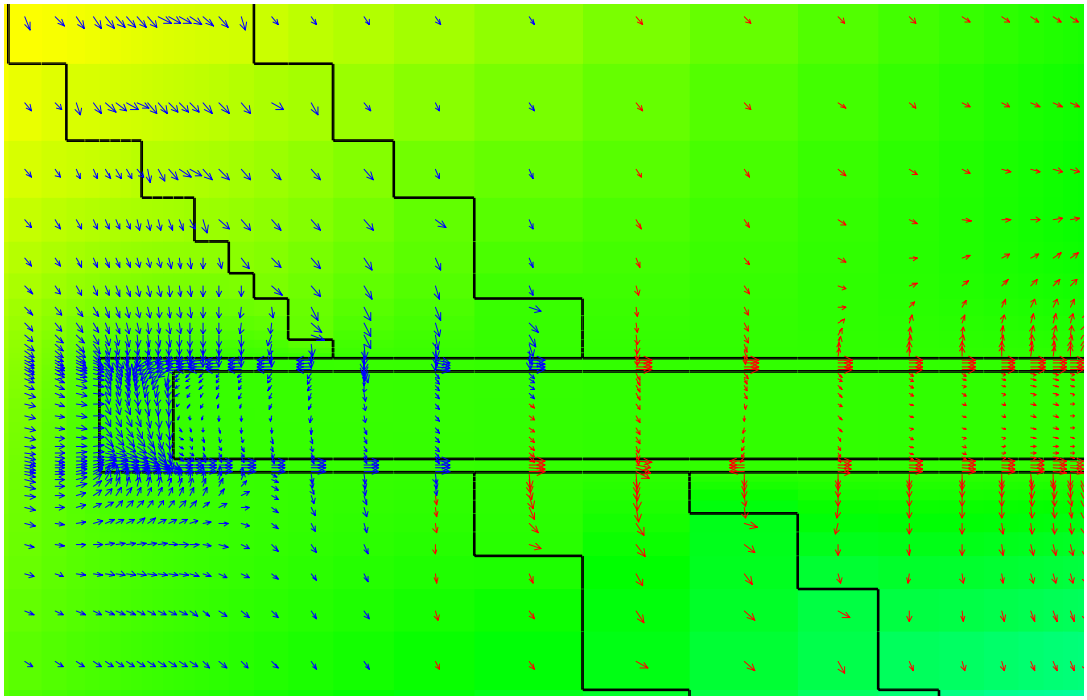

Figure 2.29: Velocity field about half way up the waste

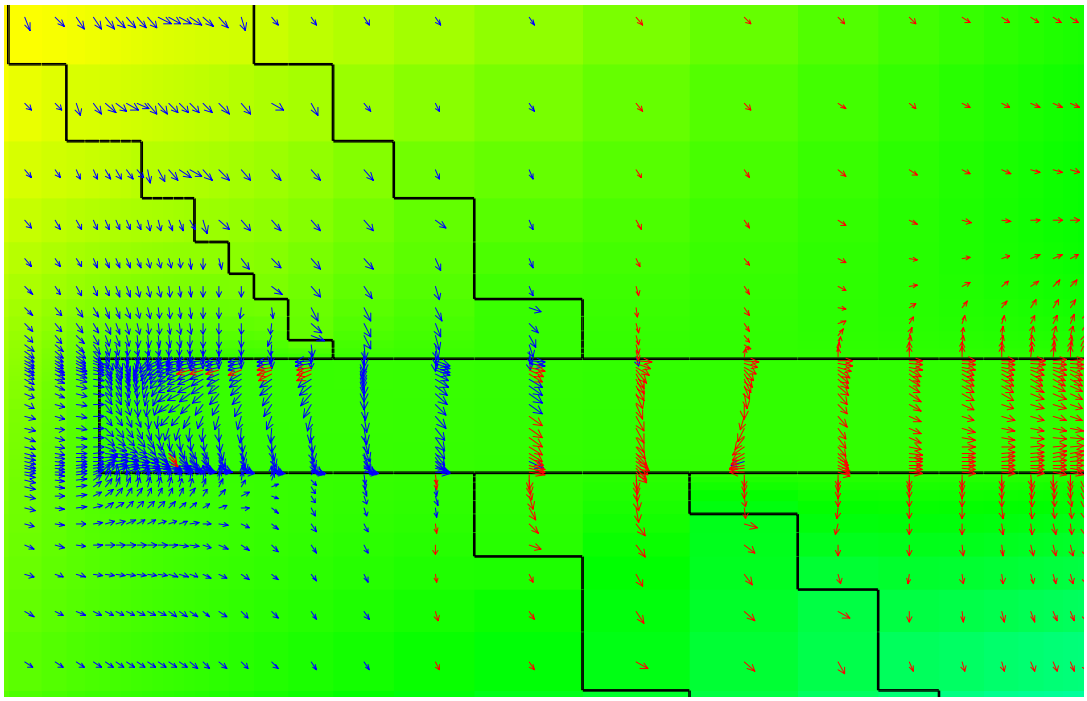

Figure 2.30: Velocity field in the backfill below the waste

The figures show the velocity field on horizontal slices through the model. The transmissive feature has a significant influence on the flow patterns within the backfill and on flow rates within the waste. Typical Darcy velocities in the model are summarised in the following table.

Location	**Darcy velocity (m/s)**
Undisturbed background flow	3×10^{-11}
Flow in transmissive feature	3×10^{-9}
Backfill upstream/downstream of waste	3×10^{-10}
Backfill above waste	1×10^{-9} / 1×10^{-8}
Backfill either side of waste	1×10^{-8} / 1×10^{-9}
Backfill below waste	1×10^{-9} / 3×10^{-8}
Encapsulated waste	1×10^{-13} / 2×10^{-12}

3 Geochemical modelling

3.1 Introduction and scope

Benbow et al. (2002) considered potential pH-buffering reactions in a gravel backfill at the particle scale. Here, attention is paid to modelling the effectiveness of pH-buffering reactions at the engineered barrier scale, incorporating realistic barrier geometry and realistic potential groundwater flow conditions at a deep repository site in Sweden. The potential flow conditions modelled using MODFLOW presented above, together with chemical data for the reaction of quartz with cement pore fluids have been incorporated into the reaction-transport computer code *Raiden2* to carry out a variety of simulations to investigate the potential for migration of hyperalkaline pore fluids beyond the confines of the barrier design for SFL 3-5.

In the simulations, the cement vault is assumed to act as an internal fixed source of high pH porewater. Unless otherwise specified, simulations were run to 10^4 years, after which time the assumption that the cement would act as a fixed source of porewater becomes questionable, due to time-dependent evolution of the cement pore water composition. Previous studies for SKI (Savage et al., 2000; Savage and Stenhouse, 2003) have shown that over this timescale concrete will be depleted of portlandite [$Ca(OH)_2$], accompanied by significant physical changes such as increased porosity and permeability.

3.2 The Raiden2 geochemical model

Both the particle-scale and repository-scale pH buffering issues have been investigated using *Raiden2*, which is a software tool for solving fully coupled geochemical transport problems in two spatial dimensions. This section describes the fundamental equations governing the geochemical evolution that are solved by *Raiden2*.

The user sets up a *Raiden2* problem by defining the initial (possibly heterogeneous) mineralogical and pore water chemical conditions in the system and some pore water boundary conditions on the system. These, together with further parameters that define the host medium (porosity, hydraulic conductivity, storativity, etc.), transport coefficients (diffusion coefficients, dispersion coefficients, etc.), groundwater boundary conditions (groundwater composition and hydraulic head) and reaction equations that are assumed for each mineral species are sufficient to prescribe a set of equations that can be solved for the evolution of the system. *Raiden2* uses a non-uniform, user-defined discretisation of the domain into cells. One or two-dimensional grids are supported in either Cartesian or cylindrical-polar coordinates.

By default, *Raiden2* will solve for coupled flow as the porosity of the system evolves, however in this study this feature of *Raiden2* was not used and instead, flows derived from the results of the flow modelling calculations in Section 2 were imposed.

In the *Raiden2* model, chemical species in the system are characterised as either

- mineral species,
- aqueous complex species, or
- basis species.

Mineral species are assumed to be stationary, and hence not susceptible to transport through the pore space, aqueous complex species are those aqueous species that are composed of a combination of the basis species, which are the fundamental building blocks of the chemical system. All of the mineral and aqueous complex species must be expressible as a combination of the basis species. The medium itself is assumed to be composed of the mineral species, with all other solid in the medium being composed of an inert solid that is not involved in any geochemical reactions.

The i^{th} mineral species is denoted by m_i (mol/m^3), i^{th} aqueous complex species is denoted by c_i (mol/l) and the i^{th} basis species is denoted by b_i (mol/l). Then, the total aqueous concentration of basis species i, b_i^{aq} (mol/l), and the total concentration per unit volume of basis species i, b_i^{tot} (mol/m^3) are given by:

$$b_i^{aq} = b_i + \sum_{j=1}^{N_c} \nu_{ij} c_j$$

$$b_i^{tot} = S\phi b_i^{aq} + \sum_{j=1}^{N_M} \gamma_{ij} m_j$$

where N_C is the number of aqueous complex species, N_M is the number of mineral species, ν_{ij} is the stoichiometry of basis i in aqueous complex j, γ_{ij} is the stoichiometry of basis i in mineral j, ϕ is the porosity and S is a volumetric scale factor. The number of basis species is denoted N_B.

The transport equation for the i^{th} basis species is then

$$\frac{\partial}{\partial t}\left[S\phi b_i^{aq} + \sum_{j=1}^{N_M} \gamma_{ij} m_j \right] = S\left\{ \nabla \cdot \left[\phi D_{B_i} \nabla b_i + \sum_{j=1}^{N_c} \phi D_{C_j} \nabla c_j \right] - \nabla \cdot \left[q b_i^{aq} \right] \right\}$$

Here, D_{Z_i} is the total dispersion coefficient of the i^{th} (either basis or aqueous complex) species,

$$\phi D_{Z_i} = \alpha_{Z_i} q + \phi D_{Z_i}^{mol}$$

where α_{Z_i} is the longitudinal dispersion coefficient (m) for the i^{th} (either basis or aqueous complex) species, q is the Darcy velocity (m/s) and $D_{Z_i}^{mol}$ is the molecular diffusion coefficient for the i^{th} (either basis or aqueous complex) species.

The rate of dissolution/precipitation of the i^{th} mineral species can be set either as an explicit kinetic rate equation, or as an implicit rate equation where instantaneous dissolution/precipitation of the mineral is assumed in order for the mineral to be instantaneously in equilibrium with the pore water. For kinetic dissolution and precipitation reactions, the user must choose a representative kinetic reaction for each mineral from *Raiden2*'s (extensible) reaction library, and parameterise it appropriately. The general form of the explicit kinetic equations is:

$$\frac{dm_i}{dt} = F\left(\{b_j : j = 1,\ldots,N_B\}, \{c_j : j = 1,\ldots,N_c\}, \{m_j : j = 1,\ldots,N_M\}, K_{M_i}(T), I, T\right)$$

where K_{M_i} is the temperature dependent equilibrium constant for the i^{th} mineral species, I is the ionic strength of the pore water, T is the temperature and $F(\cdot)$ denotes a function of the parameters, i.e. the kinetic reaction rate can be any function of the pore water chemistry, mineralogy, ionic strength and temperature in each cell in the discretisation. It is unlikely that many mineral reactions will be characterised in terms of concentrations of other minerals or complex species, instead it will usually be the case that mineral reaction rates are a function of their surface area (and hence of their concentration, specific surface area and molar volume), their equilibrium state (and hence of those basis species with non-zero stoichiometry in the mineral), and also of one or two specific basis species, most commonly H^+. However, the ability to characterise reactions in terms of other mineral concentrations and aqueous complex concentrations has been included in *Raiden2* for maximum flexibility, and can be important if considering solid solution reactions. The implicit instantaneous equilibrium equations are set up automatically in *Raiden2* (if the user chooses that this should be done).

The aqueous complex species are assumed to be in instantaneous equilibrium with the pore water at all times, so that

$$Q_{C_i} = K_{C_i}(T)$$

at all times, where K_{C_i} is the temperature dependent equilibrium constant for the i^{th} aqueous complex species, and Q_{C_i} is the equilibrium state of the i^{th} aqueous complex species, i.e.

$$Q_{C_i} = \prod_{j=1}^{N_B} \left[\mu_j(I) b_j\right]^{\nu_{ij}}$$

where μ_j is the activity coefficient of the j^{th} basis species.

Porosity change in the medium is given by:

$$\frac{d\phi}{dt} = -\sum_{i=1}^{N_M} V_i^{mol} \frac{dm_i}{dt}$$

where V_i^{mol} is the molar volume of the i^{th} mineral.

Flow in the region is fully coupled with porosity change and varies according to

$$S_s \frac{\partial h(x)}{\partial t} = \nabla \cdot \left[K(x) \nabla h\right] - \frac{\partial \phi}{\partial t} + Q$$

Here Q is the volume flow rate of pore water per unit volume (s^{-1}) and S_s is the storativity coefficient (m^{-1}), which is given by:

$$S_s = \rho_{aq} g \left[\zeta_{aq} \phi + \sum_{i=1}^{N_M} \zeta_{M_i} V_i m_i + \zeta_I (1 - \phi_I) \right],$$

where ρ_{aq} is the fluid density, g is gravitational acceleration, ζ_I is the compressibility of any inert components of the medium, ζ_{aq} is the compressibility of the fluid, ζ_{M_i} is the compressibility of the i^{th} mineral species and ϕ_I is the portion of the volume (of everything) that is filled with inert materials.

Raiden2 makes use of two databases, the reaction library (which was introduced in the previous section) and also the EQ3/6 database (Wolery, 1992). *Raiden2* uses the EQ3/6 database to determine:

- Relevant basis species for each mineral in the model;
- Relevant basis species for each aqueous complex in the model;
- Stoichiometries of the basis species in each mineral and complex species;
- Temperature-dependent equilibrium constants for each aqueous complex and mineral species;
- Molar volumes and molar weights for each mineral, aqueous complex and basis species.

3.3 Geochemical specification

The backfill for SFL 3-5 is envisaged to consist of crushed granite of size fraction 4 – 32 mm (Karlsson et al., 1999). Granite (*sensu lato*) consists of roughly 30 volume % of quartz with the remainder comprising K-feldspar, plagioclase, muscovite, biotite and Fe-Ti oxides. The total silica content of a granite is usually greater than 60 wt. %. For the modelling described here, the backfill is assumed to consist solely of quartz, so that complications arising from incorporating reaction mechanisms for different mineral types are avoided. This assumption maximises the amount of silica available for reaction with calcium and hydroxyl ions released from the cement for incorporation into reaction products and is thus a non-conservative assumption, but is consistent with the calculations made by Karlsson et al. (1999) for their assessment of pH buffering.

As assumed by Karlsson et al. (1999) the quartz backfill particles are considered to react kinetically. The reaction mechanism and kinetic data for quartz dissolution employed here are those described by Knauss and Wolery (1988) as extrapolated to 25°C. This is the same relationship employed by Karlsson et al. (1999) for their model calculations. The rate equation for quartz dissolution and precipitation is of the form:

$$\frac{dm}{dt} = Ak\left(\mathrm{H}^+\right)^n\left(1-\frac{Q}{K}\right)$$

where m = moles of quartz, A = reactive surface area of quartz, k is a rate constant, n is a coefficient to describe dependence of rate upon H^+, Q is the activity quotient for the reaction and K is the equilibrium constant. The parameter values taken in the modelling were log k = -16.3 mol m^{-2} s^{-1} at 25 °C (Knauss and Wolery, 1988), n = -0.5 (Knauss and Wolery, 1988). The surface areas of 32 mm and 4 mm spherical particles of quartz are 0.071 m^2 kg^{-1} and 0.57 m^2 kg^{-1} respectively. These areas were invariant throughout the modelling, an assumption which has already been identified as being non-conservative (Benbow et al., 2002). Surface areas of quartz are likely to decrease with time due to 'armouring' by secondary solid products, thus decreasing the available capacity to buffer pH.

A range of calcium silicate hydrate (CSH) minerals of different Ca/Si ratio were considered as solid products during the modelling calculations:

- Hillebrandite ($Ca_2SiO_3(OH)_2$:0.17H_2O),
- Afwillite ($Ca_3Si_2O_4(OH)_6$),
- Foshagite ($Ca_4Si_3O_9(OH)_2$:0.5H_2O),
- Xonotlite ($Ca_6Si_6O_{17}(OH)_2$),
- Tobermorite-14A ($Ca_5Si_6H_{21}O_{27.5}$),

- Gyrolite ($Ca_2Si_3O_7(OH)_2$:$1.5H_2O$),
- Okenite ($CaSi_2O_4(OH)_2$:H_2O).

As noted by Benbow et al. (2002), pH buffering by reaction of quartz to form calcium silicate hydrates (of general formula $Ca_xSi_yO_{(x+2y)}.wH_2O$) relies on the following generic reaction:

$$xCa^{2+} + yH_3SiO_4^- + (2x\text{-}y)OH^- = Ca_xSi_yO_{(x+2y)}wH_2O + (x+y\text{-}w)H_2O$$

Whether such reactions neutralise hyperalkaline fluids, i.e. consume OH^- (or generate H^+), depends upon the precise stoichiometry of the CSH solid concerned, and in particular the magnitude of the '$2x$-y' parameter (above). Table 3.1 (taken from Benbow et al., 2002) summarises this information for each of the CSH minerals listed above.

Mineral	**Formula**	**Ca/Si ratio**	**$OH^-/H_3SiO_4^-$**	**'$2x$-y'**
Hillebrandite	Ca_2SiO_4:$1.17H_2O$	2.00	3.00	3
Afwillite	$Ca_3Si_2O_4(OH)_6$	1.50	2.00	4
Foshagite	$Ca_4Si_3O_{10}$:$1.5H_2O$	1.33	1.66	5
Xonotlite	$Ca_6Si_6O_{18}$:H_2O	1.00	1.00	6
Tobermorite	$Ca_5Si_6O_{17}$:$10.5H_2O$	0.83	0.66	4
Gyrolite	$Ca_2Si_3O_8$:$2.5H_2O$	0.67	0.33	1
Okenite	$CaSi_2O_5$:$2H_2O$	0.50	0	0

Table 3.1: Some naturally-occurring calcium silicate hydrate minerals.

Solubility data presented in the thermodynamic database accompanying the Geochemist's Workbench software (Bethke, 1996) for these phases were included in the model calculations. If saturated in the fluid phase, these phases were assumed to precipitate/dissolve at a fast kinetic rate that approximates an instantaneous precipitation/dissolution when compared to the overall simulation time.

Aqueous species considered in the modelling were: Ca^{2+}; $CaOH^+$; H^+; OH^-; $SiO_{2(aq)}$. Again, thermodynamic data for these species were derived from the database supplied with Geochemist's Workbench.

For the input cement fluid, portlandite [$Ca(OH)_2$] was equilibrated with pure water at 25°C using the Geochemists Workbench software. The resultant fluid composition is shown in Table 3.2. It should be noted that a trivial amount of $SiO_{2(aq)}$ was assumed to be present in the cement, the amount assumed was 10^{-20} mol/l. This is a requirement of the *Raiden2* model.

Species	**Concentration (mol/l)**
H^+	4.951×10^{-13}
Ca^{2+}	1.299×10^{-2}
$CaOH^+$	2.613×10^{-3}
OH^-	2.860×10^{-2}

Table 3.2: Composition of the input cement pore fluid as calculated using the Geochemist's Workbench software (mol/l).

The inflowing pore fluid from the host rock boundary and the initial pore fluid present in the backfill was derived from the Äspö saline groundwater present in Karlsson et al. (1999). The fluid composition is shown in Table 3.3.

Species	**Concentration (mol/l)**
H^+	2.467×10^{-8}
$SiO_{2(aq)}$	1.002×10^{-4}
Ca^{2+}	4.494×10^{-2}
$CaOH^+$	1.577×10^{-7}
OH^-	6.690×10^{-7}

Table 3.3: Composition of the Äspö saline groundwater used as the initial backfill pore fluid composition and inflowing pore fluid from the host rock boundary.

3.4 Physical specification

The physical extent of the geochemical modelling has been taken to be volume occupied by the backfill and vault (see Figure 3.1). The geochemical modelling domains are 2D slices through the 3D backfill and vault. The 2D slices must pass through the vault in order to contain a source of cementitious fluid for the modelling. The positions of the 2D slices have been chosen based upon the 3D flow modelling results in section 2. Flow models that could potentially give rise to "interesting" pH plume evolutions have been chosen as a basis for the geochemical calculations. More details on the flow fields that have been chosen as a basis for the geochemical modelling is given in Section 3.5.

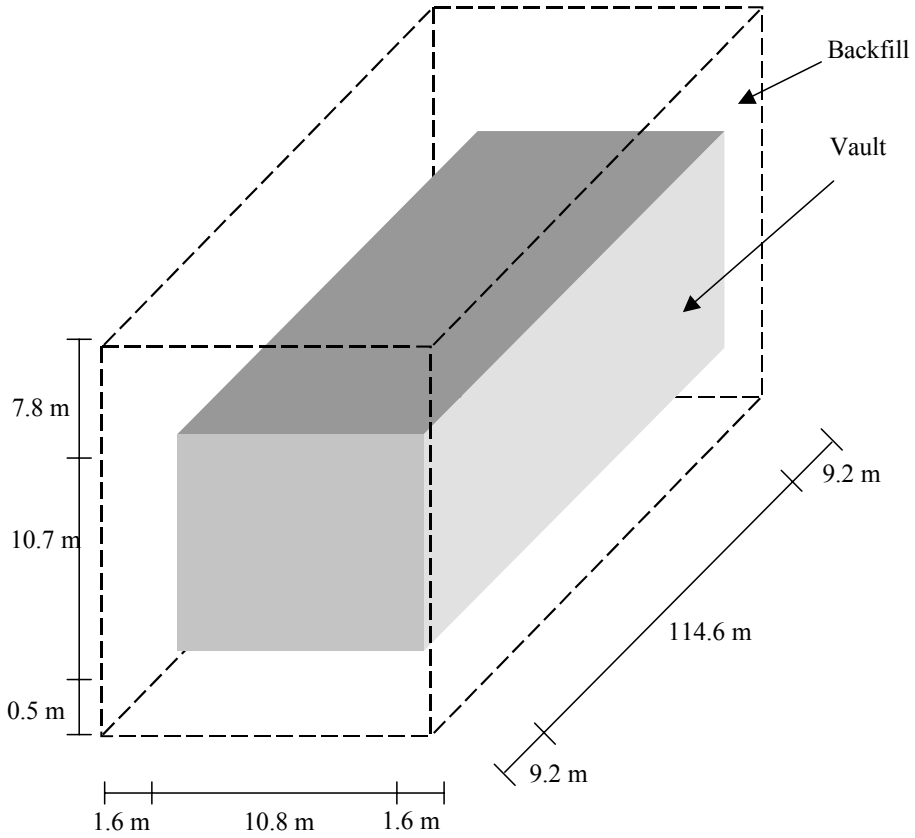

Figure 3.1: Vault and backfill geometry assumed in the geochemical modelling. The geochemical models are based on 2D slices through the backfill and vault.

The *Raiden2* flow fields have been developed by first extracting the entire flow field on the relevant slice through the entire MODFLOW grid (vault, backfill and host rock) and then interpolating that flow field onto the smaller *Raiden2* grid containing only the backfill and vault. The spatial resolution used in the *Raiden2* grid is exactly the same as that used in the MODFLOW modelling for the backfill and vault so that the

interpolation is exact. The actual *Raiden2* flow fields are shown in the results section (Section 3.6) for each 2D slice.

For each 2D cell in the *Raiden2* grid, the MODFLOW flow field provides a 3D flow vector; hence there is the potential for some flow out of the plane of the geochemical model. This flow has not been accounted for in the geochemical modelling, but the flow fields that have been chosen generally have small perpendicular flows so that this is not expected to affect the results to a great extent. Not accounting for the orthogonal flows out of the 2D grid has the effect of introducing a local symmetry assumption in the solution, i.e. parallel 2D layers are assumed to have similar chemistry. Since all of the 2D slices taken in the geochemical modelling are slices through the vault that are not close to the edges of the vault, this is considered to be a fair assumption.

The flow on the boundary of each *Raiden2* grid determines the nature of the boundary conditions that are applied in the geochemical modelling. For portions of the boundary where the flow is into the backfill (from the host rock), a fixed pore fluid chemistry boundary condition is applied using the Äspö saline groundwater composition (Section 3.3). For out-flowing portions of the boundary (flow into the host rock), it does not make sense to impose the Äspö saline groundwater composition, and so a Neumann (zero gradient) boundary condition has been imposed, which allows advective transport out of the system.

For the purposes of the geochemical modelling, the vault has been taken to be a fixed source of cementitious water, and so acts like an internal boundary condition to the model. Hence geochemical conditions only evolve in the backfill portions of the modelled domains. The simulation times have been taken to be 10^4 years (unless otherwise stated). After this time, the assumption that the vault acts as a fixed source of cementitious water may become questionable.

The backfill is assumed to have an initial porosity of 0.3 (Skagius et al., 1999). Diffusion coefficients in the backfill and vault have been taken to be equal for all porewater species and are given in Table 3.4. The values were also taken from Skagius et al., 1999; with the diffusivity in the vault being taken to be that of structural concrete.

Region	**Effective Diffusion Coefficient**
Backfill	6×10^{-10} m^2/s
Vault	1×10^{-11} m^2/s

Table 3.4: Diffusion coefficients (for all species) in the vault and backfill.

3.5 Model specifications

The 3D flow modelling in Section 2 gives rise to many potential 2D flow field slices that could be used as a basis for the geochemical modelling. It is impractical to model all possible 2D slices, so it is necessary to identify flow fields that appear to have the potential to lead to geochemical evolutions with the possibility of a migrating pH plume. The geochemical modelling has focussed in the 3D flow models that contain a transmissive feature (3D flow models 5, 6 and 7) since these lead to the greatest flows in the backfill.

Those cases that have been identified for detailed geochemical investigation are as follows.

1. 3D Flow Model 5: Horizontal slice through the middle of the vault.
2. 3D Flow Model 5: Vertical slice along the vault length.
3. 3D Flow Model 6: Vertical slice across the vault width in the plane of the intersecting transmissive feature.
4. 3D Flow Model 7: Horizontal slice through the middle of the vault.

The 2D modelled regions are shown schematically in Figure 3.2 to Figure 3.5.

In addition to these cases, one further variant case has been considered where the backfill is modelled as an inert material. The geometry and flow field that is assumed is the same as for the Model 7 case above. In this case, the only source of silica for precipitation of CSH minerals is in the initial backfill groundwater and incoming host rock groundwater. The variant case therefore provides a scenario that can highlight the role played by the quartz as a source of silica in the buffering reactions.

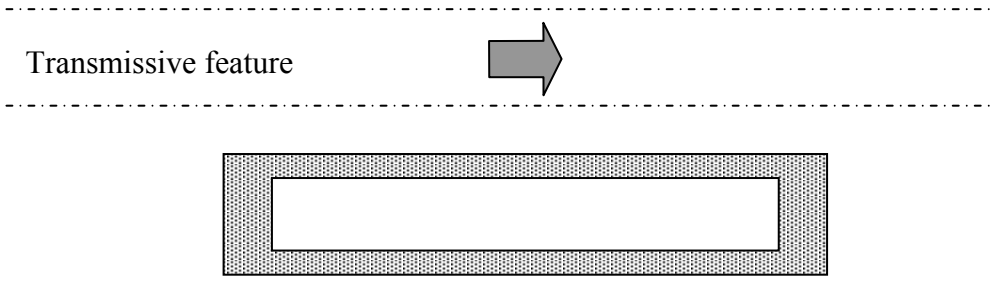

Figure 3.2: 3D Flow Model 5(plan view), 2D Horizontal slice through the middle of the vault shown as shaded region. Dominant flow direction shown by the arrow.

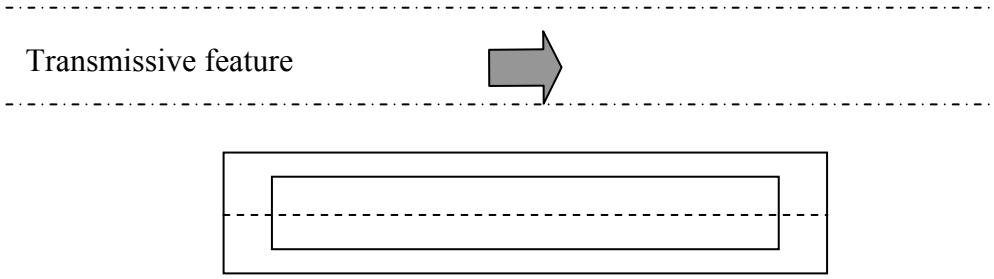

Figure 3.3: 3D Flow Model 5 (plan view), 2D Vertical slice along the vault length shown as dashed line. Dominant flow direction shown by the arrow.

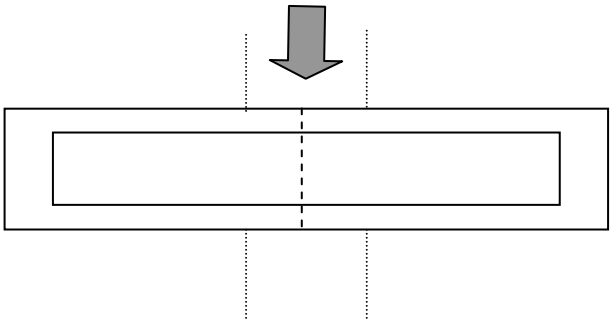

Figure 3.4: 3D Flow Model 6(plan view), 2D Vertical slice across the vault width in the plane of the intersecting transmissive feature shown as dashed line. Dominant flow direction shown by the arrow.

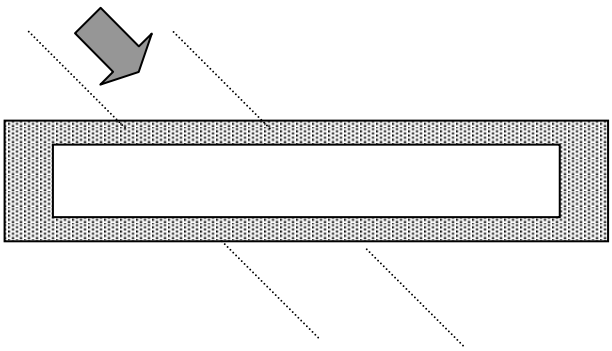

Figure 3.5: 3D Flow Model 7(plan view), 2D Horizontal slice through the middle of the vault shown as shaded region. Dominant flow direction shown by the arrow.

3.6 Results

The results for the four modelling cases and the variant case that were described in the previous subsection are presented here. Backfills composed of 4 mm and 32 mm particles were simulated for each of the four main cases, resulting in a total of nine modelled scenarios.

In all the scenarios, the only CSH minerals that are observed to precipitate are tobermorite and gyrolite. In some cases, both of these CSH minerals are observed, whilst in other cases only one or the other is observed. It is difficult to predict *a-priori*, which of the CSH minerals will precipitate, since the onset and progress of precipitation is sensitive to the porewater chemistry at the point, which in turn is dependent on the balance of chemical gradients and flow rates across the backfill.

3.6.1 Model 5: horizontal slice

This case is based upon the 3D flow modelling case model 5 (see Section 2.3.2), where a transmissive feature is assumed to be parallel to the vault at a distance of approximately two vault widths from the vault. The geochemical model considers a 2D slice through the 3D flow model corresponding to a horizontal slice through the vault approximately half-way up the waste. The geometrical extent of the geochemical model is the region comprising the backfill and the vault. The host rock and transmissive feature are not represented in the model.

The 2D grid used in the geochemical modelling corresponds to a 2D slice through the 3D MODFLOW grid used for the flow modelling, i.e. the (2D) resolutions of the flow and geochemical models are the same. The flow field calculated for the 3D Model 5 was mapped onto the 2D Raiden grid. Figure 3.6 shows the resulting Raiden flow field, which corresponds to the flow field shown in Figure 2.21.

Simulations for 32 mm and 4 mm backfill particles were performed to 10^4 years.

It should be noted that the vertical direction in the geochemical modelling figures is reversed with respect to the corresponding vertical direction in the flow modelling figures, because the y-coordinate is increasing from the top to the bottom of the flow figures, hence the geochemical modelling figures in this section may appear to be upside-down with respect to the flow figures.

Results: 32 mm backfill particles

The pH profile at 10^4 years is shown in Figure 3.7. The pH varies considerably through the backfill, and reaches its highest value of pH~11 on the backfill/host rock boundary at the outflowing points along the length of the vault. The pH profiles along the boundaries along the length of the vault are shown in Figure 3.9 and Figure 3.10. The

downstream boundary across the width of the vault has a higher pH than the upstream end with pH~9.5.

The total amount of quartz dissolved per 1 m thickness of backfill is shown as a function of time in Figure 3.11. After 10^4 years, the total amount of quartz dissolved is approximately 4×10^4 moles, which corresponds to approximately 0.2% of the initial quartz inventory (in the 1 m thick slice). The dissolution profile of the quartz is shown in Figure 3.8. The only significant quartz dissolution occurs adjacent to the concrete vault with the majority occurring along the long edges of the vault. Using a mass balance approach, Karlsson et al. (1999) calculated that, in SFL3 and SFL 5, between 5% and 6% of the total quartz content in the backfill would need to react in order to completely buffer the total leachable amount of OH^-. The calculations here would tend to suggest that for a diffusive release of OH^- from the vault, a much smaller fraction of the total quartz content in the backfill would be consumed. This is not to say that the quartz in the backfill is easily sufficient to buffer the pH plume, the pH profile graphs show that it is not. Rather it would tend to suggest that the quartz is not able to react sufficiently quickly for complete buffering to take place.

Figure 3.11 also shows the total precipitated amounts of silica in the secondary CSH minerals. The only secondary minerals to precipitate in this case are tobermorite and gyrolite. Tobermorite precipitation is the more significant of the two minerals by a factor of approximately five. It is clear from the figure that the total amount of precipitated silica is almost exactly equal to the amount of dissolved quartz, which indicates that all of the dissolved quartz is converted to tobermorite and gyrolite.

Figure 3.12 and Figure 3.13 show the profiles of the precipitated tobermorite and gyrolite at 10^4 years. The major precipitation occurs in the cell adjacent to the vault (where the only significant quartz dissolution took place), with only a small amount of gyrolite precipitating in cells at a greater distance from the vault, as can be seen in the concentration profile slices across the vault in Figure 3.14 and Figure 3.15.

Results: 4 mm backfill particles

The pH profile at 10^4 years is shown in Figure 3.16 and profiles along the backfill/host rock boundary are shown in Figure 3.18 and Figure 3.19. The figures are barely distinguishable from the analogous profiles for the 32 mm backfill particle case. However, a close inspection reveals that for times earlier than 10^3 years, the pH rises fractionally slower in the 4 mm particle case, due to the slightly faster quartz dissolution rate, which allows faster precipitation of secondary minerals and hence a slightly increased buffering capacity. Beyond 10^3 years, the results are indistinguishable.

In contrast to the 32 mm particle case, the only secondary mineral to precipitate is gyrolite. No tobermorite is present in this case. The final gyrolite profile at 10^4 years is

shown in Figure 3.21. Again, the only significant quartz dissolution and gyrolite precipitation occurs adjacent to the vault. The total amount of quartz dissolved assuming a 1 m thickness of backfill in this case is ~4.8×10^4 moles (0.25% of the initial amount in the slice) and ~1.6×10^4 moles of gyrolite precipitates, which confirms that the SiO_2 released from the quartz is almost entirely converted into gyrolite (the stoichiometry of SiO_2 in gyrolite being 3). This can be seen in Figure 3.20.

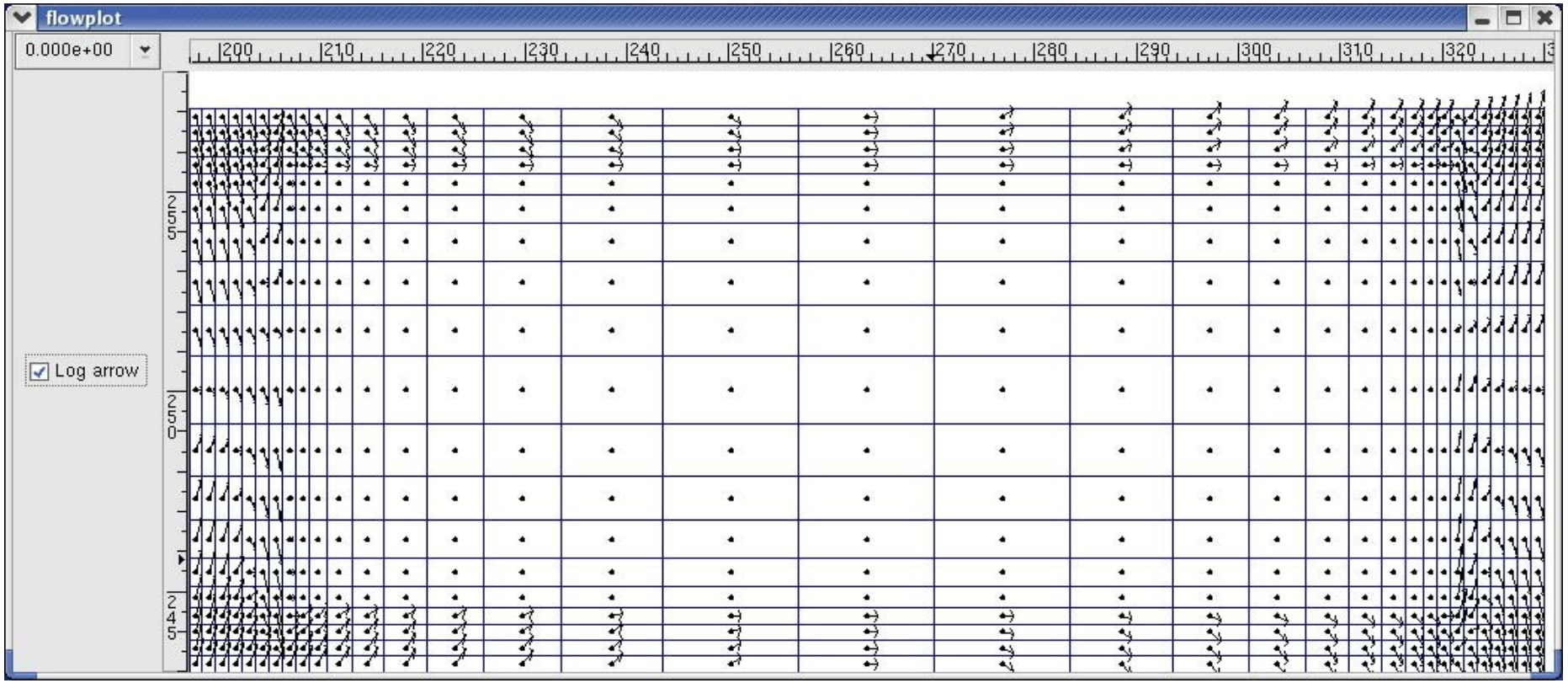

Figure 3.6: 2D flow field used for the geochemical calculations based on 3D flow calculation model 5 (c.f. Figure 2.21). The figure depicts a horizontal slice through the vault. The transmissive feature is situated in the host rock below to the bottom of the figure.

Figures: 32 mm quartz particles

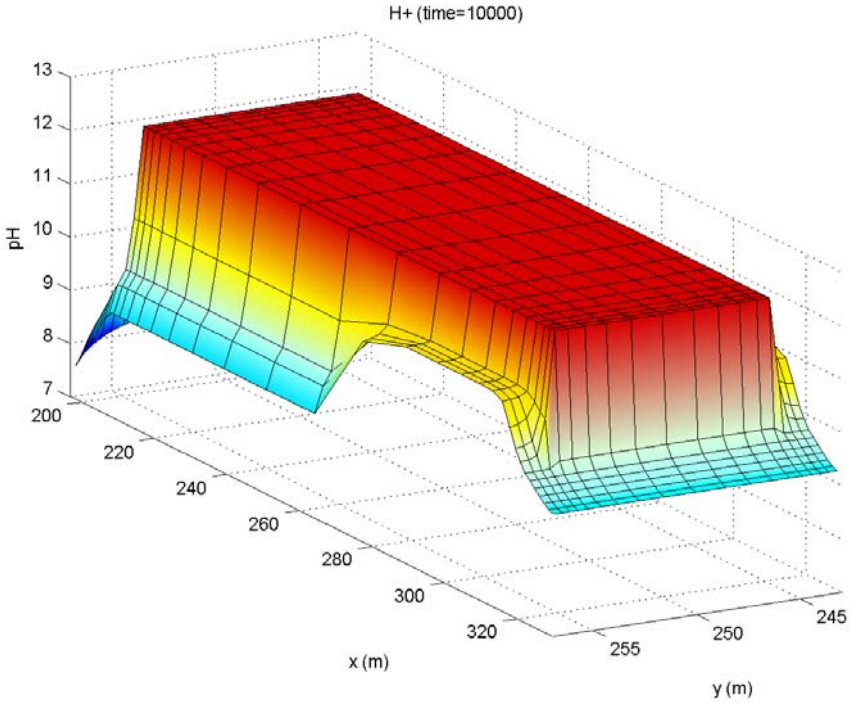

Figure 3.7: (Model 5 horizontal slice, 32 mm backfill particles) - pH profile at 10^4 years.

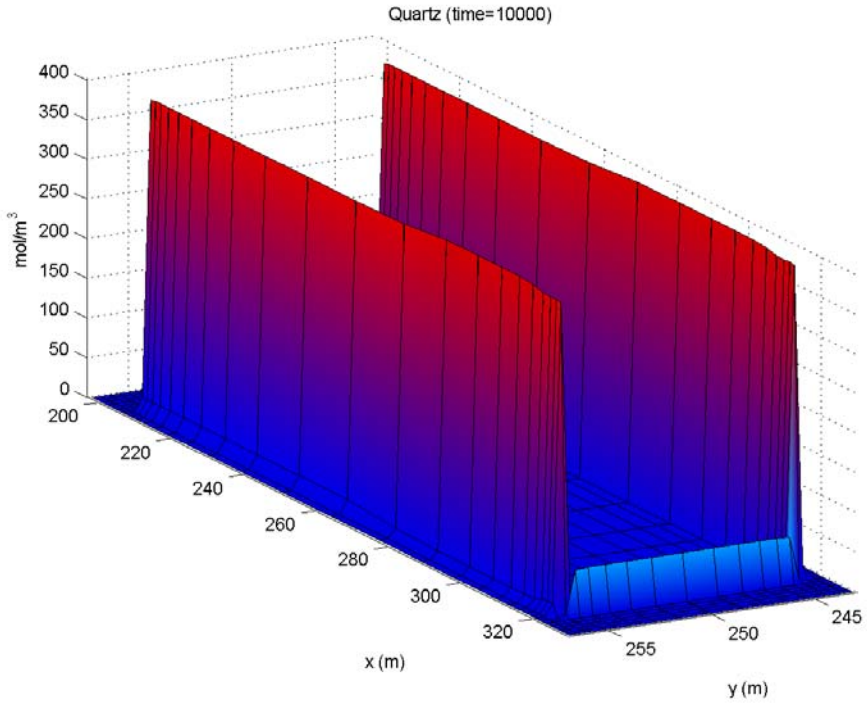

Figure 3.8: (Model 5 horizontal slice, 32 mm backfill particles)– profile of concentration of dissolved quartz in the backfill.

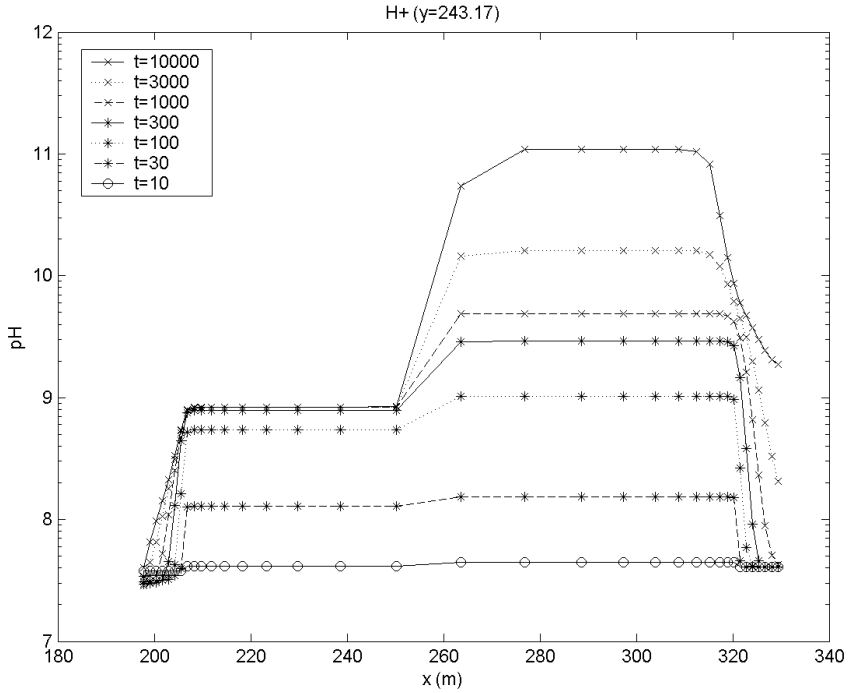

Figure 3.9: (Model 5 horizontal slice, 32 mm backfill particles) – pH profile along the backfill/host rock interface (bottom edge of Figure 3.6).

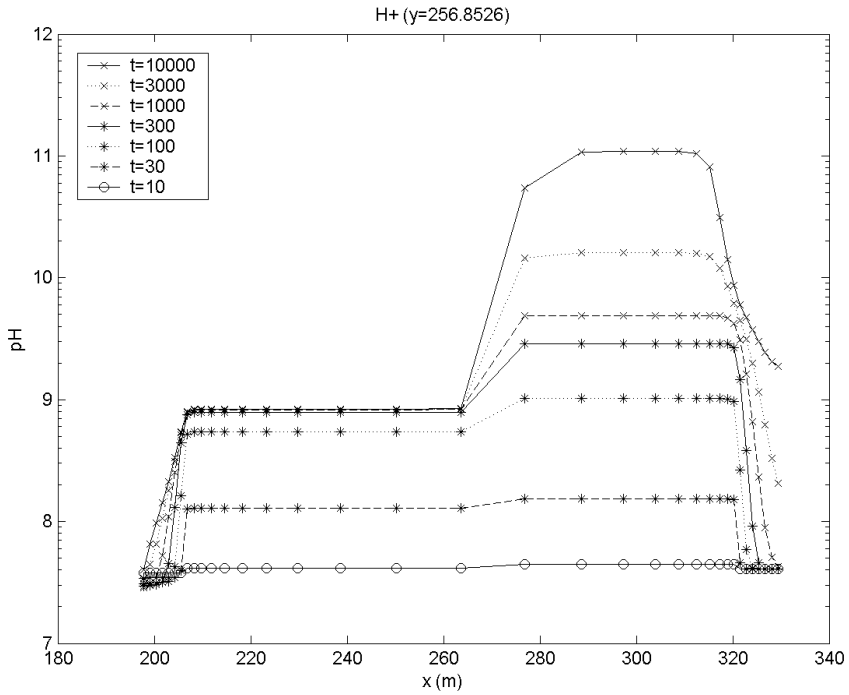

Figure 3.10: (Model 5 horizontal slice, 32 mm backfill particles) – pH profile along the backfill/host rock interface (top edge of Figure 3.6).

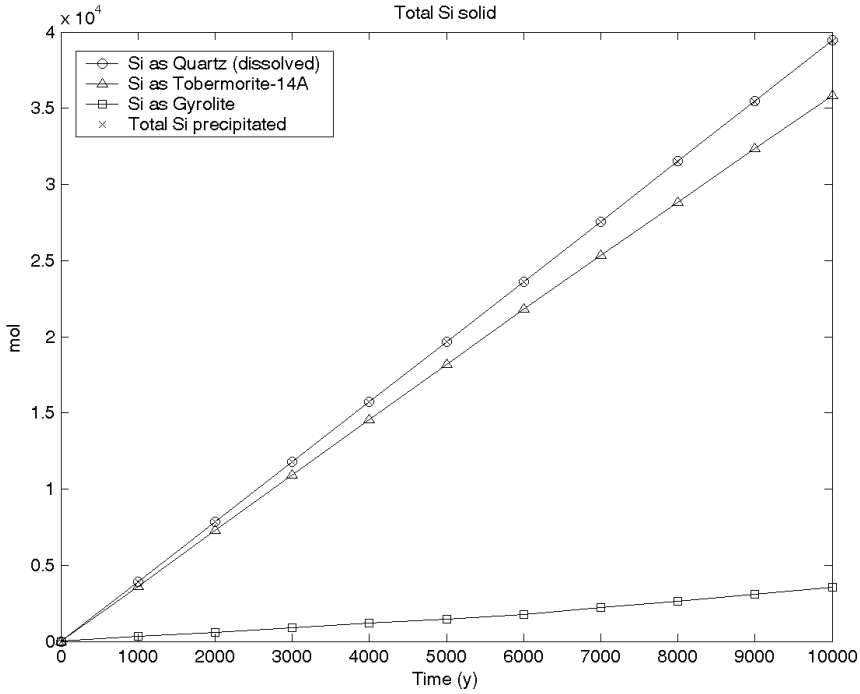

Figure 3.11: (Model 5 horizontal slice, 32 mm backfill particles) – total quartz dissolved per 1m height of backfill, and total silica precipitated in secondary CSH phases.

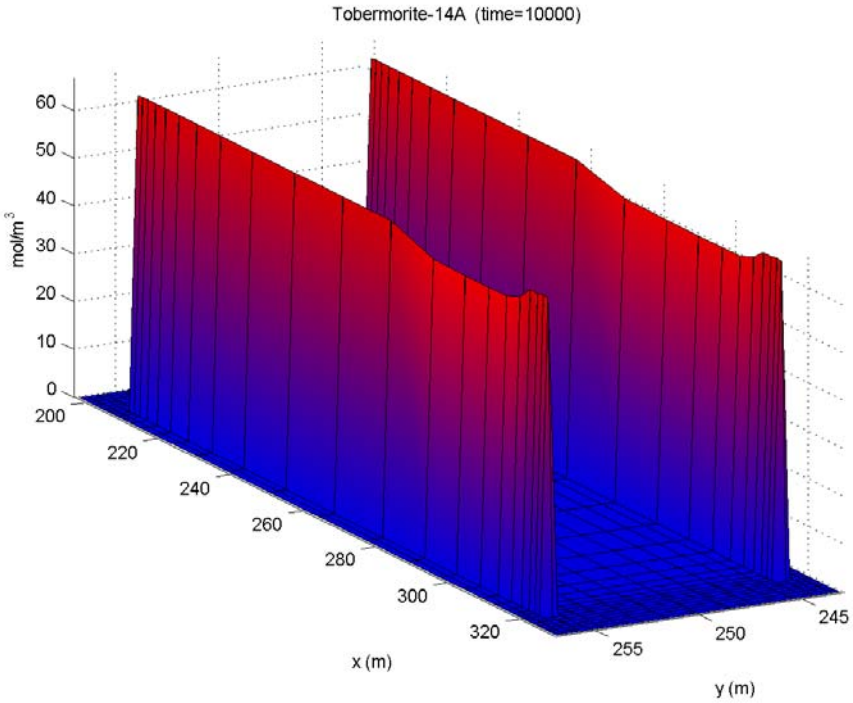

Figure 3.12: (Model 5 horizontal slice, 32 mm backfill particles)– tobermorite concentration profile at 10^4 years.

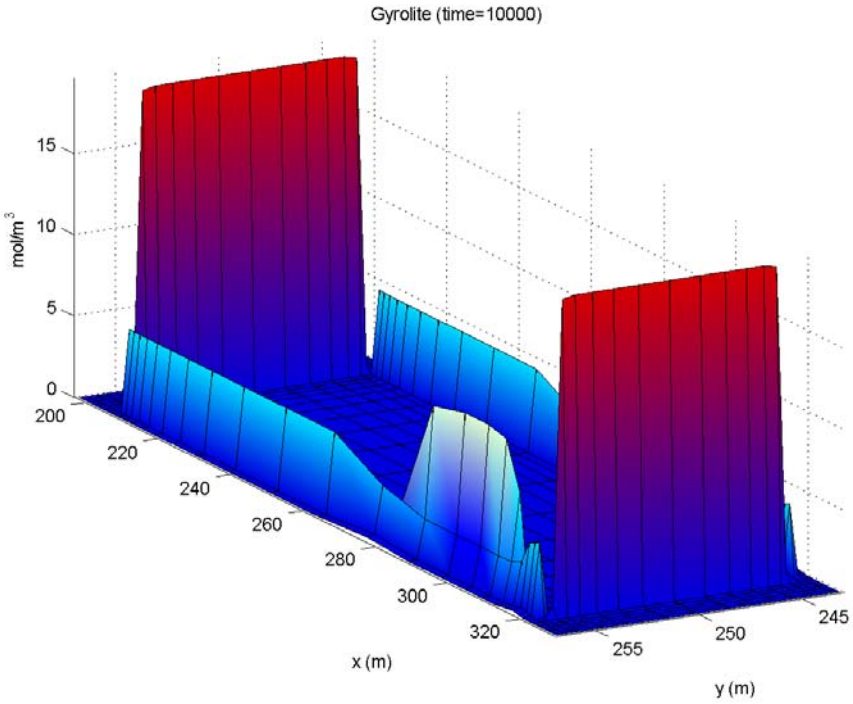

Figure 3.13: (Model 5 horizontal slice, 32 mm backfill particles)– gyrolite concentration profile at 10^4 years.

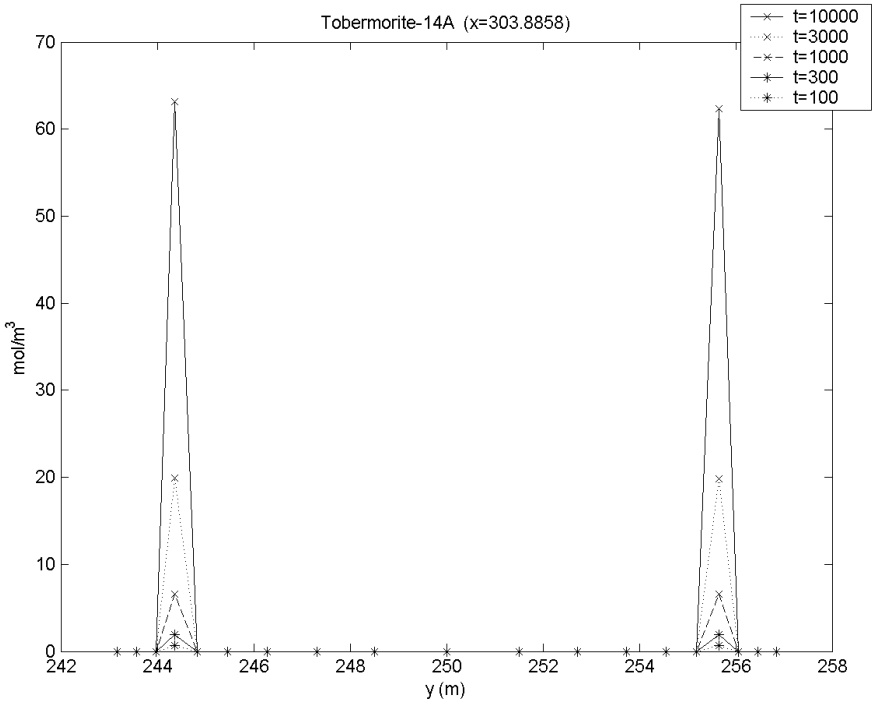

Figure 3.14: (Model 5 horizontal slice, 32 mm backfill particles)– tobermorite concentration profile across the vault at x~304m.

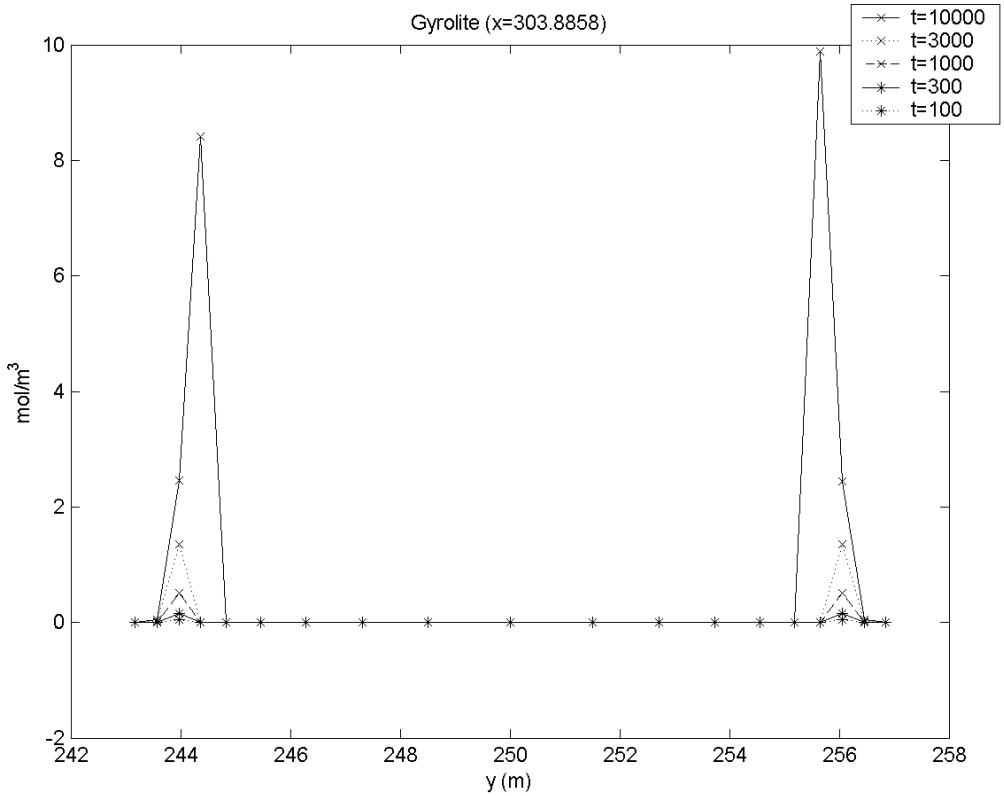

Figure 3.15: (Model 5 horizontal slice, 32 mm backfill particles) - gyrolite concentration profile across the vault at x~304m.

Figures: 4 mm quartz particles

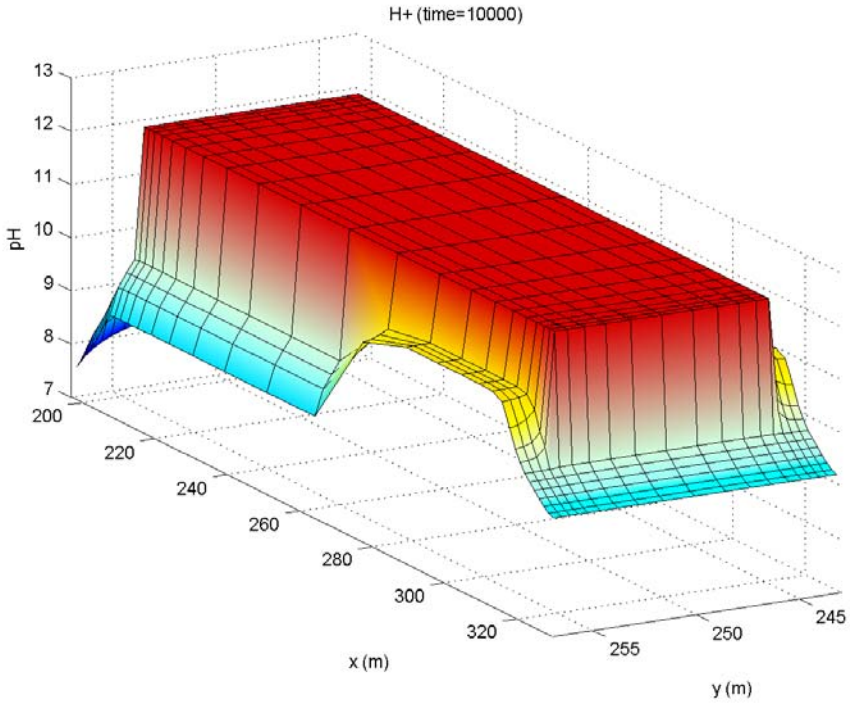

Figure 3.16: (Model 5 horizontal slice, 4 mm backfill particles) - pH profile at 10^4 years.

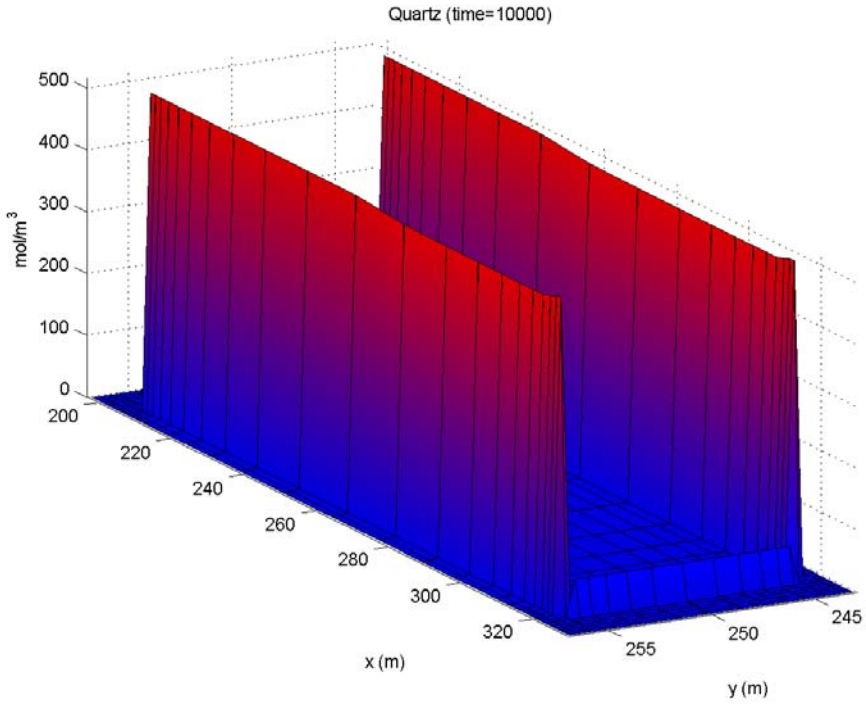

Figure 3.17: (Model 5 horizontal slice, 4 mm backfill particles)– profile of concentration of dissolved quartz in the backfill.

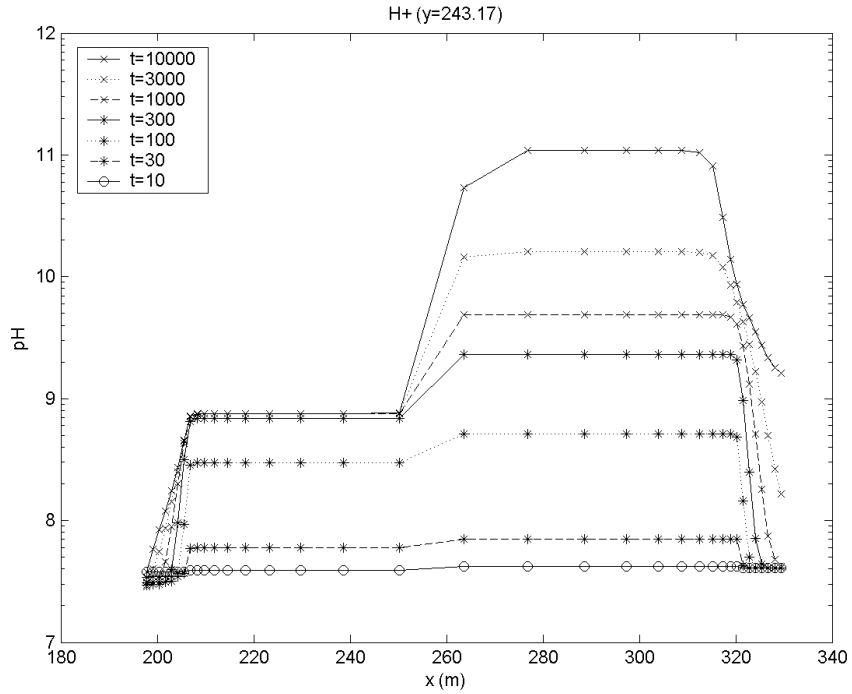

Figure 3.18: (Model 5 horizontal slice, 4 mm backfill particles)– pH profile along the backfill/host rock interface (bottom edge of Figure 3.6).

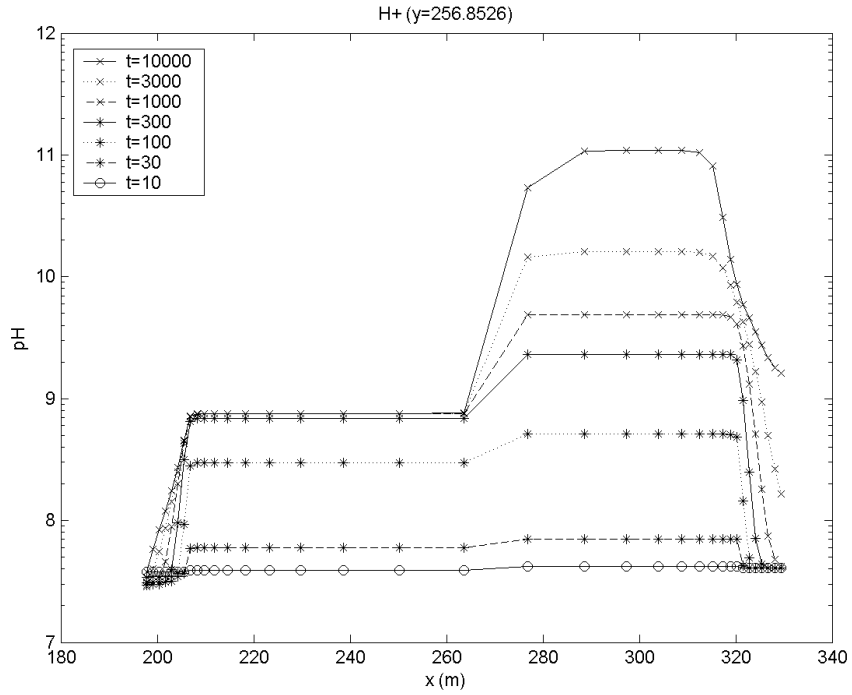

Figure 3.19: (Model 5 horizontal slice, 4 mm backfill particles)– pH profile along the backfill/host rock interface (top edge of Figure 3.6).

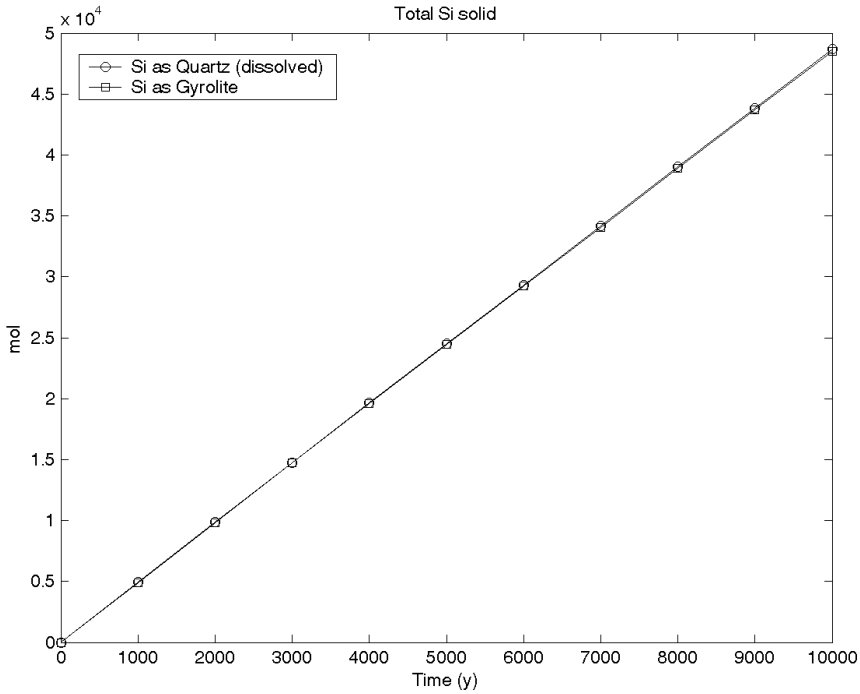

Figure 3.20: (Model 5 horizontal slice, 4 mm backfill particles)– total quartz dissolved per 1m height of backfill, and total silica precipitated in secondary CSH phases.

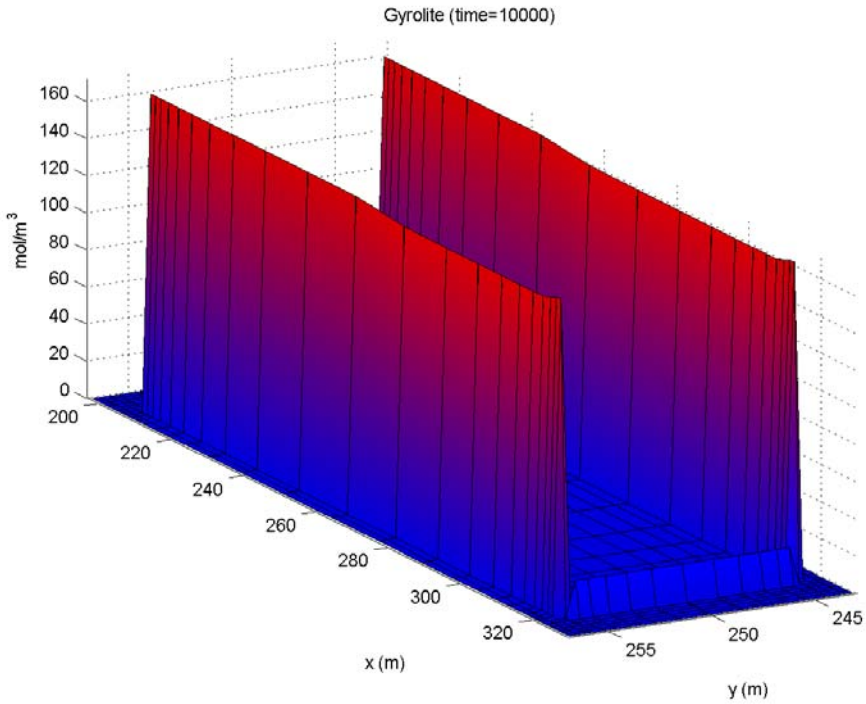

Figure 3.21: (Model 5 horizontal slice, 4 mm backfill particles)– gyrolite concentration profile at 10^4 years.

3.6.2 Model 5: vertical slice along vault length

This case is based upon the 3D flow modelling case model 5 (see Section 2.3.2), where a transmissive feature is assumed to be parallel to the vault at a distance of approximately two vault widths from the vault. The geochemical model considers a 2D slice through the 3D flow model corresponding to a vertical slice along the length of the vault approximately in the middle of the width of the vault. The geometrical extent of the geochemical model is the region comprising the backfill and the vault from the bottom to the top of the backfill. The host rock and transmissive feature are not represented in the model.

The 2D grid used in the geochemical modelling corresponds to a 2D slice through the 3D MODFLOW grid used for the flow modelling, i.e. the (2D) resolutions of the flow and geochemical models are the same. The flow field calculated for the 3D Model 5 was mapped onto the 2D Raiden grid. Figure 3.22 shows the resulting Raiden flow field. Notice the narrow backfill area available for flow in the backfill beneath the vault compared to that available above the vault.

Simulations for 32 mm and 4 mm backfill particles were performed to 10^4 years.

Results: 32 mm backfill particles

The pH profile at 10^4 years is shown in Figure 3.23 and Figure 3.24 (the two figures show the same results, but viewed from above and below the backfill respectively). The pH varies dramatically in the backfill above and below the vault. Above the vault at the interface between the backfill and the host rock, the pH reaches a maximum of approximately 9; below the vault at the interface between the backfill and host rock the pH exceeds 11. The maxima above and below the vault are achieved on the out-flowing portions of the boundaries. The pH profiles along the boundaries along the length of the vault are shown in Figure 3.25 and Figure 3.26. The downstream boundary across the width of the vault has a higher pH than the upstream end (pH varies between 9 and 9.5 on the out-flowing boundary).

The total amount of quartz dissolved in a 1 m thick backfill slice is shown as a function of time in Figure 3.27. After 10^4 years, the total amount of quartz dissolved is approximately 5×10^4 moles (0.13% of the initial amount in the slice). The dissolution profile of the quartz is shown in Figure 3.28. The only significant quartz dissolution occurs in the backfill below the vault, with the majority occurring along the long edges of the vault. Figure 3.29 shows a cross-section of the quartz profile.

The only secondary minerals to precipitate in this case are tobermorite and gyrolite; Figure 3.27 shows the total precipitated amounts of silica. Tobermorite precipitation is the more significant of the two minerals. All of the dissolved quartz is converted to tobermorite and gyrolite.

Figure 3.30 to Figure 3.33 show the profiles of the precipitated tobermorite and gyrolite at 10^4 years. The major tobermorite precipitation occurs in the cells adjacent to the vault. Between 3000 and 10000 years, the amount of gyrolite adjacent to the vault decreases, but increases at greater distance from the vault, which suggests that a wave of gyrolite precipitation propagates at the front of the tobermorite.

Results: 4 mm backfill particles

The pH profile at 10^4 years is shown in Figure 3.34 and Figure 3.35. Once again the late pH profiles are similar to the 32 mm particle case, although the pH at early times is slightly lower due to the faster buffering made possible by the greater surface area of quartz available for reaction.

There is less quartz dissolution away from the cells adjacent to the vault than in the 32 mm particle case, although overall slightly more quartz dissolves in the 4 mm particle case. See Figure 3.36 to Figure 3.38.

In contrast to the horizontal cross-section 32 mm particle case (see Section 3.6.1), the vertical section witnesses precipitation of both tobermorite and gyrolite. All of the SiO_2 freed from the quartz is precipitated in these two minerals. Both minerals only precipitate adjacent to the vault, with tobermorite precipitation exceeding gyrolite precipitation by a factor of approximately three. See Figure 3.39 to Figure 3.42.

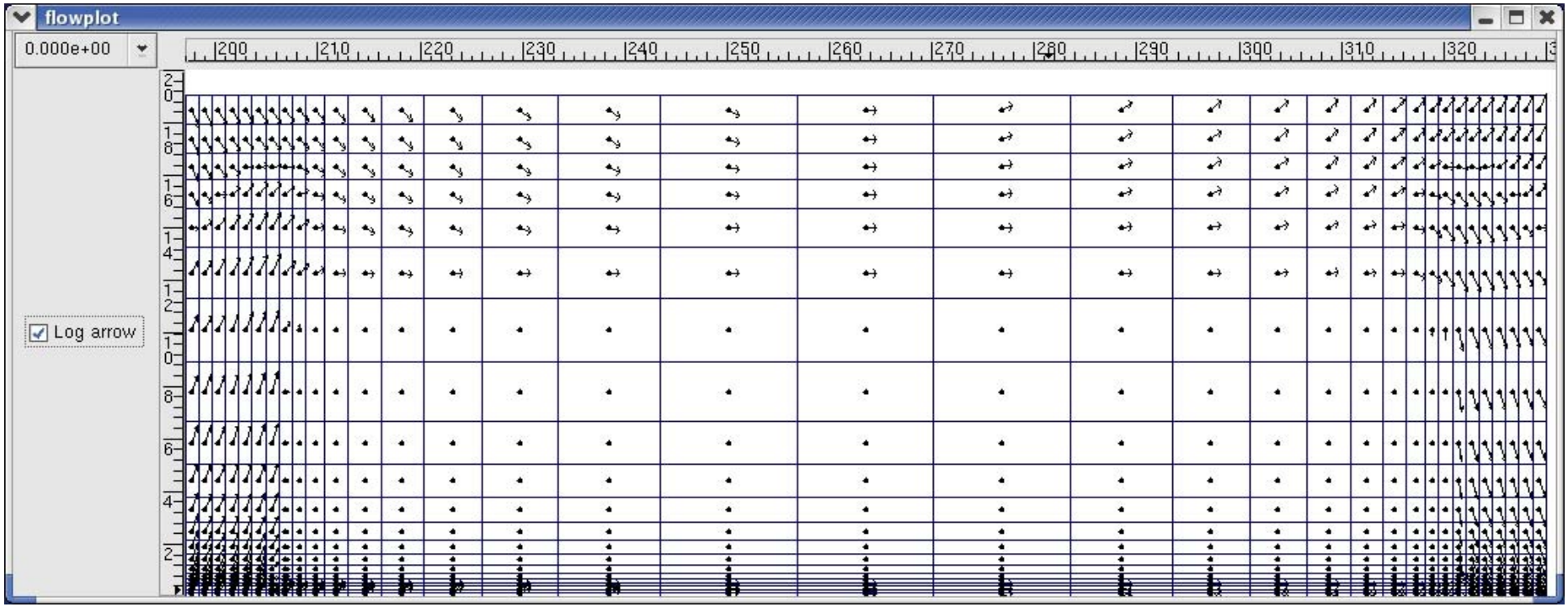

Figure 3.22: 2D flow field used for the geochemical calculations based on 3D flow calculation model.5. Figure depicts a vertical slice along the length of the vault.

Figures: 32 mm quartz particles

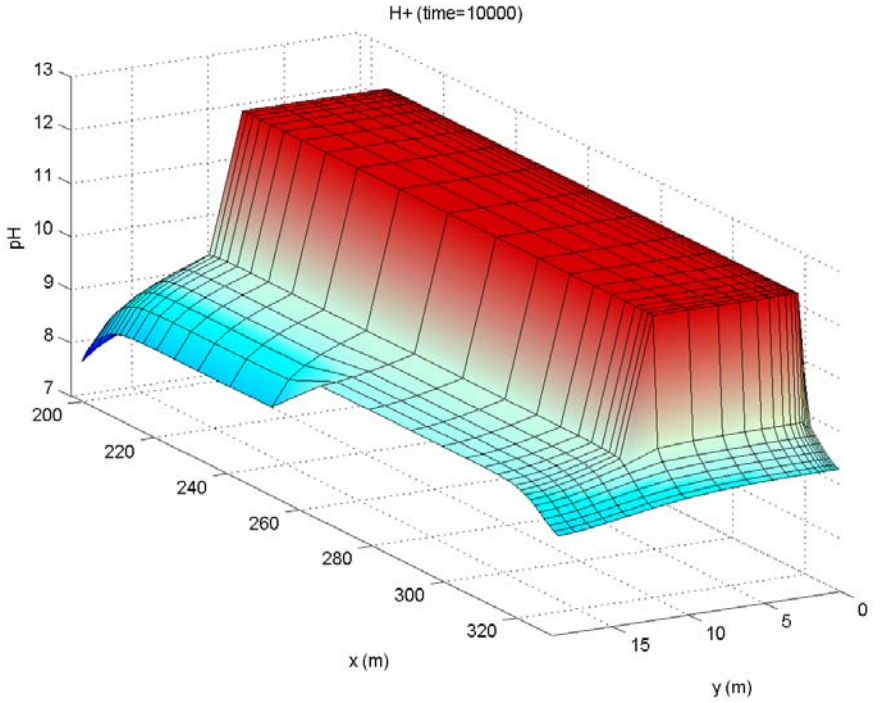

Figure 3.23: (Model 5 vertical slice, 32 mm backfill particles) - pH profile at 10^4 years (view from the top of the backfill).

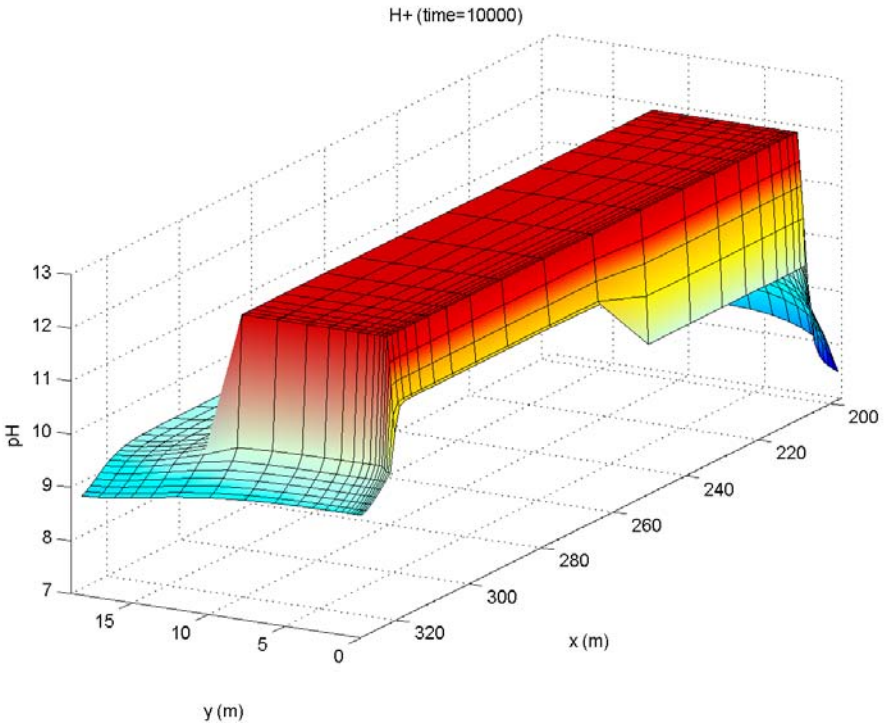

Figure 3.24: (Model 5 vertical slice, 32 mm backfill particles) - pH profile at 10^4 years (view from the bottom of the backfill).

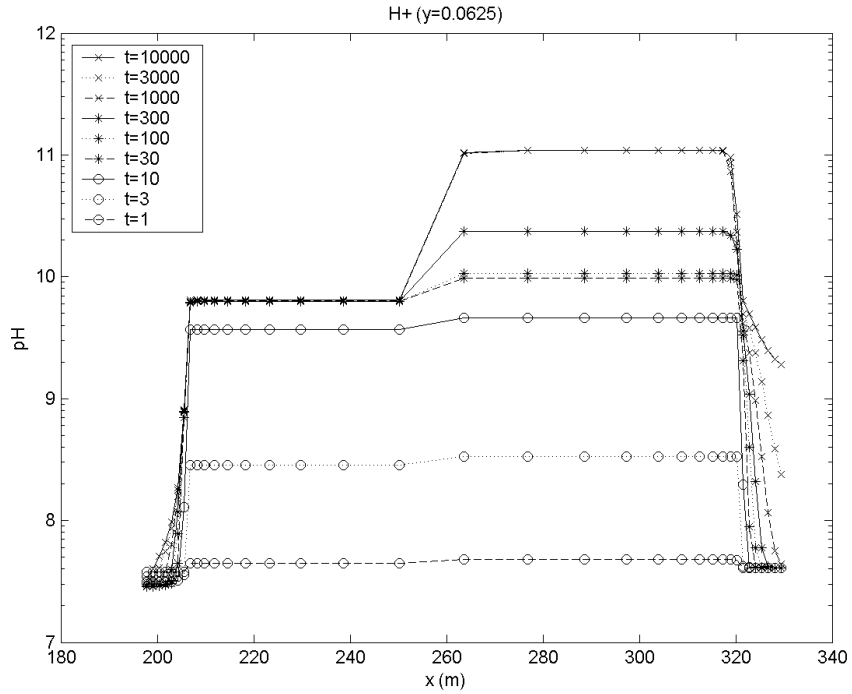

Figure 3.25: (Model 5 vertical slice, 32 mm backfill particles)– pH profile along the bottom of the backfill/host rock interface.

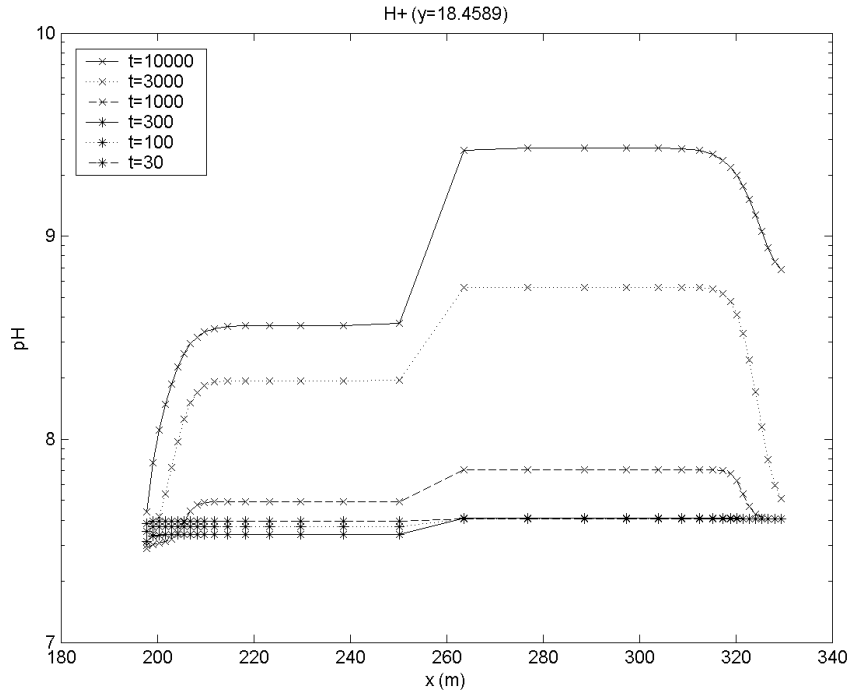

Figure 3.26: (Model 5 vertical slice, 32 mm backfill particles)– pH profile along the top of the backfill/host rock interface.

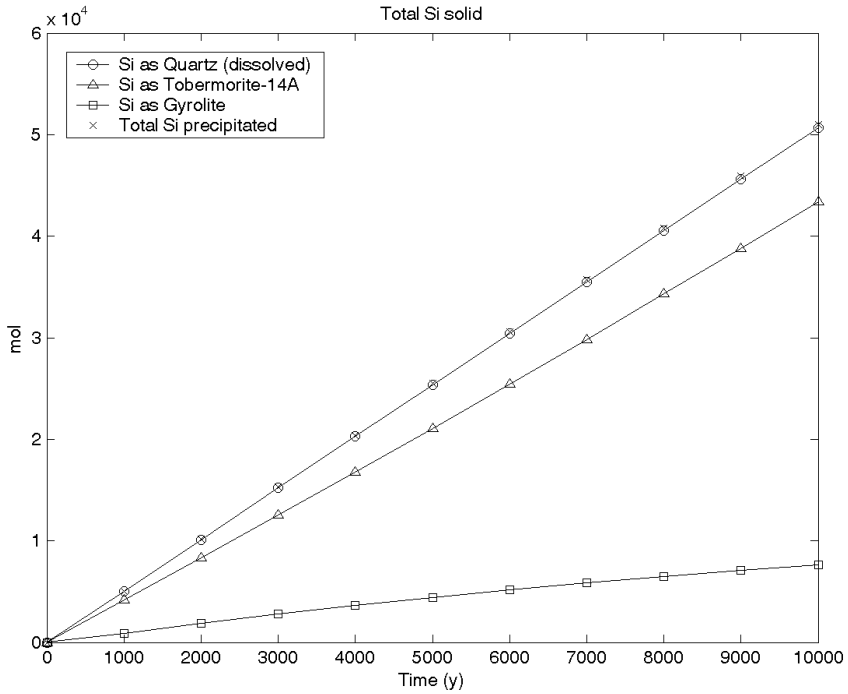

Figure 3.27: (Model 5 vertical slice, 32 mm backfill particles)– total quartz dissolved per 1m width of backfill, and total silica precipitated in secondary CSH phases.

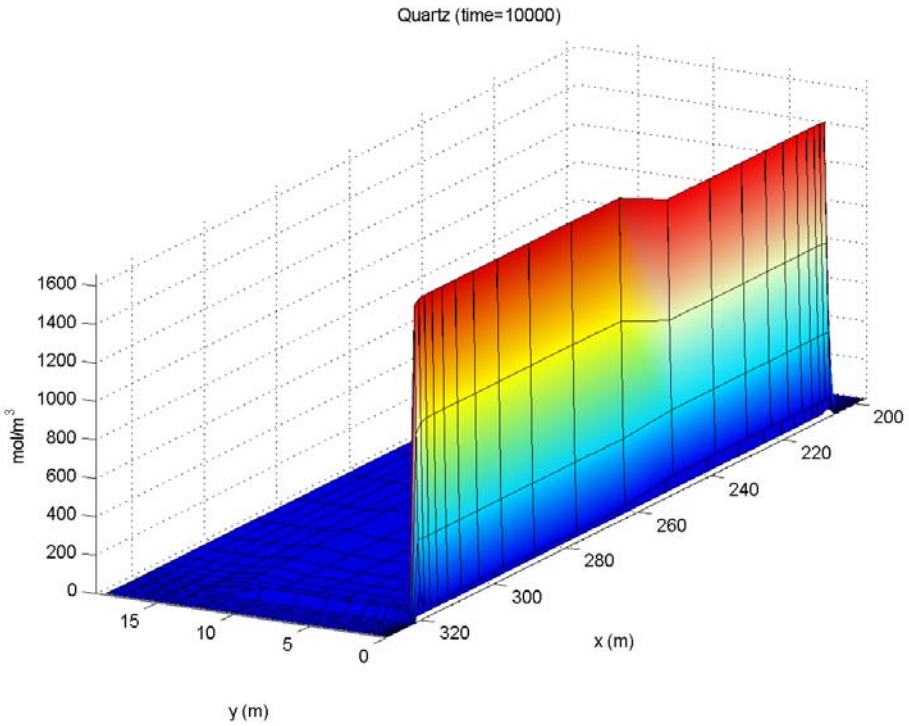

Figure 3.28: (Model 5 vertical slice, 32 mm backfill particles)– profile of concentration of dissolved quartz in the backfill at 10^4 years.

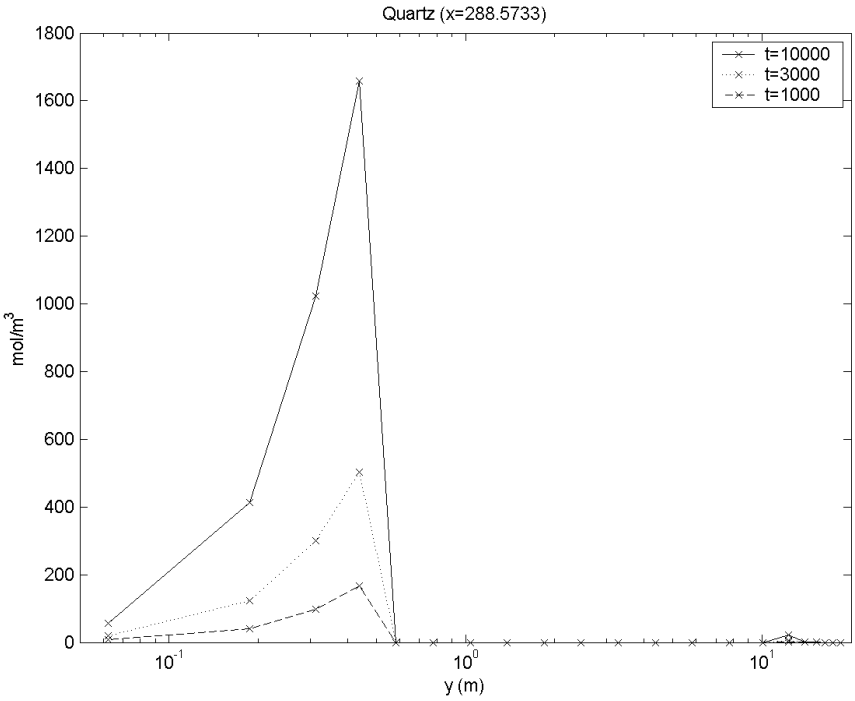

Figure 3.29: (Model 5 vertical slice, 32 mm backfill particles)– cross-section of profile of concentration of dissolved quartz in the backfill. The only significant dissolution is in the backfill below the vault.

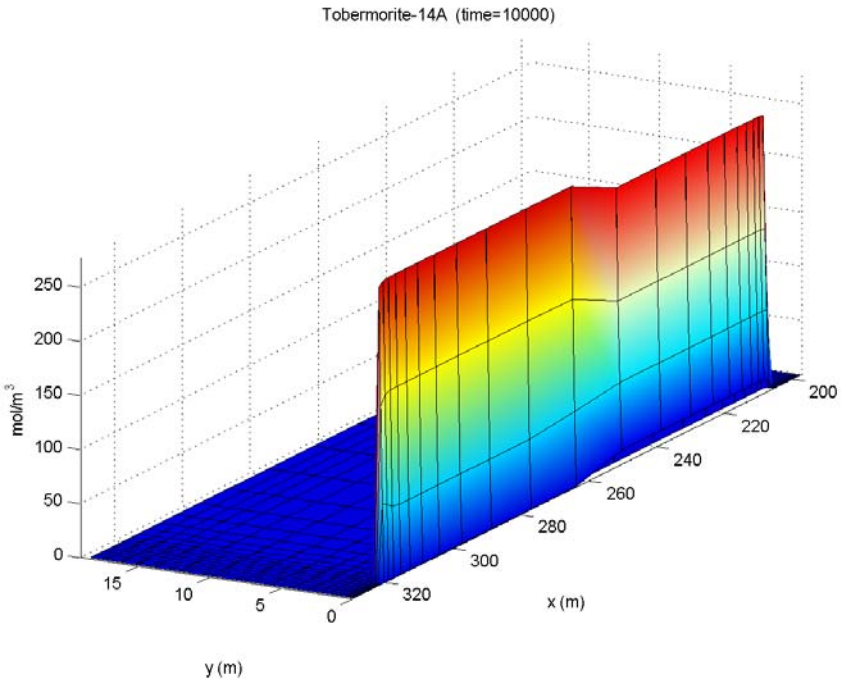

Figure 3.30: (Model 5 vertical slice, 32 mm backfill particles)– tobermorite concentration profile at 10^4 years.

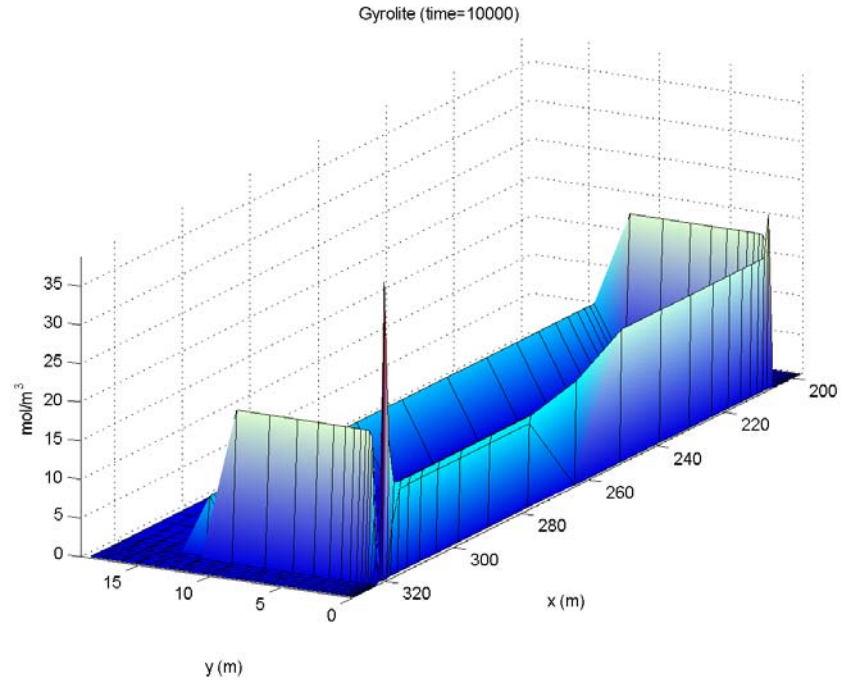

Figure 3.31: (Model 5 vertical slice, 32 mm backfill particles)– gyrolite concentration profile at 10^4 years. The spike in the gyrolite concentration is most likely due to silica-rich porewater flowing down the side of the vault meeting with silica-depleted, but calcium rich water flowing along the bottom of the vault. The cells in the discretisation are very small in this region, so the high concentration has little effect on the overall amount of CSH.

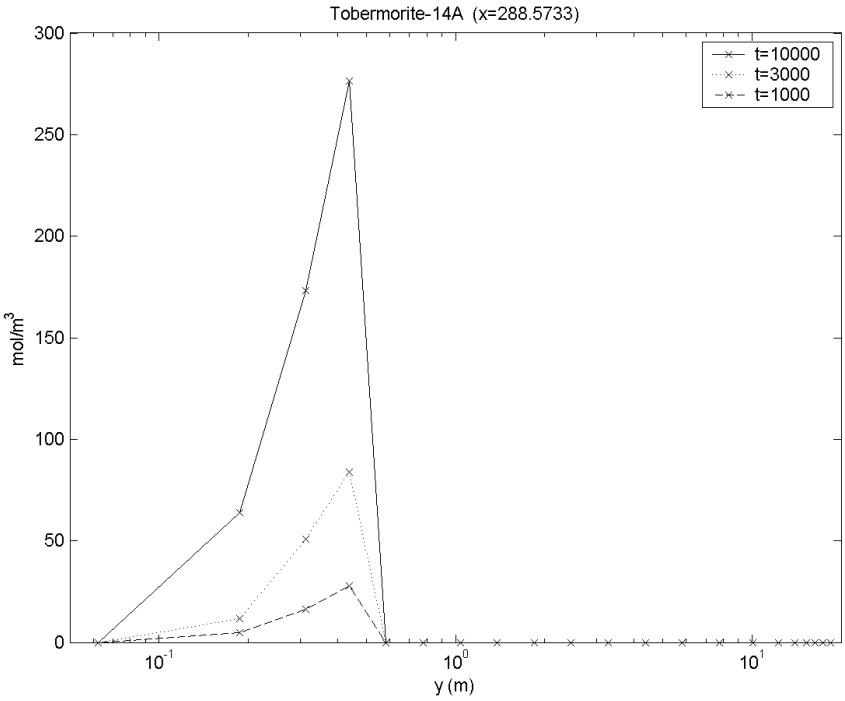

Figure 3.32: (Model 5 vertical slice, 32 mm backfill particles)– cross-section of profile of concentration of tobermorite in the backfill. The only significant precipitation is in the backfill below the vault.

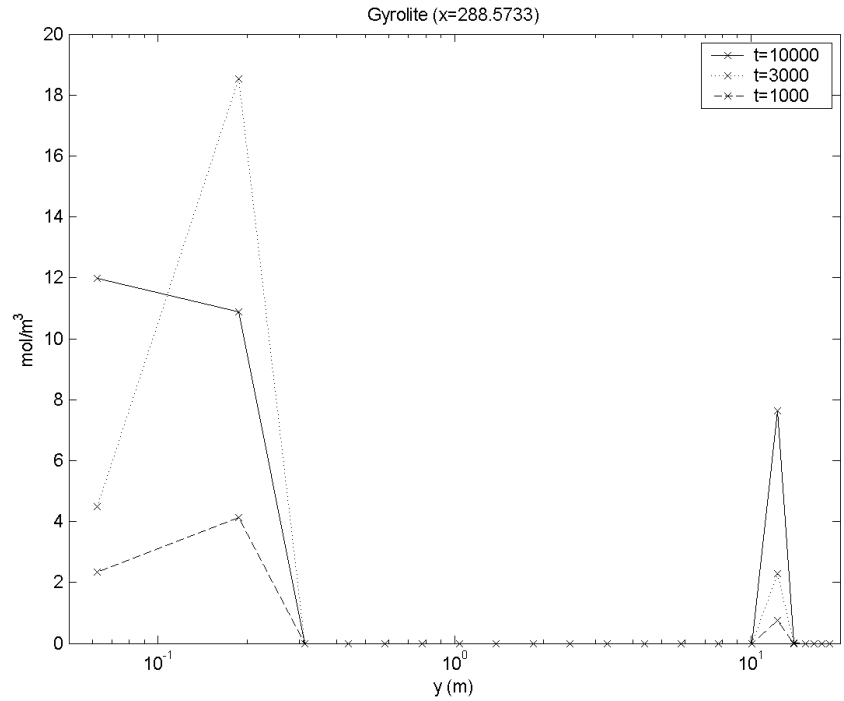

Figure 3.33: (Model 5 vertical slice, 32 mm backfill particles)– cross-section of profile of concentration of gyrolite in the backfill. The only significant precipitation is in the backfill below the vault.

Figures: 4 mm quartz particles

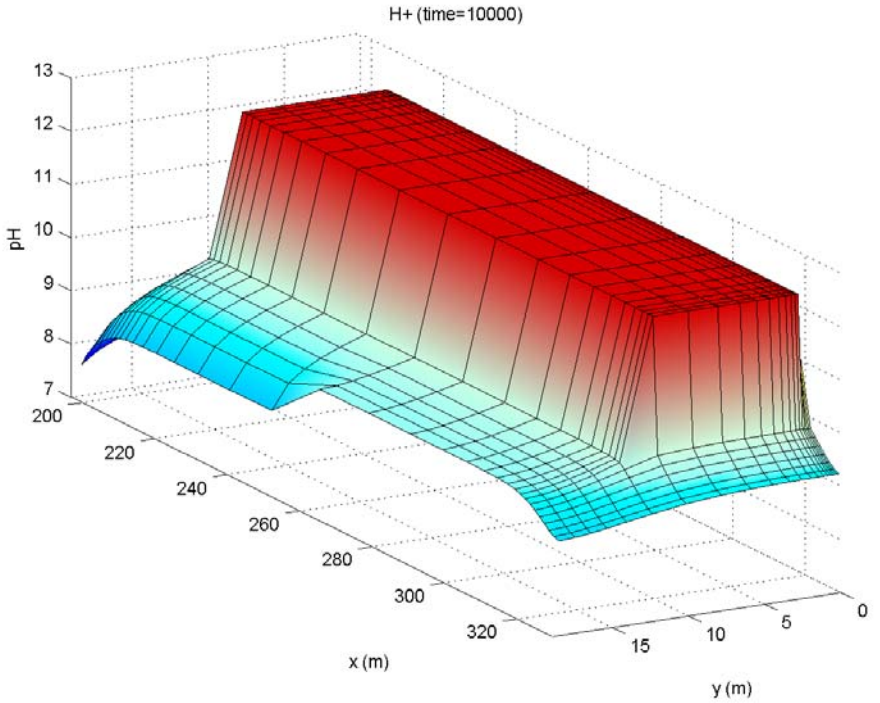

Figure 3.34: : (Model 5 vertical slice, 4 mm backfill particles) - pH profile at 10^4 years (view from the top of the backfill).

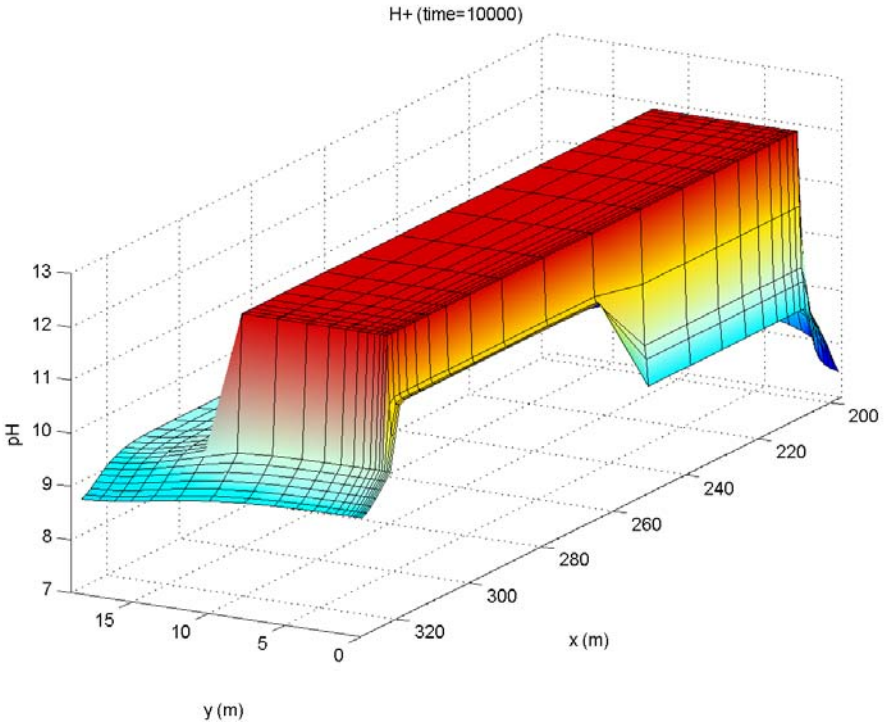

Figure 3.35: : (Model 5 vertical slice, 4 mm backfill particles) - pH profile at 10^4 years (view from the bottom of the backfill).

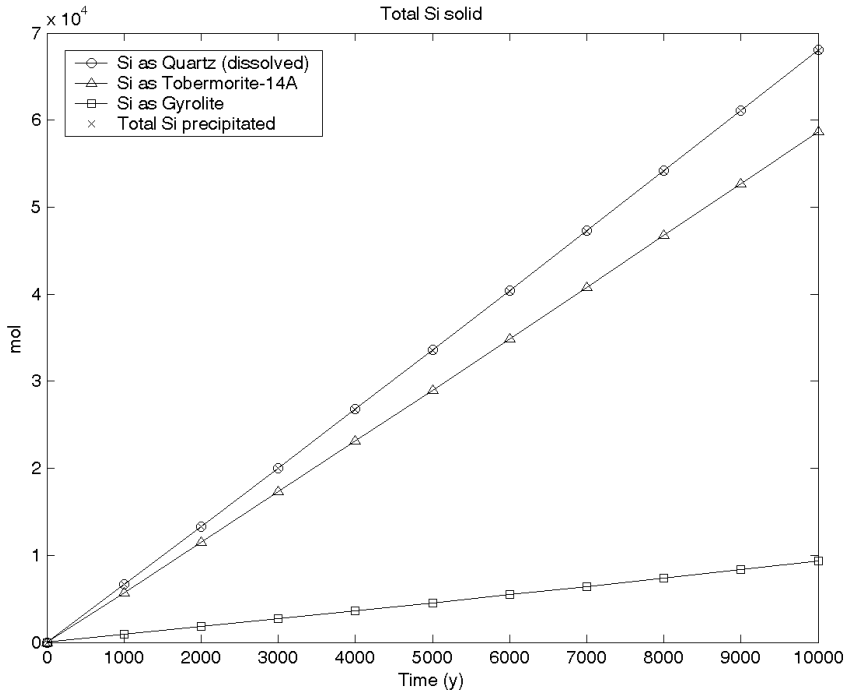

Figure 3.36: (Model 5 vertical slice, 4 mm backfill particles)– total quartz dissolved per 1m width of backfill, and total silica precipitated in secondary CSH phases.

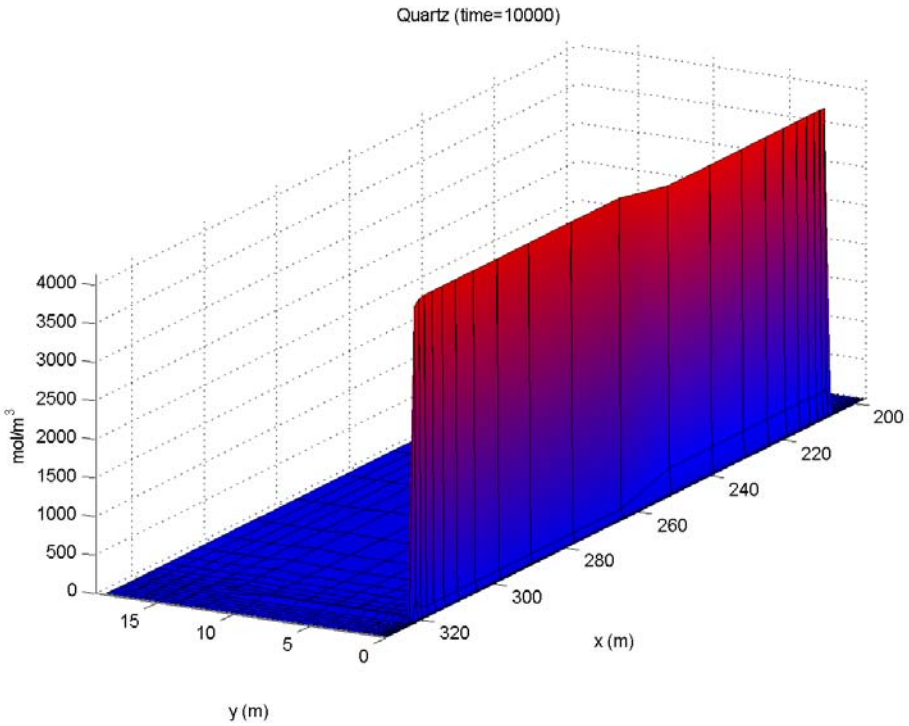

Figure 3.37: (Model 5 vertical slice, 4 mm backfill particles)– profile of concentration of dissolved quartz in the backfill at 10^4 years.

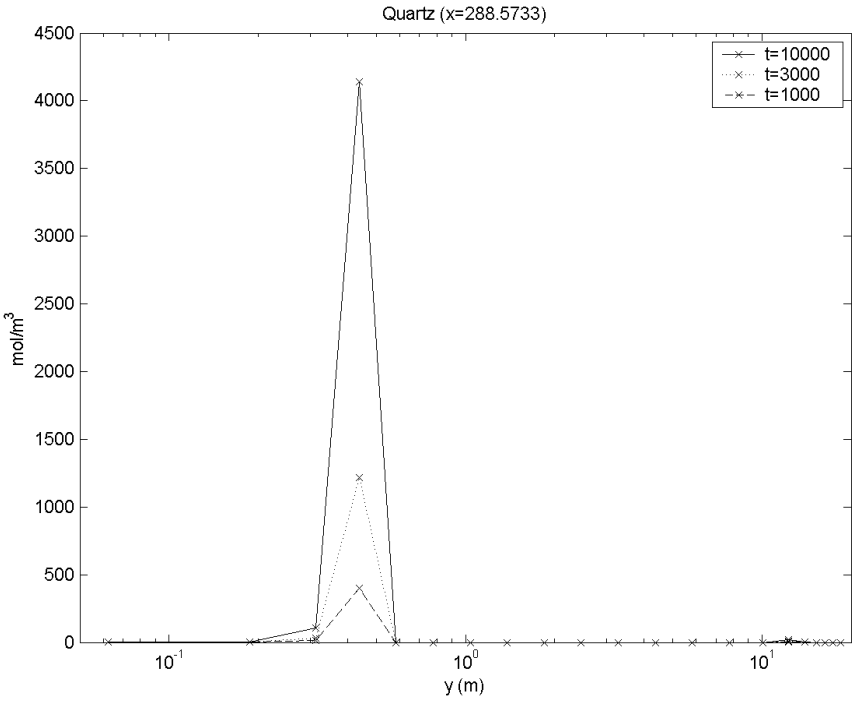

Figure 3.38: (Model 5 vertical slice, 4 mm backfill particles)– cross-section of profile of concentration of dissolved quartz in the backfill. The only significant dissolution is in the backfill below the vault.

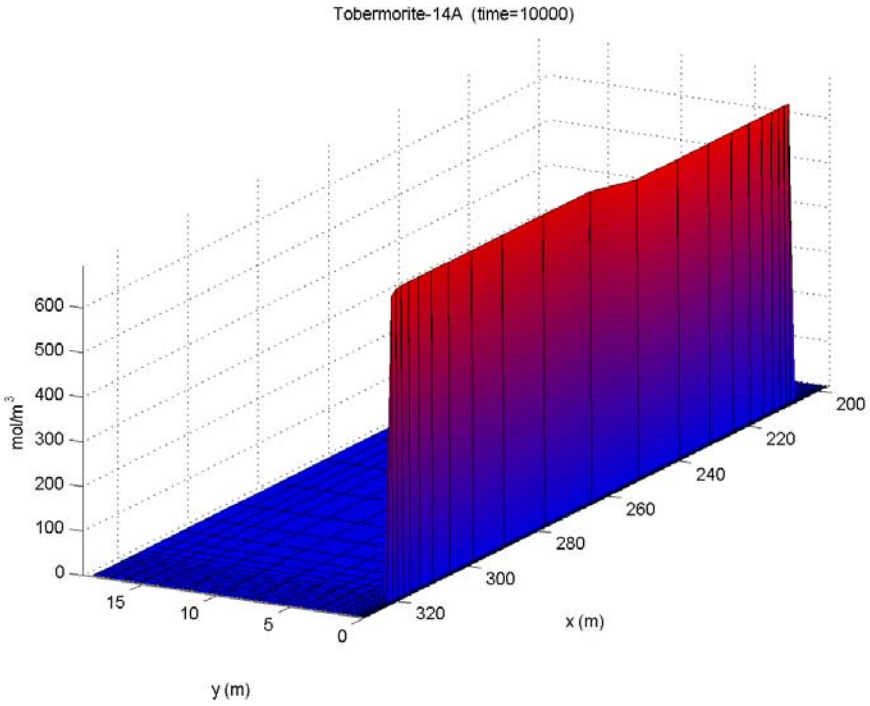

Figure 3.39: (Model 5 vertical slice, 4 mm backfill particles)– tobermorite concentration profile at 10^4 years.

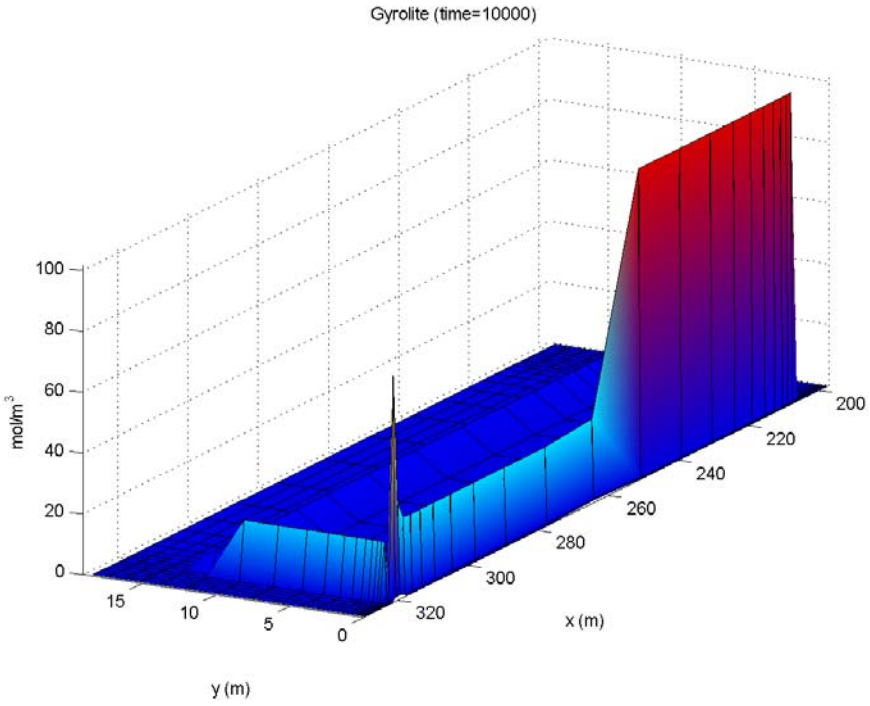

Figure 3.40: (Model 5 vertical slice, 4 mm backfill particles)– gyrolite concentration profile at 10^4 years. The spike in the concentration is most likely a result of the same arguments put forward in the caption to Figure 3.31, however the effect is less significant when compared to the higher upstream concentrations of gyrolite in this case.

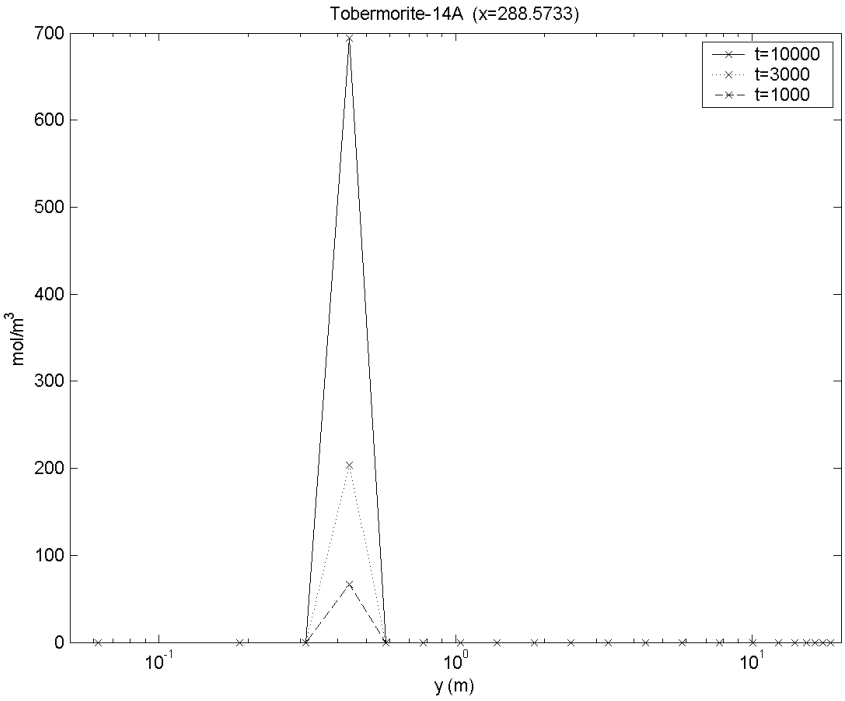

Figure 3.41: (Model 5 vertical slice, 4 mm backfill particles)– cross-section of profile of concentration of tobermorite in the backfill. The only significant precipitation is in the backfill below the vault.

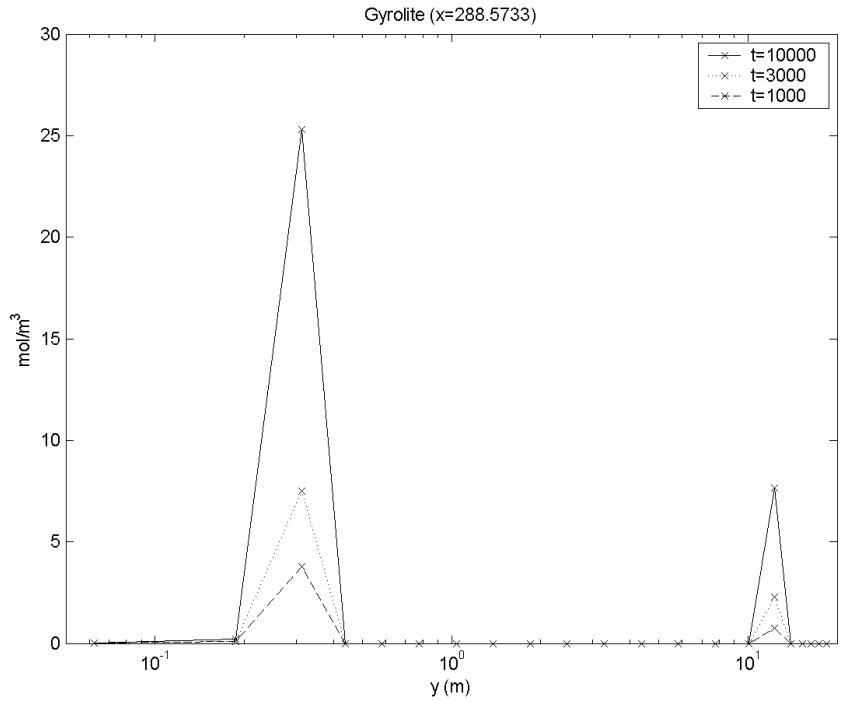

Figure 3.42: (Model 5 vertical slice, 4 mm backfill particles)– cross-section of profile of concentration of gyrolite in the backfill. The only significant precipitation is in the backfill below the vault.

3.6.3 Model 6: vertical slice across vault width

This case is based upon the 3D flow modelling case model 6 (see Section 2.3.2), where a transmissive feature is assumed to cut through the vault at 90°. The geochemical model considers a 2D slice through the 3D flow model corresponding to a vertical slice along the width of the vault approximately in the middle of the transmissive feature. This case represents the shortest travel path between the in-flowing to the out-flowing boundaries. The geometrical extent of the geochemical model is the region comprising the backfill and the vault from the bottom to the top of the backfill. The host rock and transmissive feature are not represented in the model.

The 2D grid used in the geochemical modelling corresponds to a 2D slice through the 3D MODFLOW grid used for the flow modelling, i.e. the (2D) resolutions of the flow and geochemical models are the same. The flow field calculated for the 3D Model 6 was mapped onto the 2D Raiden grid. Figure 3.43 shows the resulting Raiden flow field. Notice again the narrow backfill area available for flow in the backfill beneath the vault compared to that available above the vault.

The ratio of the fast flow beneath the vault, and the small cell size in the discretisation in this region led to a much longer run-time for this scenario compared to the other scenarios that were considered. For this reason, the run for the 32 mm particle was stopped after a simulation time of 9000 years and the 4 mm particle was stopped after 7000 years.

Results: 32 mm backfill particles

The pH profile at 9000 years is shown in Figure 3.44 and Figure 3.45 (the two figures show the view from above and below the backfill respectively). Above the vault at the interface between the backfill and the host rock, the pH reaches a maximum of approximately 9; below the vault at the interface between the backfill and host rock the pH almost reaches 11. The maximum above the vault is achieved on the out-flowing portion of the boundary. The pH profiles along the boundaries above and below the vault are shown in Figure 3.46 and Figure 3.47. The downstream boundary on the side of the vault has a higher pH than the upstream end (pH is approximately 9 in this out-flowing boundary).

The total amount of quartz dissolved in a 1 m thick slice of backfill is shown as a function of time in Figure 3.48. After 9000 years, the total amount of quartz dissolved is approximately 7500 moles (0.16% of the initial amount in the slice). The dissolution profile of the quartz is shown in Figure 3.49. The only significant quartz dissolution occurs in the backfill below the vault, with the majority occurring along the long edges of the vault. Figure 3.50 shows a cross-section of the quartz profile.

Again, tobermorite and gyrolite precipitate in the backfill; Figure 3.48 shows the total precipitated amount of silica in each mineral. Tobermorite precipitation is the more significant of the two minerals. All of the dissolved quartz is converted to tobermorite and gyrolite.

Figure 3.51 to Figure 3.54 show the profiles of the precipitated tobermorite and gyrolite at 9000 years. The major tobermorite precipitation occurs beneath and to the side of the vault in the cells adjacent to the vault. Gyrolite appears to propagate at the front of the tobermorite, away from the vault.

Results: 4 mm backfill particles

The pH profile at 7000 years is shown in Figure 3.55 to Figure 3.58. The late pH profiles are similar to the 32 mm particle case, with very little difference between the profile at 7000 years for the 4 mm particles and the profile at 9000 years from the 32 mm particles. Again the pH at early times is slightly lower in the 4 mm particle case due to the faster buffering made possible by the faster quartz dissolution reaction.

There is less quartz dissolution away from the cells adjacent to the vault than in the 32 mm particle case, although overall slightly more quartz dissolves in the 4 mm particle case (by 7000 years, more quartz has dissolved than that by 9000 years in the 32 mm particle case). See Figure 3.59 to Figure 3.60.

Again tobermorite and gyrolite precipitate, tobermorite precipitating predominantly below the vault and gyrolite to the sides, the total amounts of silica precipitated in the minerals is shown in Figure 3.59. Tobermorite and gyrolite profiles at 7000 years are shown in Figure 3.61 and Figure 3.62 respectively.

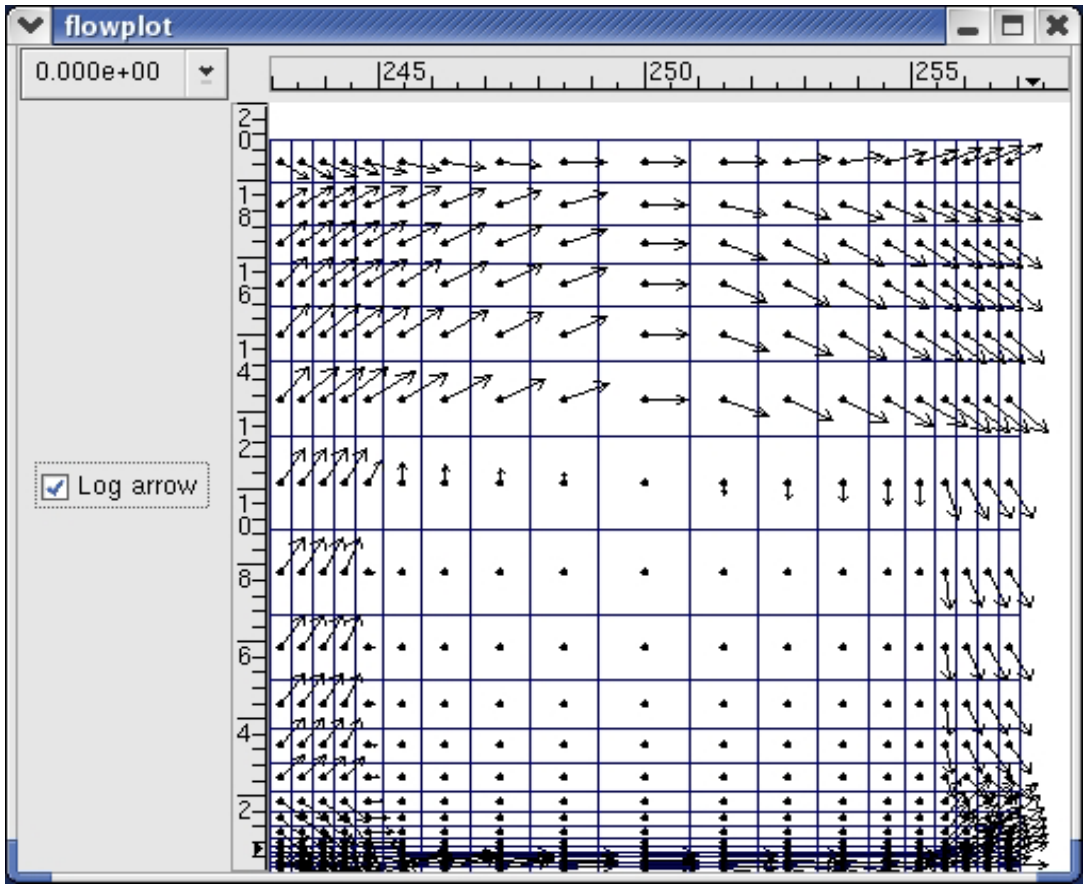

Figure 3.43: 2D flow field used for the geochemical calculations based on 3D flow calculation model.6. Figure depicts a vertical slice across the width of the vault.

Figures: 32 mm quartz particles

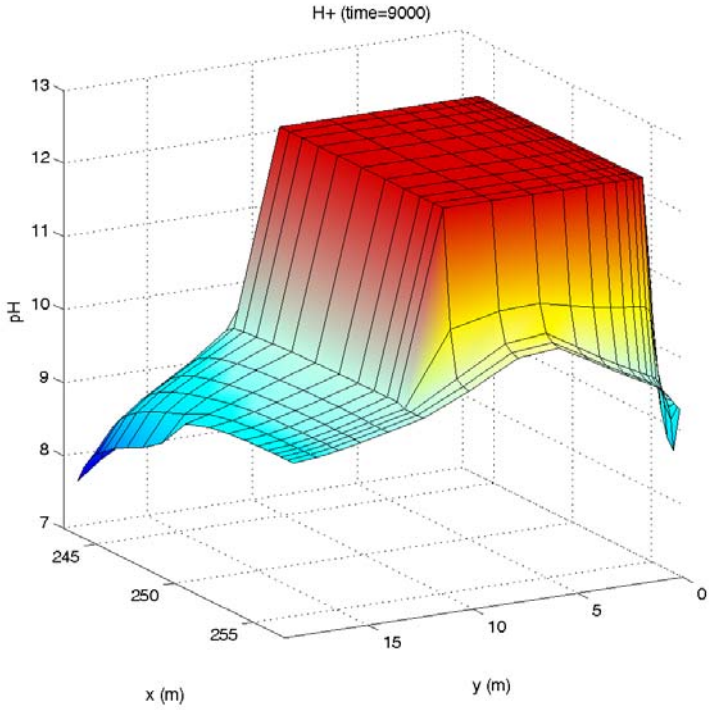

Figure 3.44: (Model 6 vertical slice, 32 mm backfill particles) - pH profile at 9000 years (view from the top of the backfill).

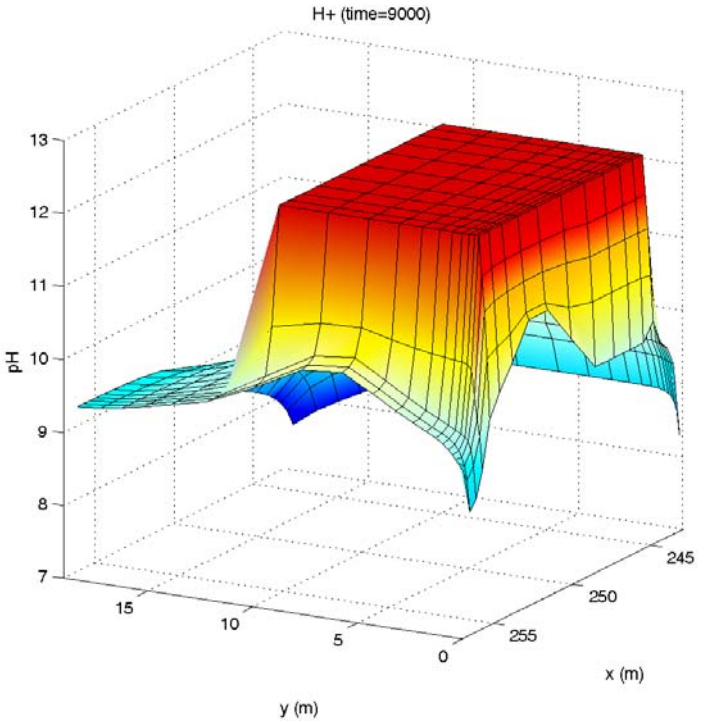

Figure 3.45: (Model 6 vertical slice, 32 mm backfill particles) - pH profile at 9000 years (view from the bottom of the backfill).

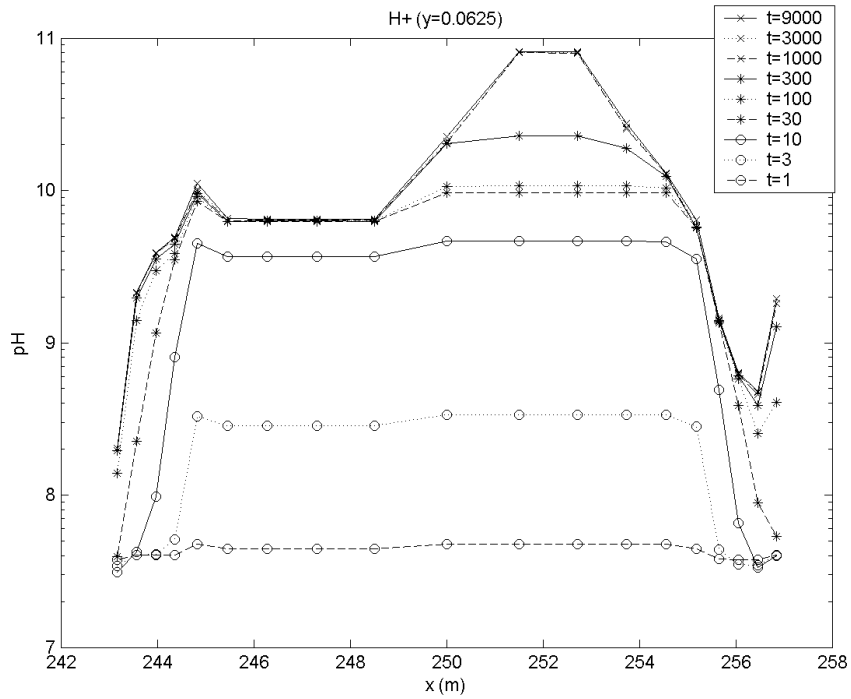

Figure 3.46: (Model 6 vertical slice, 32 mm backfill particles) - pH profile along the bottom of the backfill/host rock interface.

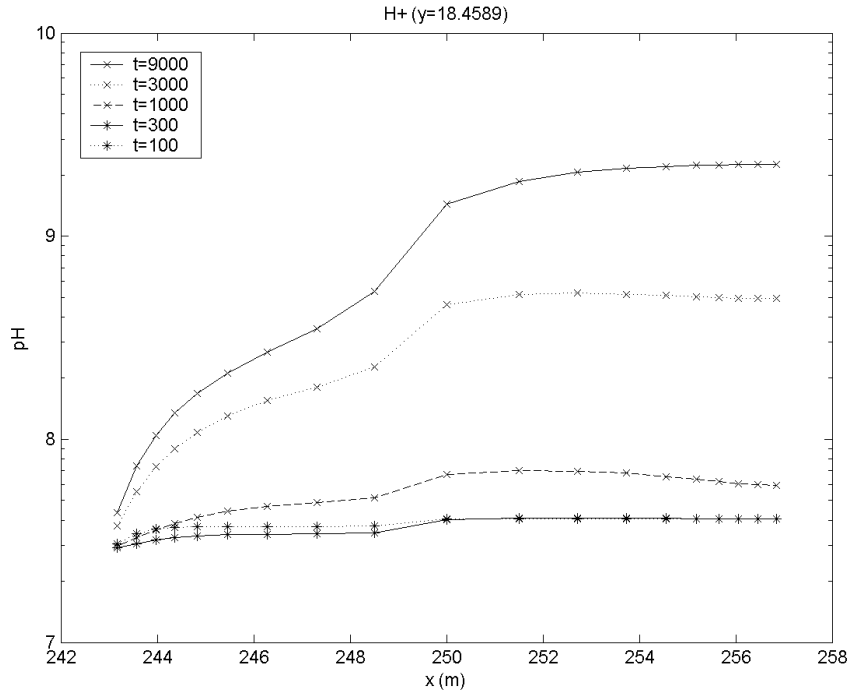

Figure 3.47: (Model 6 vertical slice, 32 mm backfill particles) - pH profile along the top of the backfill/host rock interface.

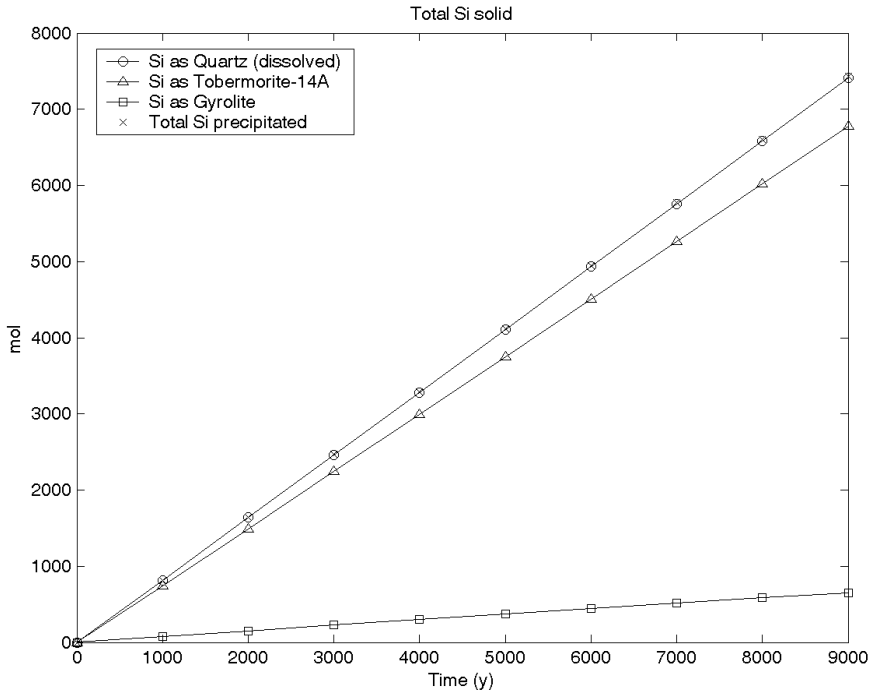

Figure 3.48: (Model 6 vertical slice, 32 mm backfill particles) - total quartz dissolved per 1m width of backfill, and total silica precipitated in secondary CSH phases.

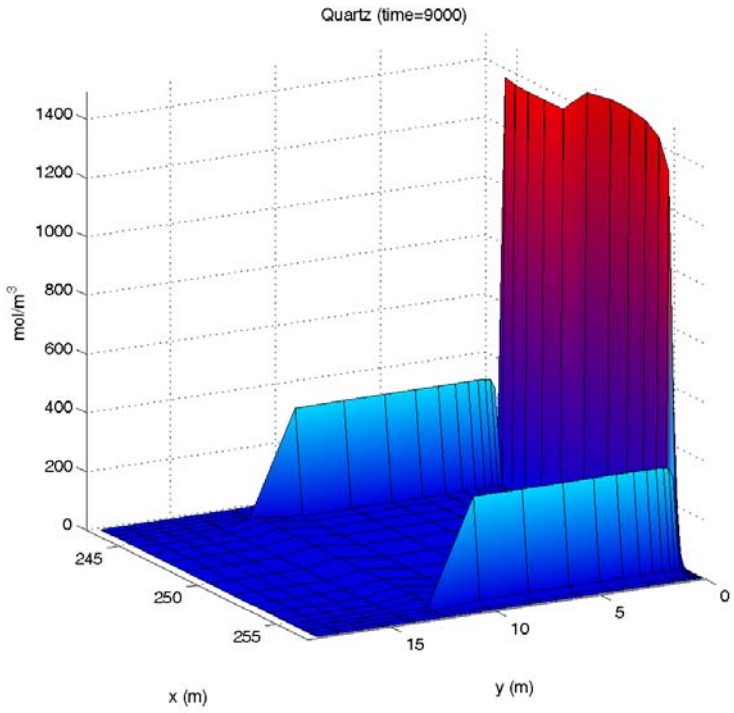

Figure 3.49: (Model 6 vertical slice, 32 mm backfill particles) - profile of concentration of dissolved quartz in the backfill at 9000 years.

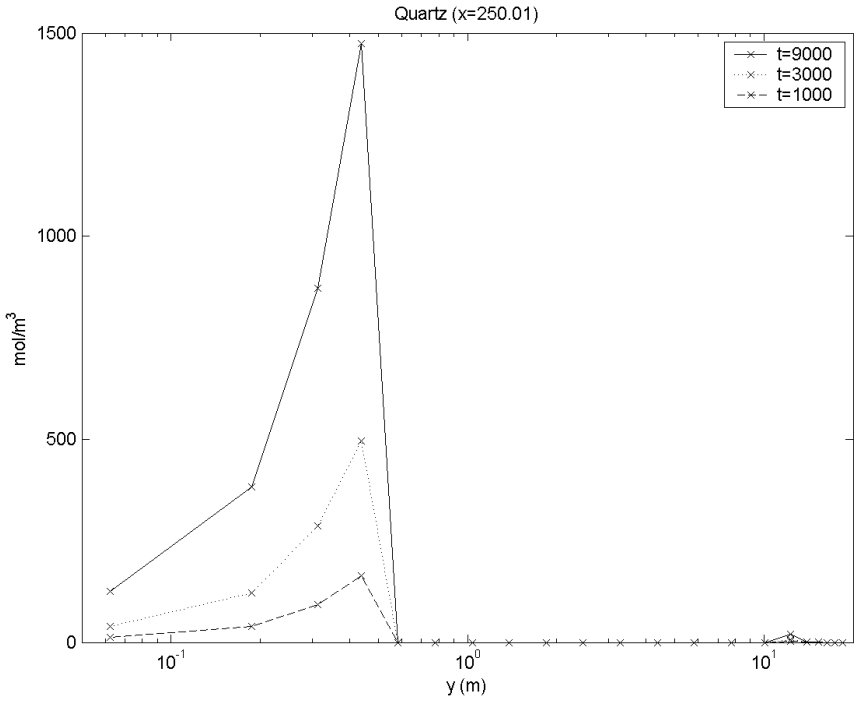

Figure 3.50: (Model 6 vertical slice, 32 mm backfill particles) - cross-section of profile of concentration of dissolved quartz in the backfill. The only significant dissolution is in the backfill below the vault.

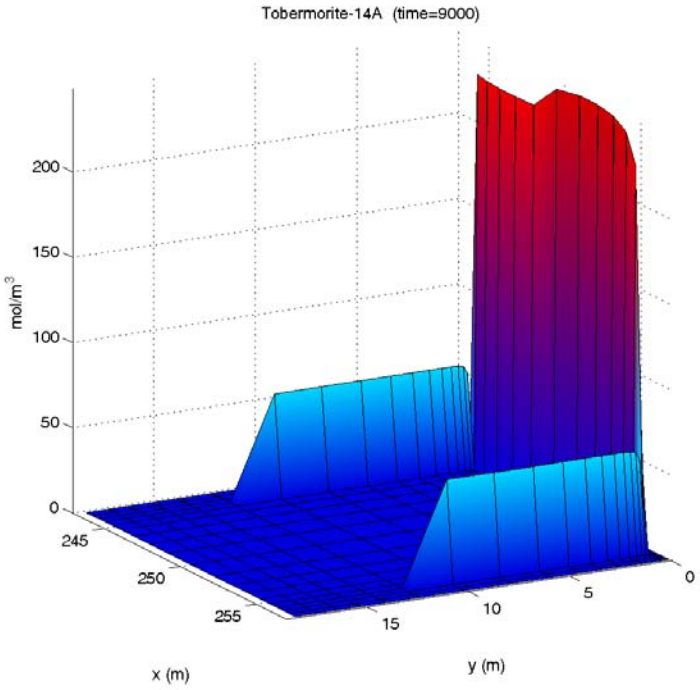

Figure 3.51: (Model 6 vertical slice, 32 mm backfill particles) - tobermorite concentration profile at 9000 years.

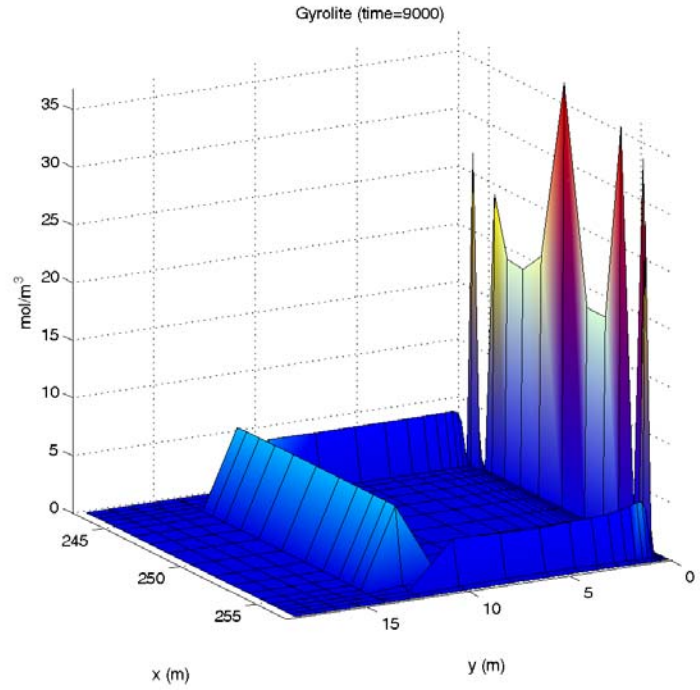

Figure 3.52: (Model 6 vertical slice, 32 mm backfill particles) - gyrolite concentration profile at 9000 years. The spikes in the gyrolite concentration along the bottom of the domain are due to the alternating Dirichlet and Neumann boundary conditions that are applied along the bottom boundary, corresponding to the alternating in and out-flows that were calculated in the flow modelling.

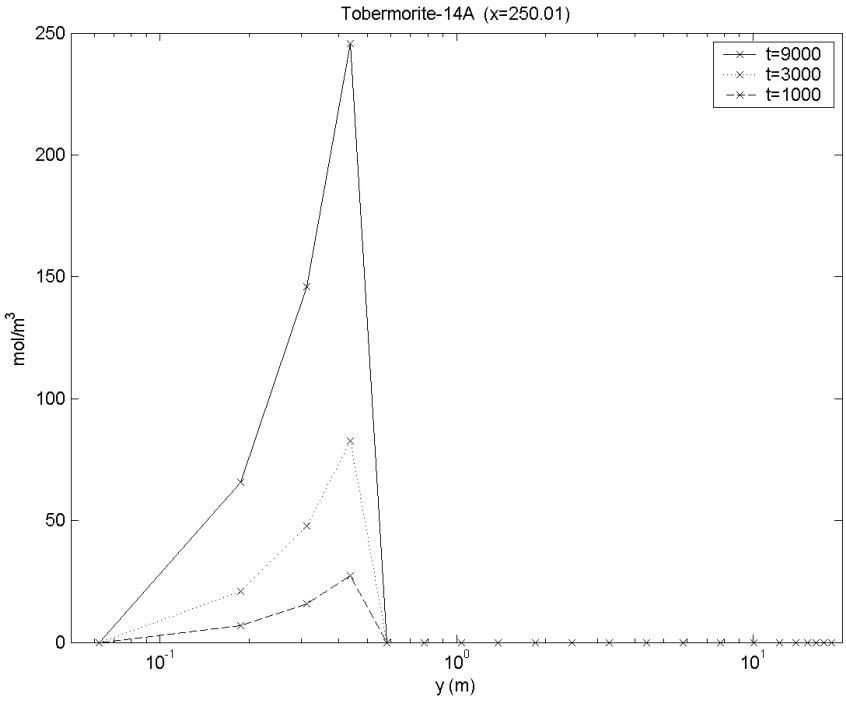

Figure 3.53: (Model 6 vertical slice, 32 mm backfill particles) - cross-section of profile of concentration of tobermorite in the backfill. The only significant precipitation is in the backfill below the vault.

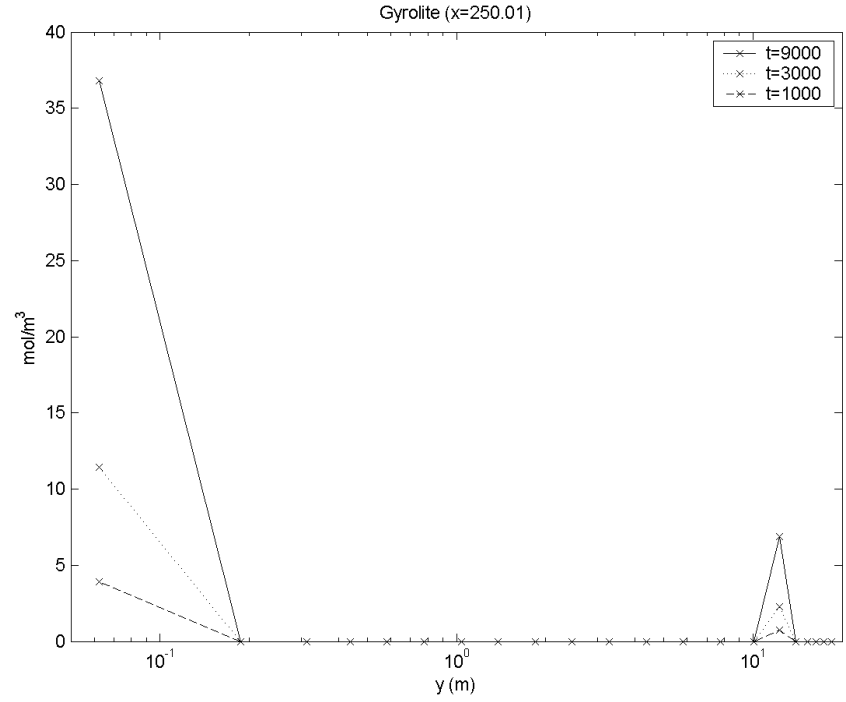

Figure 3.54: (Model 6 vertical slice, 32 mm backfill particles) - cross-section of profile of concentration of gyrolite in the backfill. The only significant precipitation is in the backfill below the vault.

Figures: 4 mm quartz particles

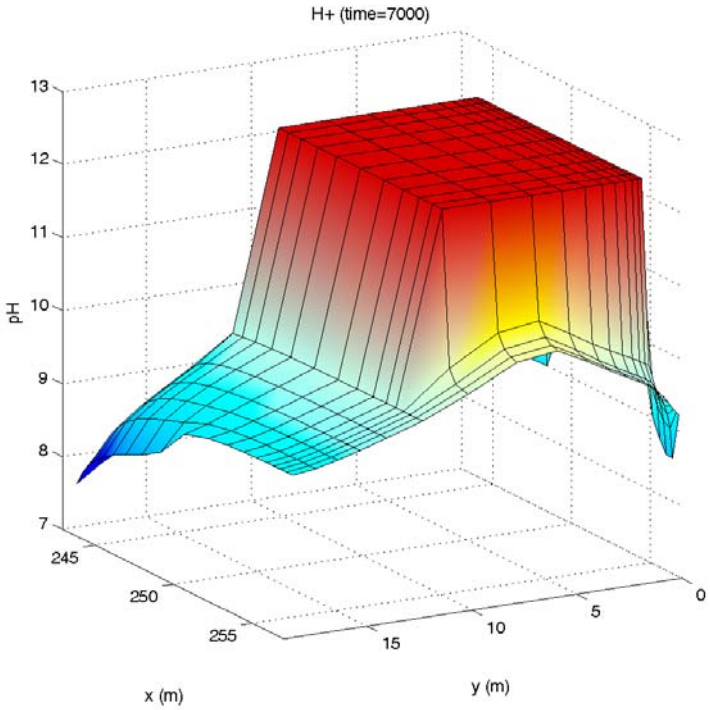

Figure 3.55: (Model 6 vertical slice, 4 mm backfill particles) - pH profile at 7000 years (view from the top of the backfill).

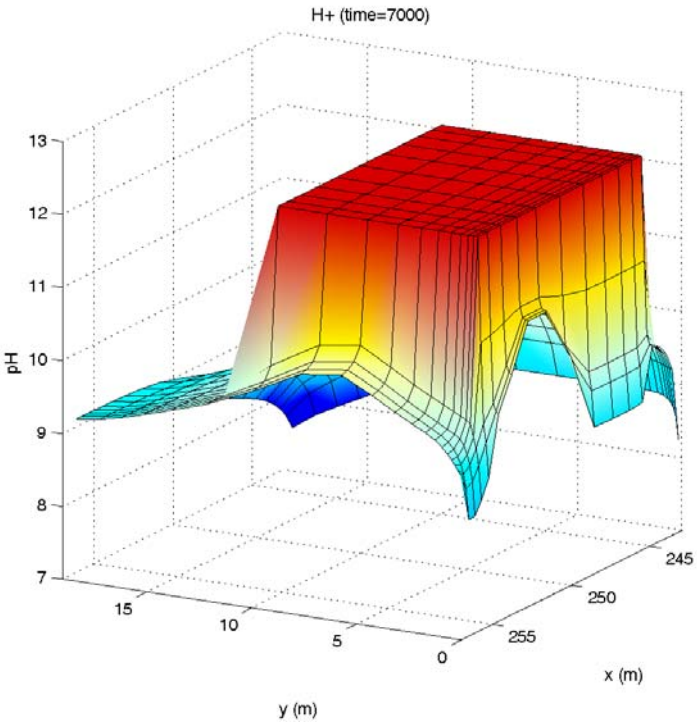

Figure 3.56: (Model 6 vertical slice, 4 mm backfill particles) - pH profile at 7000 years (view from the bottom of the backfill).

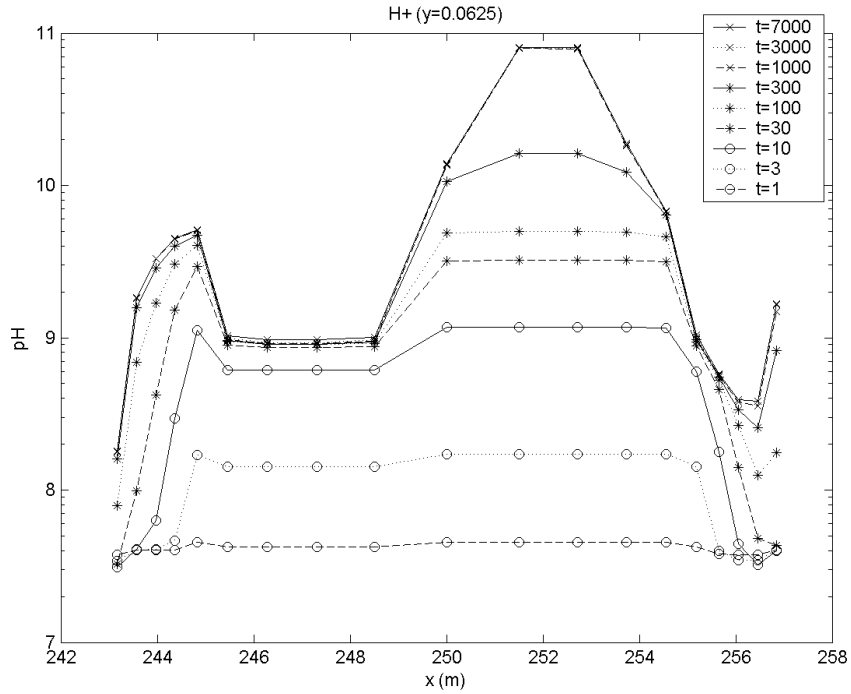

Figure 3.57: (Model 6 vertical slice, 4 mm backfill particles) - pH profile along the bottom of the backfill/host rock interface.

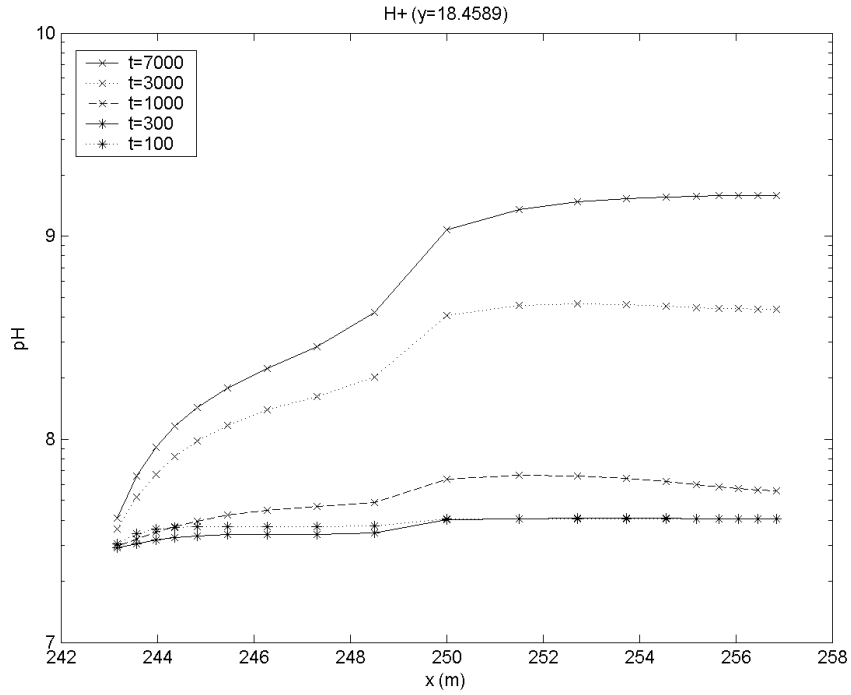

Figure 3.58: (Model 6 vertical slice, 4 mm backfill particles) - pH profile along the top of the backfill/host rock interface.

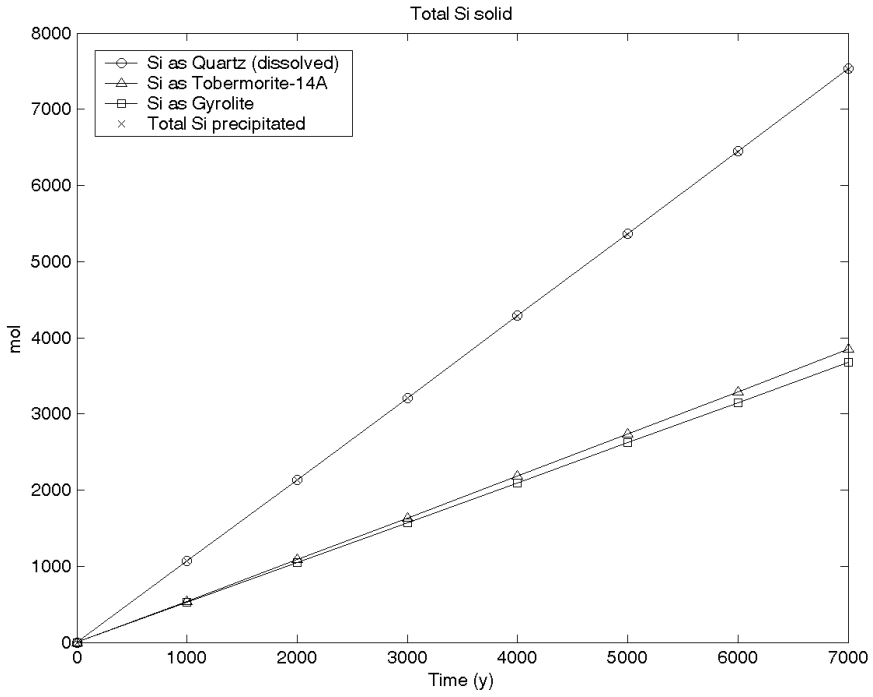

Figure 3.59: (Model 6 vertical slice, 4 mm backfill particles) - total quartz dissolved per 1m width of backfill, and total silica precipitated in secondary CSH phases.

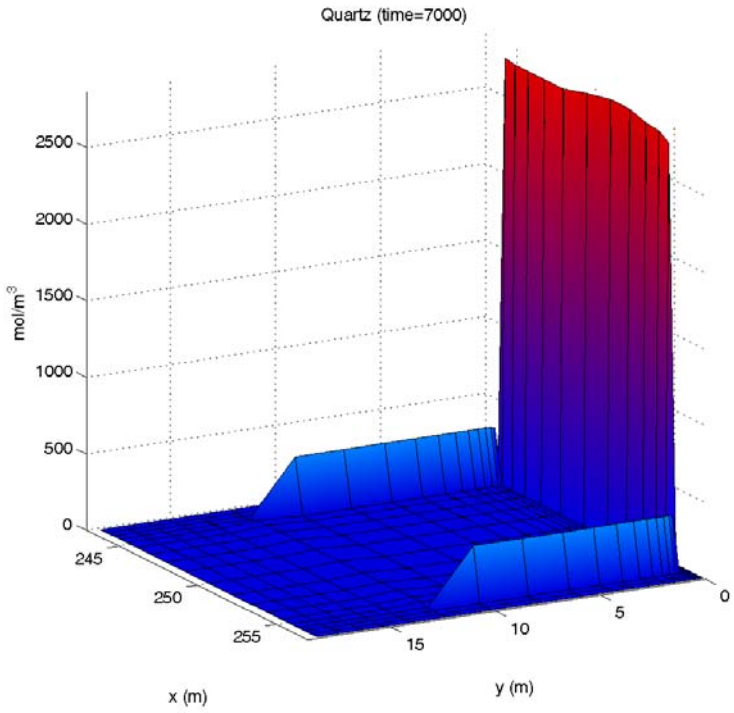

Figure 3.60: (Model 6 vertical slice, 4 mm backfill particles) - profile of concentration of dissolved quartz in the backfill at 7000 years.

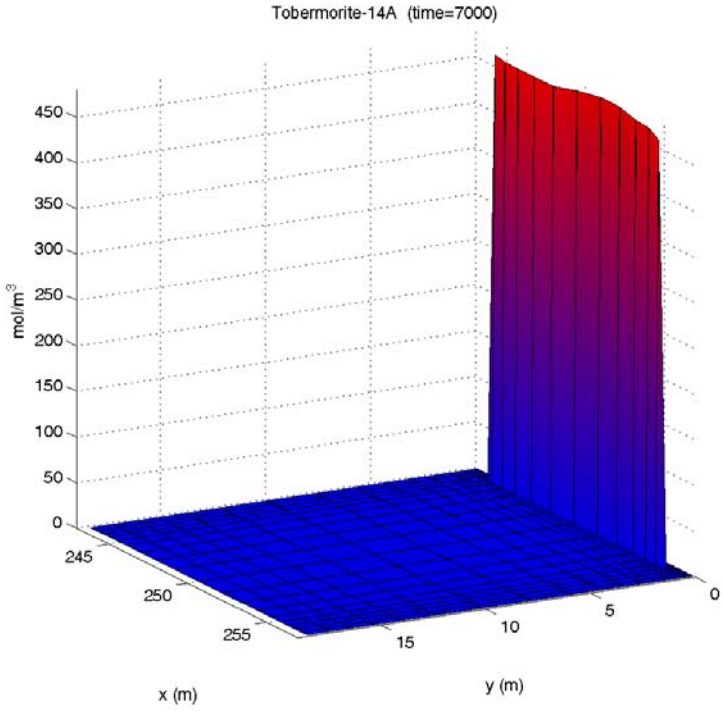

Figure 3.61: (Model 6 vertical slice, 4 mm backfill particles) - tobermorite concentration profile at 7000 years.

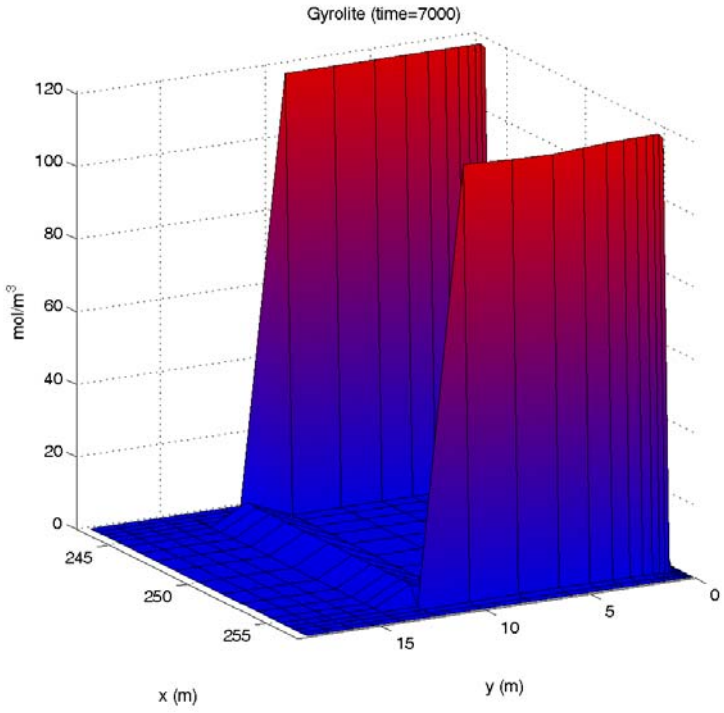

Figure 3.62: (Model 6 vertical slice, 4 mm backfill particles) - gyrolite concentration profile at 7000 years.

3.6.4 Model 7: horizontal slice

This case is based upon the 3D flow modelling case model 7 (see Section 2.3.2), where a transmissive feature is assumed to cut through the vault at 45°. The geochemical model considers a 2D slice through the 3D flow model corresponding to a horizontal slice along the length of the vault approximately half way up the waste. The geometrical extent of the geochemical model is the region comprising the backfill and the vault. The host rock and transmissive feature are not represented in the model.

The 2D grid used in the geochemical modelling corresponds to a 2D slice through the 3D MODFLOW grid used for the flow modelling, i.e. the (2D) resolutions of the flow and geochemical models are the same. The flow field calculated for the 3D Model 7 was mapped onto the 2D Raiden grid. Figure 3.63 shows the resulting Raiden flow field. In relation to the flow modelling, the direction of the y-axis is flipped, so that inflowing part of the transmissive feature is on the bottom boundary, and flow is out of the top boundary.

Simulations for 32 mm and 4 mm backfill particles were performed to 10^4 years.

Results: 32 mm backfill particles

The pH profiles viewed from the out-flowing and in-flowing boundaries at 10^4 years are shown in Figure 3.64 and Figure 3.65 respectively. Figure 3.66 and Figure 3.67 show the profile of pH along the boundaries. The maximum pH (exceeding 11) occurs at the out-flowing interface with the transmissive feature. On the in-flowing interface, the pH is highest at the downstream end where it reaches approximately 10.2.

The total amount of quartz dissolved in a 1 m thick slice of backfill is shown as a function of time in Figure 3.68 and the dissolved quartz profile at 10^4 years is shown in Figure 3.69. After 10^4 years, the total amount of quartz dissolved is approximately 4×10^4 moles (0.2% of the initial quartz amount in the slice). Again the only significant quartz dissolution occurs along the long edges of the vault.

Tobermorite and gyrolite precipitate in the backfill; Figure 3.68 shows the total precipitated amounts of silica in each mineral. Tobermorite precipitation is the more significant of the two minerals by a factor of approximately five. All of the dissolved quartz is converted to tobermorite and gyrolite. Figure 3.70 and Figure 3.71 show the profile of the precipitated minerals at 10^4 years. The majority of the precipitated minerals lie along the long edges of the vault.

Results: 4 mm backfill particles

The pH evolution for the 4 mm particle case are close to those for the 32 mm particle case, but with a slightly slower rate of increase early on due to the more rapid quartz

dissolution. However after 1000 years, the difference is small. See Figure 3.72 to Figure 3.75.

In contrast to the 32 mm particle case, the only secondary mineral that precipitates is gyrolite. The total amount of quartz dissolved is 5×10^{4} moles (0.25% of the initial amount of quartz in the slice), mostly along the long edges of the vault, the liberated SiO_2 precipitating as gyrolite before it can travel away from the vault. See Figure 3.76 and Figure 3.77.

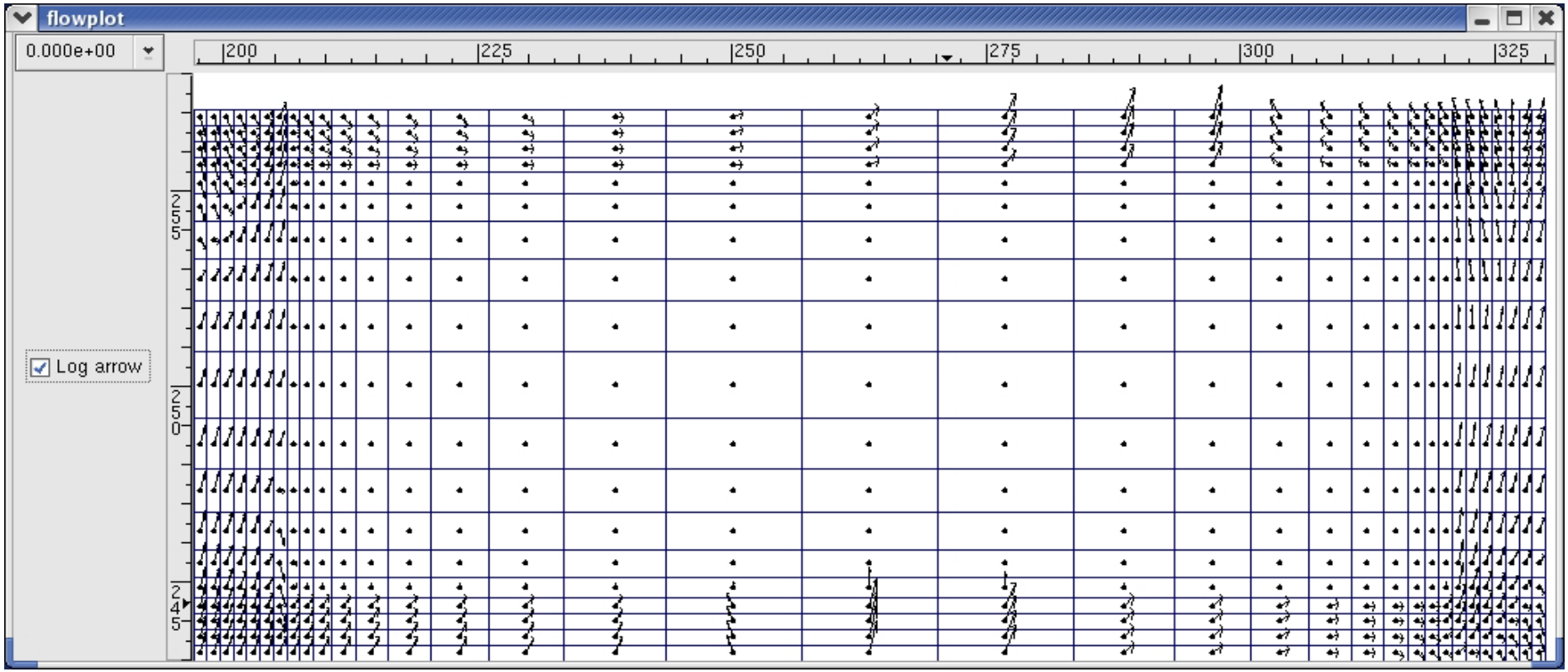

Figure 3.63: 2D flow field used for the geochemical calculation based on 3D flow calculation model.7. Figure depicts a horizontal slice through the vault. Note the flip in the y-axis from the flow modelling (Section 2.3.2) - the in-flowing boundary is at the bottom of the picture and the out-flowing boundary is at the top.

Figures: 32 mm quartz particles

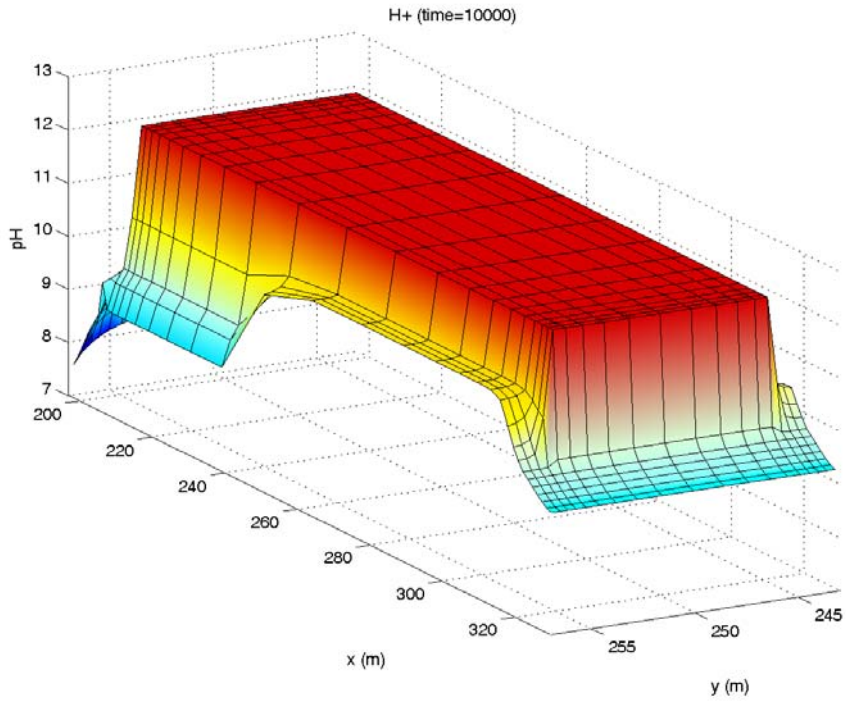

Figure 3.64: (Model 7 horizontal slice,32 mm backfill particles) - pH profile at 10^4 years (view from the out-flowing side of the backfill).

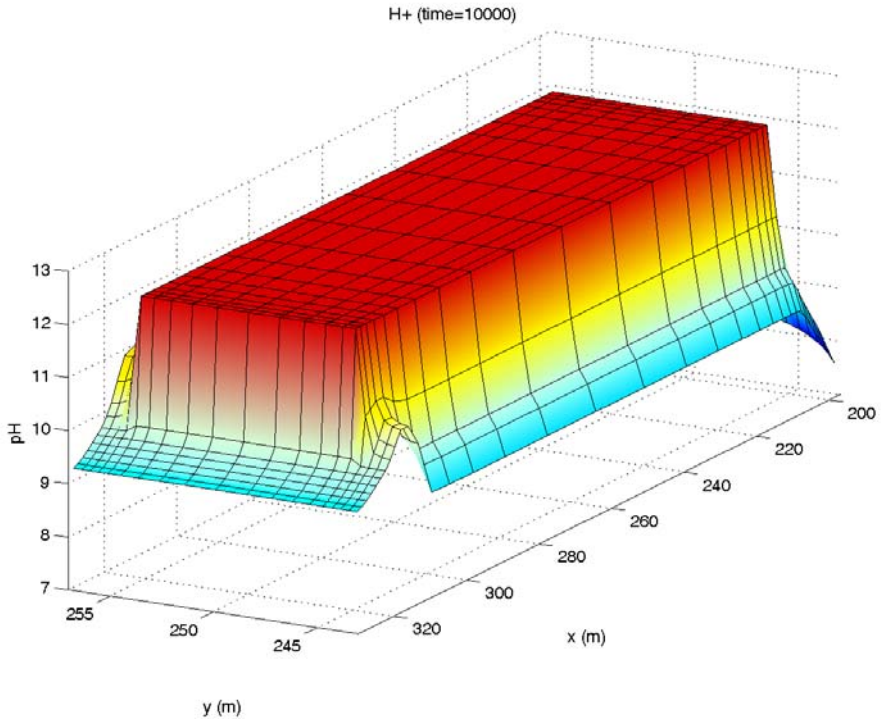

Figure 3.65: (Model 7 horizontal slice,32 mm backfill particles) - pH profile at 10^4 years (view from the in-flowing side of the backfill).

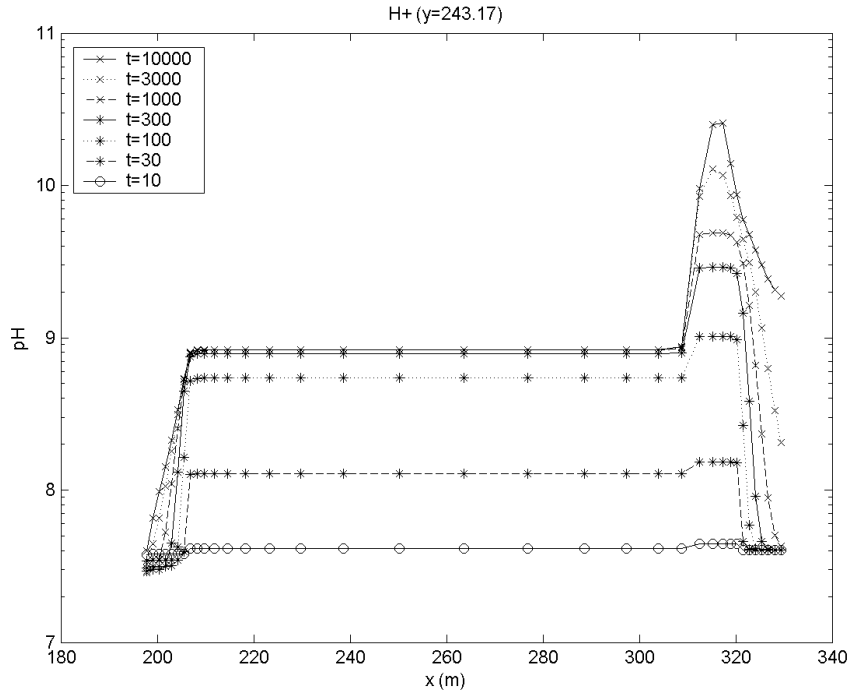

Figure 3.66: (Model 7 horizontal slice,32 mm backfill particles) - pH profile along the backfill/host rock interface at the in-flowing side.

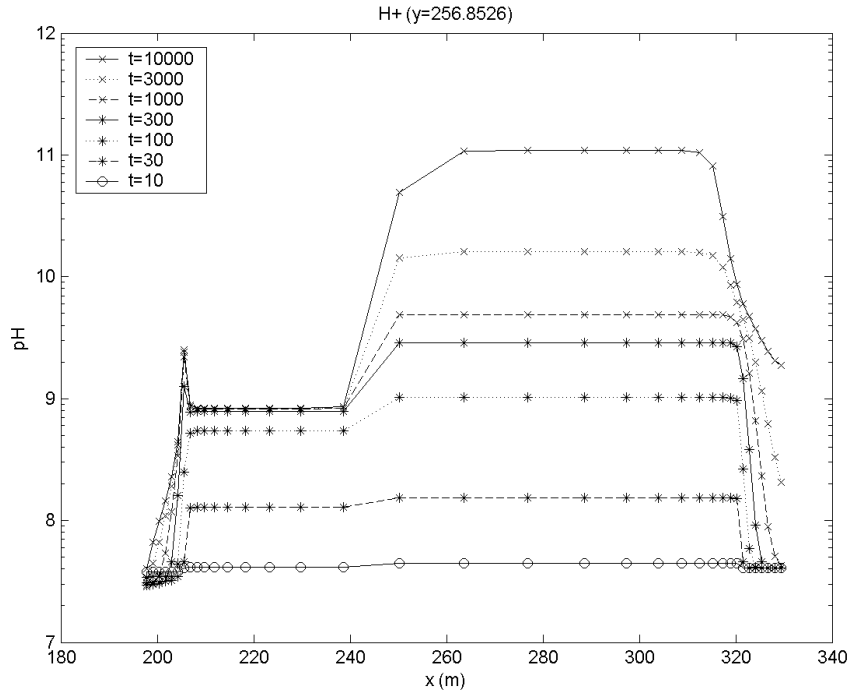

Figure 3.67: (Model 7 horizontal slice,32 mm backfill particles) - pH profile along the backfill/host rock interface at the out-flowing side.

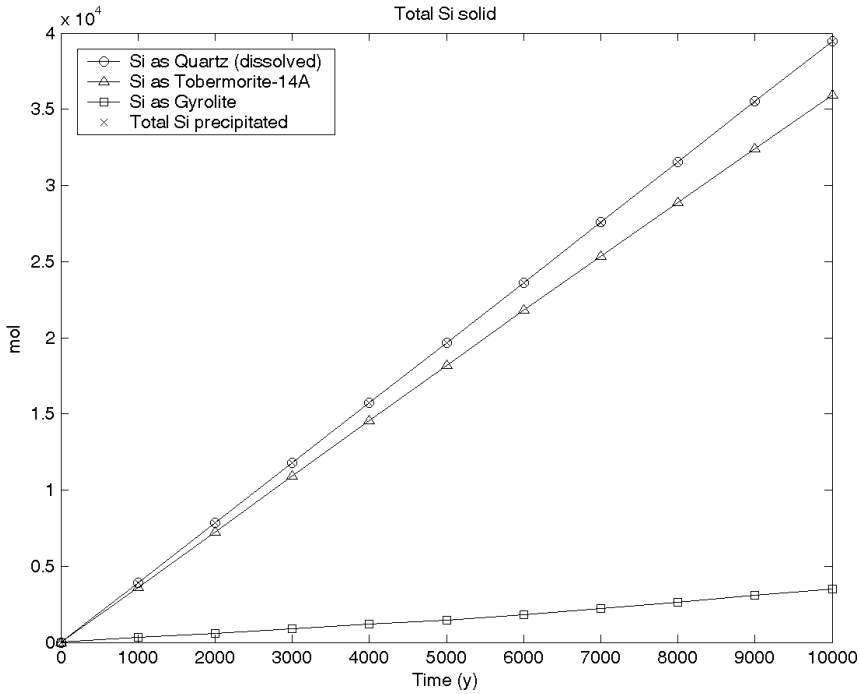

Figure 3.68: (Model 7 horizontal slice,32 mm backfill particles) - total quartz dissolved per 1m height of backfill, and total silica precipitated in secondary CSH phases.

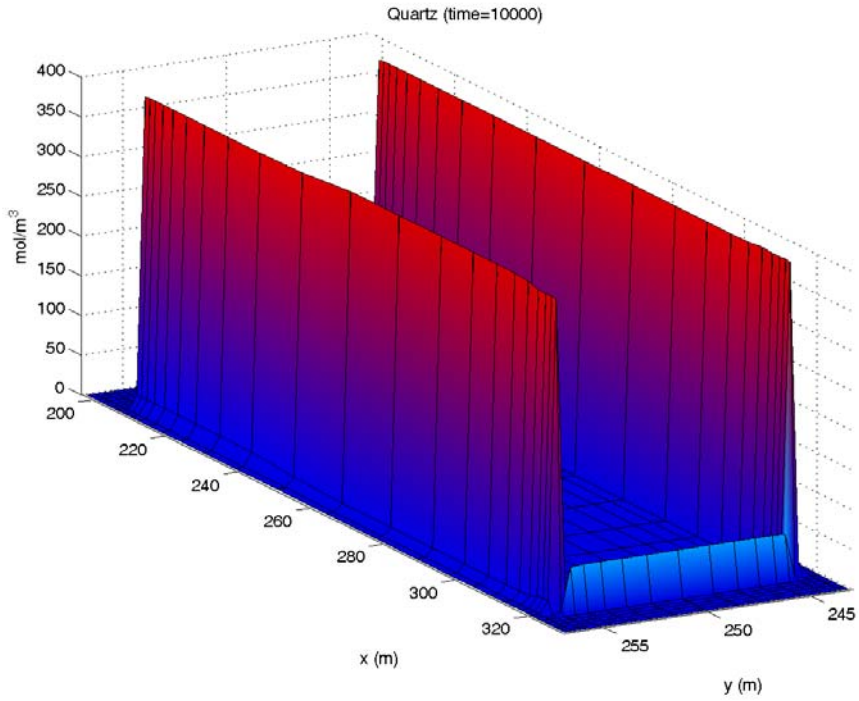

Figure 3.69: (Model 7 horizontal slice,32 mm backfill particles) - profile of concentration of dissolved quartz in the backfill at 10^4 years.

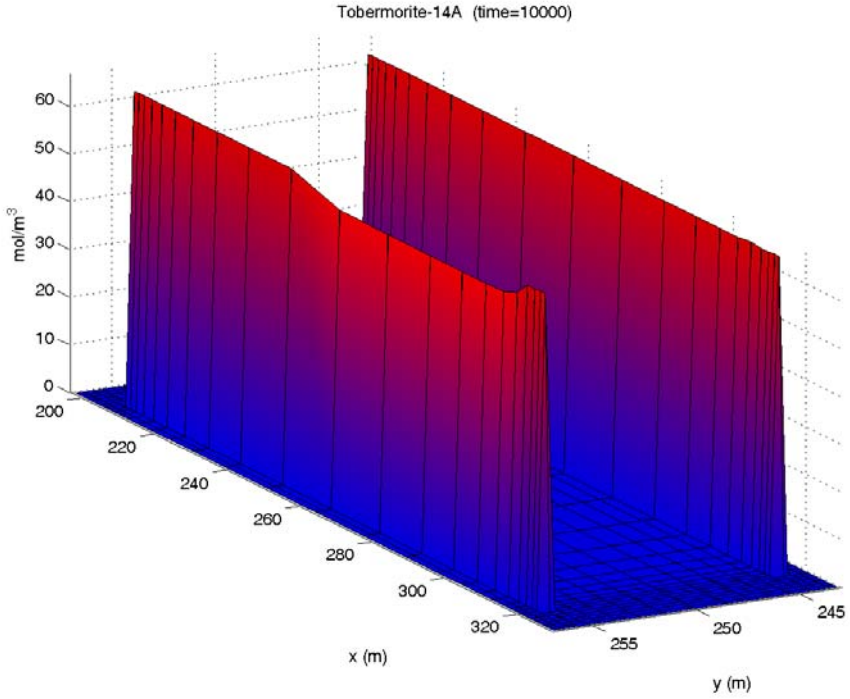

Figure 3.70: (Model 7 horizontal slice,32 mm backfill particles) - profile of concentration of tobermorite in the backfill at 10^4 years.

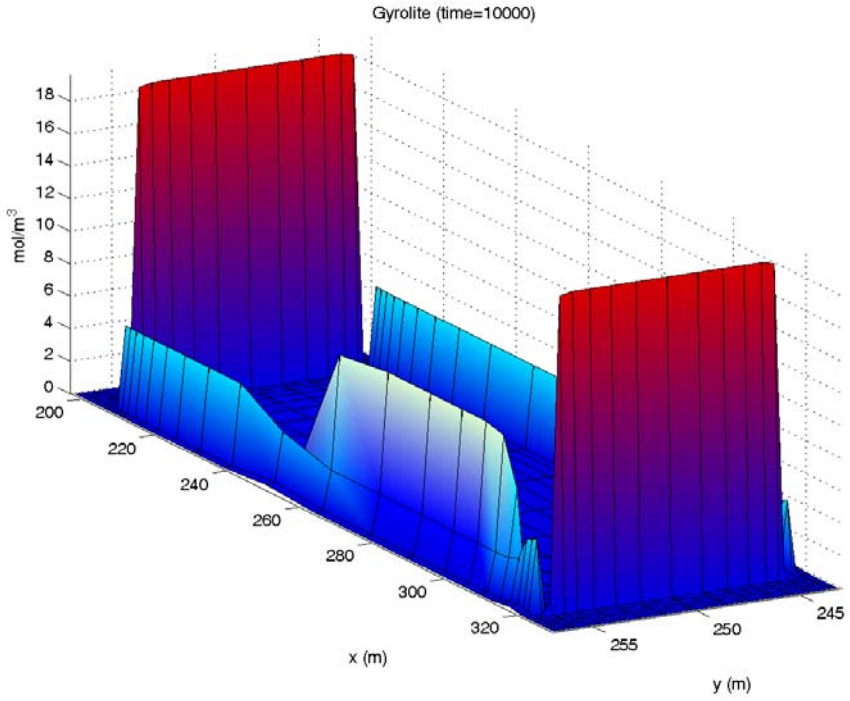

Figure 3.71: (Model 7 horizontal slice,32 mm backfill particles) - profile of concentration of gyrolite in the backfill at 10^4 years.

Figures:4 mm quartz particles

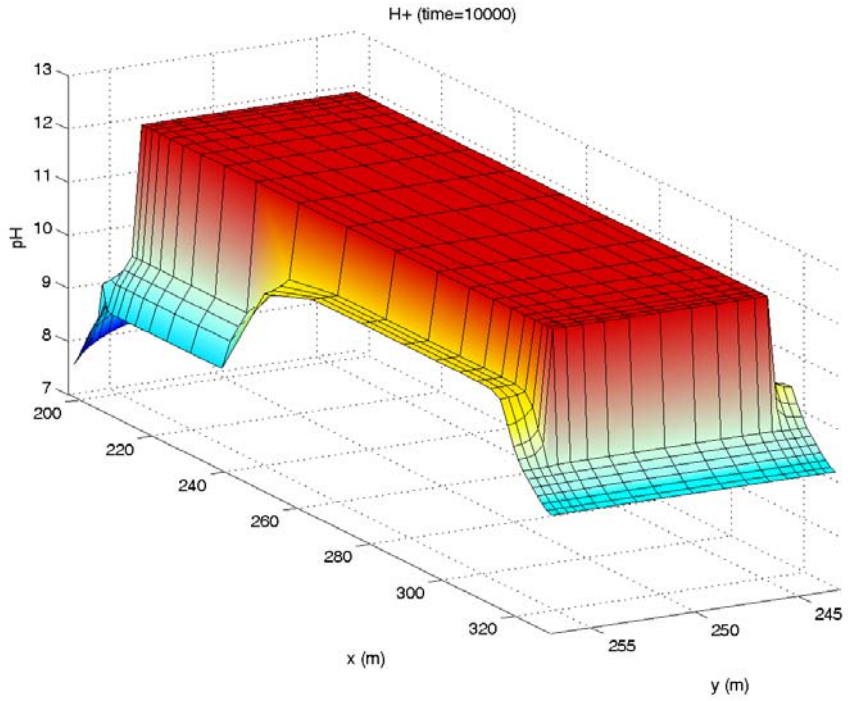

Figure 3.72: (Model 7 horizontal slice,4 mm backfill particles) - pH profile at 10^4 years (view from the out-flowing side of the backfill).

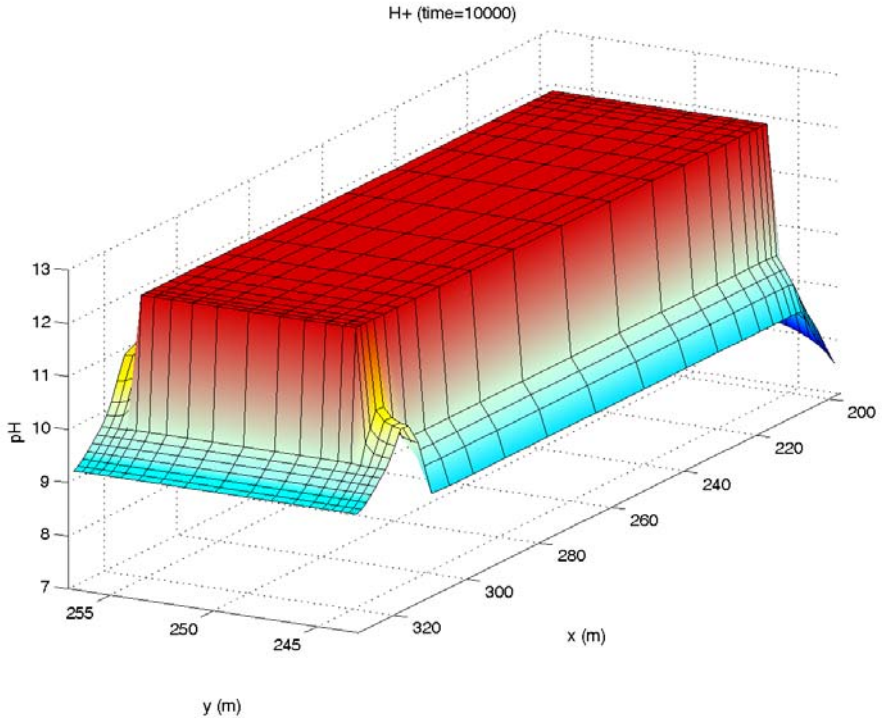

Figure 3.73: (Model 7 horizontal slice,4 mm backfill particles) - pH profile at 10^4 years (view from the in-flowing side of the backfill).

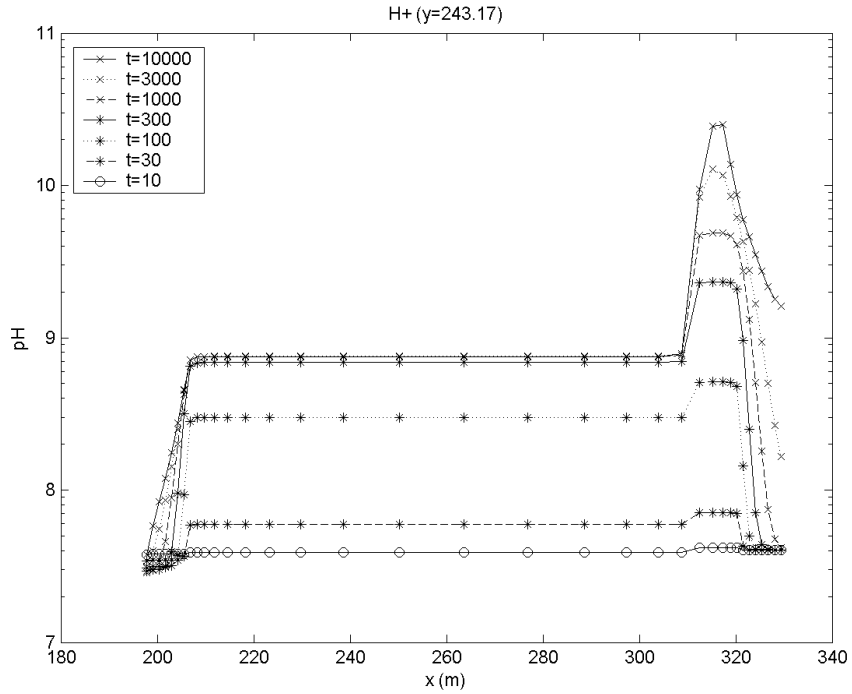

Figure 3.74: (Model 7 horizontal slice,4 mm backfill particles) - pH profile along the backfill/host rock interface at the in-flowing side.

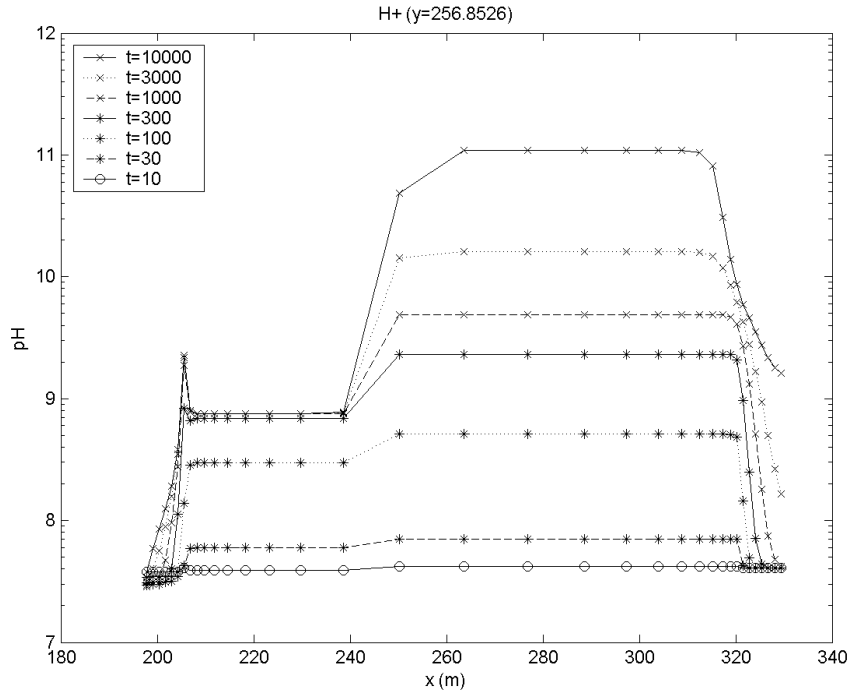

Figure 3.75: (Model 7 horizontal slice,4 mm backfill particles) - pH profile along the backfill/host rock interface at the out-flowing side.

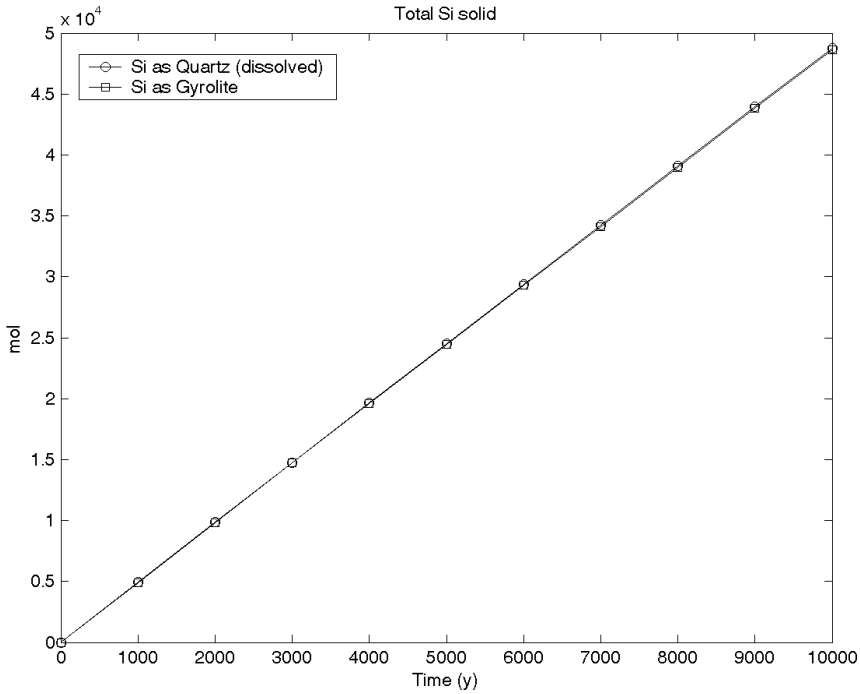

Figure 3.76: (Model 7 horizontal slice,4 mm backfill particles) - total quartz dissolved per 1m height of backfill, and total silica precipitated in secondary CSH phases.

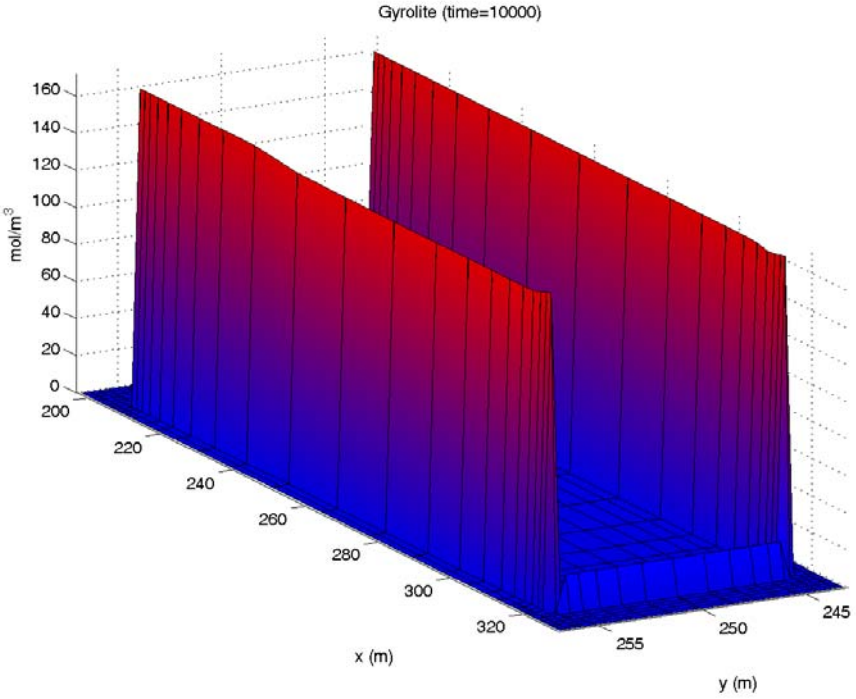

Figure 3.77: (Model 7 horizontal slice,4 mm backfill particles) - profile of concentration of gyrolite in the backfill at 10^4 years.

3.6.5 Variant case – Model 7 horizontal slice with inert backfill

A variant case of the horizontal slice through Model 7 (Section 3.6.4) was run to simulate the buffering capacity of an inert backfill and thereby check that the buffering role of the incoming groundwater is small. The quartz reaction was switched off so that the only source of SiO_2 was from the incoming porewater.

The results are plotted in Figure 3.78 to Figure 3.79. Compared to the cases in which the quartz backfill is present, the pH rapidly increases and by 3000 years exceeds 11 almost everywhere on the downstream long edge boundary between the backfill and the host rock. The only mineral that precipitates is tobermorite. Only a small amount precipitates, mostly adjacent to the inflowing boundary which is the only source of SiO_2.

This case highlights the role played by the quartz backfill in the previous cases and indicates that almost all of the buffering that was seen in the previous examples is as a result of silica made available from quartz dissolution, as opposed to silica that is present in the incoming porewater.

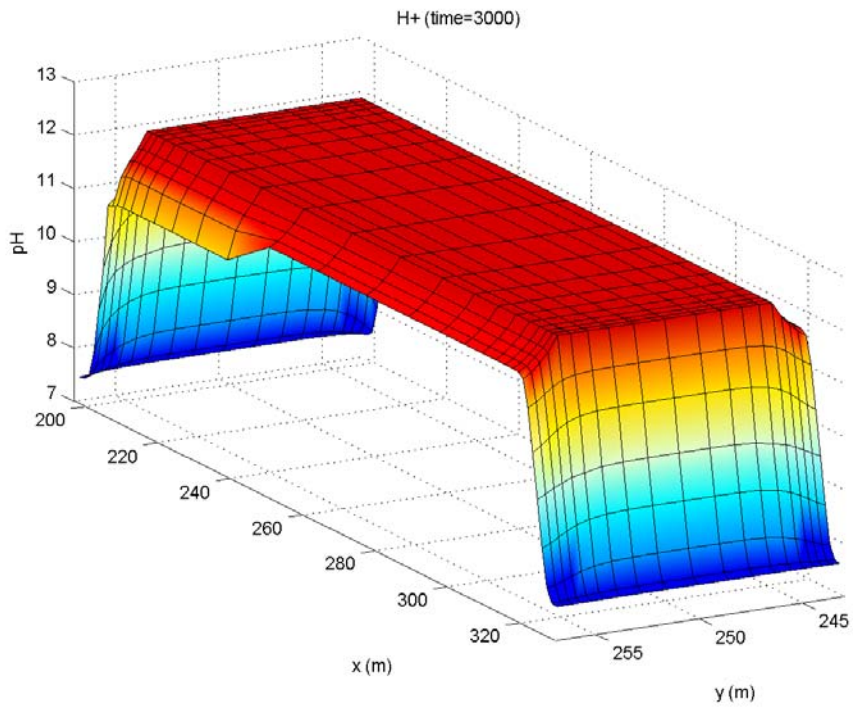

Figure 3.78: (Inert backfill variant case) - pH profile at 3000 years

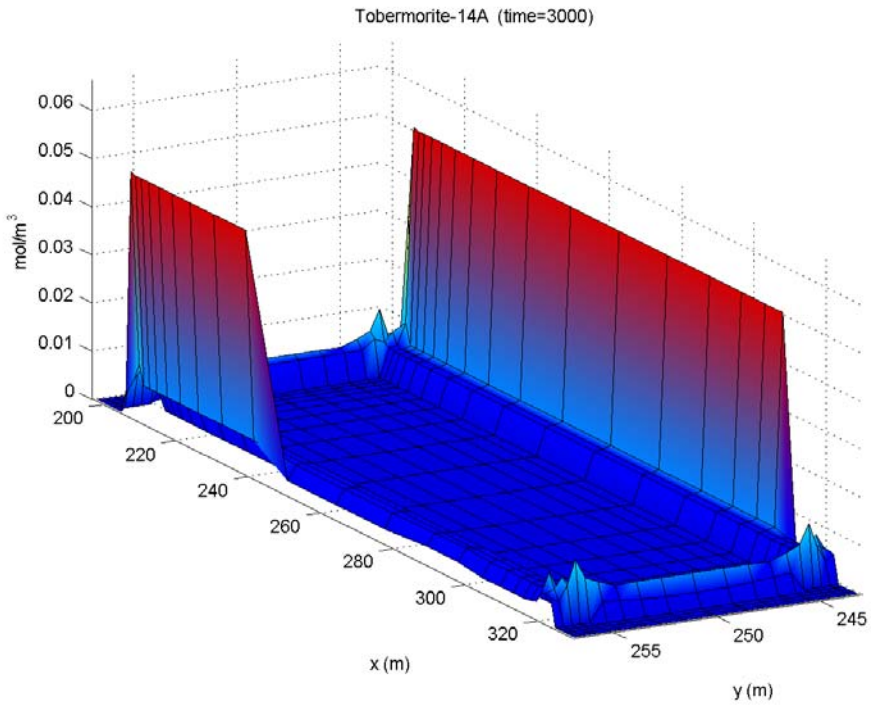

Figure 3.79: (Inert backfill variant case) -profile of concentration of tobermorite in the backfill at 3000 years.

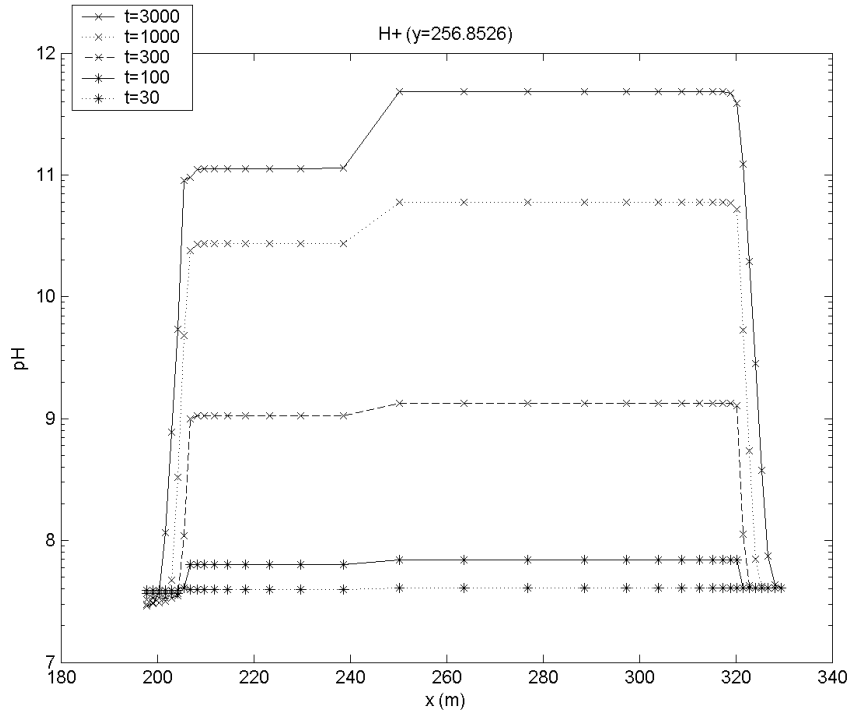

Figure 3.80: (Inert backfill variant case) - pH profiles along the backfill/host rock interface at the out-flowing side

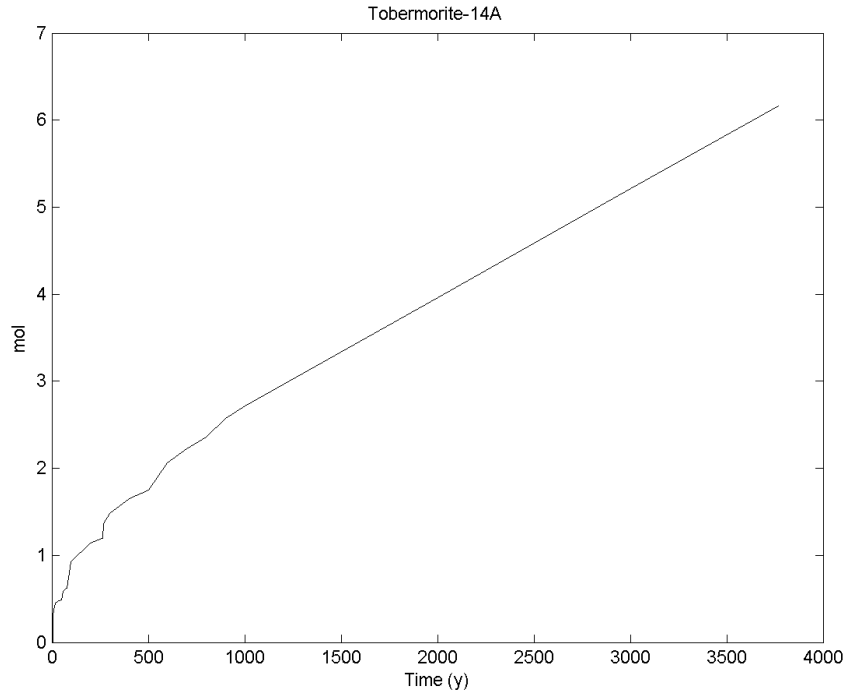

Figure 3.81: (Inert backfill variant case) - total tobermorite precipitated per 1m height of backfill.

4 Summary and conclusions

Potential groundwater flow conditions through gravel backfill for the SFL 3-5 repository concept were modelled in 3D using MODFLOW. The regional groundwater flow field was assumed to be horizontal and its interaction with a homogeneous backfill of dimensions in accord with published designs for the SKB SFL 3-5 repository, with uniform physical and hydraulic properties was investigated. The host rock also had uniform properties, except for explicitly represented transmissive features.

Calculations of cement pore fluid migration and reaction with backfill were carried out using *Raiden2*, a fully-coupled reaction-transport simulator. Flow fields generated in 3D with MODFLOW were converted to 2D 'slices' for reaction-transport calculations. The backfill was assumed to consist of grains of quartz of uniform size of either 4 mm or 32 mm diameter. The cement pore fluid diffusing from the waste package was assumed to be pure water saturated with portlandite [$Ca(OH)_2$] at 25 °C. The pore fluid saturating the backfill was assumed to be pure water equilibrated with quartz at 25 °C. A number of different simulations were carried out for both 4 and 32 mm diameter gravel backfill grains.

1. A 2D horizontal slice through the vault length with a transmissive feature in the host rock parallel to the vault length, at a distance of roughly 2 vault widths from the vault.
2. As (1) above, but considering a 2D *vertical* slice through the vault.
3. A 2D horizontal slice through the vault *width* with a transmissive feature in the host rock normal to the vault length.
4. A 2D horizontal slice through the vault length with a transmissive feature in the host rock intersecting the vault at 45 ° to the vault.

An additional simulation was also carried out for the geometry considered in model variant (4) above where reaction of quartz was excluded so that only reaction of $Ca(OH)_2$-saturated fluid was with ambient groundwater.

The results of the model variants incorporating reaction of quartz were broadly similar, with few differences apparent for the different orientations of the transmissive feature in the host rock. Most simulations showed that the gravel backfill is capable of maintaining pH < 11 in the backfill adjacent to the waste package and pH < 9.5 adjacent to the host rock, at timescales up to 10 000 years. However, some model variants showed pH ~11 in the backfill adjacent to the host rock at certain locations (beneath the waste package in some simulations, or at outflow regions in others). In all simulations, gradients of pH across the backfill were marked. The thin backfill layer beneath the vault was a region of poor buffering in all simulations where the layer was considered.

In this region, steep chemical gradients can exist across the relatively thin layer, which would probably lead to a rapid transport of the hyperalkaline plume across the thin backfill layer regardless of the flow conditions that are present.

Appreciable amounts of quartz (in the order of 10^4 moles after 10 000 years in a representative 1 m thick slice through the backfill) were dissolved in the gravel adjacent to the waste package to achieve pH buffering. All of the dissolved quartz is converted to CSH solids (tobermorite and gyrolite). Reactions in simulations with the 4 mm diameter backfill grains were slightly faster, but the results were otherwise identical to those for the 32 mm diameter grains.

The model variant with no chemical reaction of the backfill particles was considerably different from the other simulations with pH > 11 throughout the backfill volume after 3000 years of simulated time. Only trace amounts of a CSH solid (tobermorite) precipitated in this simulation, reflecting the trace amount of silica in the backfill pore fluid. This simulation confirmed the role of quartz/granite reactivity in retarding the migration of the hyperalkaline pore fluid.

The results of the modelling reported here broadly confirm the conclusions of Karlsson et al. (1999) in that a gravel backfill (here represented by quartz) is generally capable of limiting the extent of high pH pore fluids derived from hydrolysis of a cement/concrete waste package. However, the situation is more complicated than the simple mass-balance arguments presented Karlsson et al. (1999) would suggest, and some model variants investigated here suggest that pore fluid pH at the backfill-host rock boundary may increase to pH ~11, particularly beneath waste packages or at outflow regions of the EBS. These pore fluids have a pH considerably above that expected for groundwaters in Swedish granites (e.g. Karlsson et al., 1999) and may thus be reactive with respect to minerals lining groundwater pathways. Dissolution of fracture-lining silicates and carbonates may be expected, with concomitant precipitation of solids such as zeolites. These reactions may serve to increase radionuclide retardation, but may need to be considered explicitly in safety assessment.

Moreover, there are a couple of non-conservative assumptions in the modelling conducted here and that presented by Karlsson et al., 1999 which create further uncertainty in the ability of a gravel backfill to buffer pH.

- The granite backfill is not wholly composed of quartz, so that the amount of silica available for reaction is exaggerated, probably by 30-40 %.
- The reactive surface area of granite gravel grains will decrease with time due to ‘armouring’ by reaction products. This will result in decreased reactivity (less buffering capacity) with time.

The effects of these assumptions could be investigated in further studies of this type.

References

Benbow S., Robinson P., and Savage D., *Buffering capacity of pH in backfill*, SKI Technical Report 02:39, Swedish Nuclear Power Inspectorate, Stockholm, Sweden, 2002.

Bethke C. M., *Geochemical Reaction Modelling*, Oxford University Press, 1996.

Börjesson S., *Computer modelling of the interaction between water and complex solid phases. PhD Thesis*, Department of Nuclear Chemistry, Chalmers University of Technology, Göteborg, Sweden, 1997.

Holmén, J. G., *On the flow of groundwater in closed tunnels. Generic hydrogeological modelling of nuclear waste repository SFL 3-5*, SKB Report TR-97-10, Swedish Nuclear Fuel and Waste Management Company, Stockholm, Sweden, 1997.

Karlsson F., Lindgren M., Skagius K., Wiborgh M., and Engkvist I., *Evolution of geochemical conditions in SFL 3-5*, SKB Report R-99-15, Swedish Nuclear Fuel and Waste Management Company, Stockholm, Sweden, 1999.

Knauss K. G., and Wolery T. J., *The dissolution kinetics of quartz as a function of pH and time at 70 °C*, Geochimica et Cosmochimica Acta 52: 43-53, 1988.

Marsic N., Hartley L., Jackson P., Poole M., Morvik A., *Development of hydrogeological modelling tools based on NAMMU*, SKB Report R-01-49, Swedish Nuclear Fuel and Waste Management Company, Stockholm, Sweden, 2001.

McDonald M. G. and Harbaugh A.W., *A Modular Three-Dimensional Finite-Difference Ground-Water Flow Model*, U.S. Geological Survey, Techniques of Water-Resources Investigations, Book 6, Chapter A1, 1988.

Savage D., Stenhouse M. and Benbow S., *Evolution of near-field physico-chemical characteristics of the SFR repository*, SKI Technical Report 00:49, Swedish Nuclear Power Inspectorate, Stockholm, Sweden, 2000.

Savage D. and Stenhouse M., *SFR1 vault database*, SKI Technical Report 02:53, Swedish Nuclear Power Inspectorate, Stockholm, Sweden, 2003.

Skagius K., Pettersson M., Wiborgh M., *Compilation of data for the analysis of radionuclide migration from SFL 3-5*, SKB Report R-99-13, Swedish Nuclear Fuel and Waste Management Company, Stockholm, Sweden, 1999.

Wolery T.J., *EQ3NR, a computer program for geochemical aqueous speciation-solubility calculations: Theoretical manual, user's guide, and related documentation (version 7.0).* Lawrence Livermore Report UCRL-MA-110662 PT III. Lawrence Livermore National Laboratory, Livermore, California, USA, 1992.

www.ski.se

STATENS KÄRNKRAFTINSPEKTION
Swedish Nuclear Power Inspectorate

POST/POSTAL ADDRESS SE-106 58 Stockholm
BESÖK/OFFICE Klarabergsviadukten 90
TELEFON/TELEPHONE +46 (0)8 698 84 00
TELEFAX +46 (0)8 661 90 86
E-POST/E-MAIL ski@ski.se
WEBBPLATS/WEB SITE www.ski.se